Numerical Solution Methods for Shock and Detonation Jump Conditions

S. Browne, J. Ziegler, and J. E. Shepherd
Aeronautics and Mechanical Engineering
California Institute of Technology
Pasadena, CA USA 91125

Abstract

Selected algorithms are described for the numerical solution of shock and detonation jump conditions in ideal gas mixtures with realistic thermochemical properties. An iterative technique based on a two-variable Newton's method is selected as being the most robust method for both reactive and nonreactive flows. In the implementations of this solution algorithm, we have used the Cantera software library to evaluate gas properties and carry out chemical equilibrium computations. A library of routines is described for Python or Matlab computations of post-shock conditions and Chapman-Jouguet detonation velocity.

Note Added in Revision March 2015 This is a hypertext document with links to Python and Matlab scripts that can be downloaded and executed by the reader. These scripts were revised in 2014 by Neal Bitter and Bryan Schmidt for use with Cantera version 2.1 and Python V2.7. In order to use these scripts, the reader must install the Cantera software and Python or Matlab. Instructions about installation are available on the SDToolbox website.

Disclaimer and Copyright The software tools described in this document are based on the Cantera software library and offered under the same licensing terms, which are as follows:

Contents

List of Figures

List of Tables

1 Introduction

Numerical solution methods are necessary for solving the conservation equations or jump conditions that determine the properties of shock and detonation waves in a multi-component, reacting, ideal gas mixture. Only the idealized situations of perfect (constant heat-capacity) gases with fixed chemical energy release can be treated analytically (see the results given in Appendix A and B.1). Although widely used for simple estimates and mathematical analysis, the results of perfect gas models are not suitable for analysis of laboratory experiments and carrying out numerical simulations based on realistic thermochemical properties.

There are four situations that are commonly encountered.

1. Non-reactive shock wave. If the chemical reactions occur sufficiently slowly compared to translational, rotational, and vibrational equilibrium,[1] then a short distance behind a shock wave flow can be considered to be in thermal equilibrium but chemical nonequilibrium. This is often referred to as a "frozen shock" since the chemical composition is considered to be fixed through the shock wave. Computations of post-shock conditions are used as initial conditions for the subsequent reaction zone and are therefore a necessary part of computing shock or detonation structure. Usually, these computations proceed from specified upstream conditions and shock speed; the aim of the computation is to determine the downstream thermodynamic state and fluid velocity. On occasion, we consider the inverse problem of starting from a specified downstream state and computing the upstream state.
   Function PostShock_fr: Demos - Matlab: demo_PSfr.m Python: demo_PSfr.py

2. Reactive shock wave. The region sufficiently far downstream from the shock wave is considered in thermodynamic equilibrium. Thermodynamics can be used to determine the chemical composition, but this is coupled to the conservation equation solutions since the entropy and enthalpy of each species is a function of temperature. As a consequence, the solution of the conservation equations and chemical equilibrium must be self-consistent, requiring an iterative solution for the general case. In the case of endothermic reactions (i.e., dissociation of air behind the bow shock on re-entry vehicle), there are no limits on the specified shock velocity and the computation of the downstream state for specified upstream conditions is straightforward. For exothermic reactions, solutions are possible only for a range of wave speeds separated by a forbidden region. The admissible solutions are detonation (high velocity, i.e., supersonic) and deflagration (low velocity, i.e., subsonic) waves, and there are usually two solutions possible for each case.
   Function PostShock_eq: Demos - Matlab: demo_PSeq.m Python: demo_PSeq.py

3. Chapman-Jouguet (CJ) detonation. This is the limiting case of the minimum wave speed for the supersonic solutions to the jump conditions with exothermic reactions. The Chapman-Jouguet solution is often used to approximate the properties of an ideal steady detonation wave. In particular, detonation waves are often observed to propagate at speeds within 5-10% of their theoretical CJ speeds in experimental situations where the waves are far from failure.
   Function CJSpeed: Demos - Matlab: demo_CJ.m Python: demo_CJ.py

4. Reflected shock wave. When a detonation or shock wave is incident on a hard surface, the flow behind the incident wave is suddenly stopped, creating a reflected shock wave that propagates in the opposite direction of the original wave. If we approximate the reflecting surface as rigid, then we can compute the speed of the reflected shock wave given the incident shock strength. This computation is frequently carried out in connection with estimating structural loads from shock or detonation waves.
   Function reflected_eq and reflected_fr:
   Demos - Matlab: demo_reflected_eq.m and demo_reflected_fr.m Python: demo_reflected_eq.py and demo_reflected_fr.py

There are other special situations such as oblique and curved shock or detonation waves. If the structure of the wave can be neglected, waves can locally be considered planar and by transforming to a wave-fixed frame, oblique shock waves can be analyzed by the same methods as used for planar shocks (Thompson, 1972, Shepherd, 1994).

---

[1] The structure of shock waves with vibration non-equilibrium is discussed at length by Clarke and McChesney (1964) and Vincenti and Kruger (1965)

In the last 60 years, many numerical solution methods have been developed and made available as application software, some of which are described briefly in Section 2. However, there are issues with using the older software including limited availability due to national security or proprietary concerns and lack of support for legacy software. In response to this situation, we have developed a library of software tools that we are making freely available for academic research. In doing so, we have taken advantage of recent developments in programming environments such as Matlab and Python and modern software libraries such as Cantera (Goodwin).

In this report, we describe the historical background in Section 2 and discuss the governing equations and classical analysis methods in Section 3. A simple functional iteration algorithm is described in Section 7.1. A more sophisticated algorithm based on Newton's method for calculating both the post-shock state and the Chapman-Jouguet detonation speed is described in Sections 7.2 and 7.3 . Section 8 discusses the basis of the Newton algorithm and the order of convergence of the iterative scheme. Section 8 also gives a comparison between results obtained with the Matlab implementation and with legacy Fortran programs (Shepherd, 1986) that we have previously used in our laboratory. Programs for simulating idealized (constant volume or constant pressure) explosions and idealized ZND[2] detonation structure are described in a companion report Browne et al. (2005).

2   Background

Methods for solving shock and detonation jump conditions were initially developed in order to test theories about wave propagation and later, to make quantitative predictions for explosive engineering. Efforts to test the Chapman-Jouguet model of detonation through the comparison of measured and predicted detonation wave speeds played an important role in this process. The early history of shock and detonation wave studies is described by Bone and Townend (1927) (Chap XV and XVI) and Jost (1946) (Chap V); some of the original theoretical papers on shock waves are reproduced in Johnson and Chéret (1998).

1848 Stokes notes the problem of wave steepening in acoustic waves with finite amplitude and derives jump conditions for mass and momentum. He is skeptical about the possibility of discontinuous motion and creates a half-century of confusion about the role of dissipation and energy conservation in shock waves by using the isentropic relationship instead of the correct energy equation, which was still in development at that time. (See Thompson 1972 and for more detail Salas 2007)

1860 Riemann develops the first finite amplitude theory of sound waves and discusses how wave steepening will generate shock waves, but does not consider energy conservation in his jump relations. (Reproduced in translation in Johnson and Chéret, 1998)

1870 Rankine derives the correct energy jump condition based on modern ideas about thermodynamics and energy conservation, clearly states that the wave is adiabatic, and explicitly solves the jump conditions for perfect gases. (Reproduced in Johnson and Chéret, 1998)

1881 Berthelot & Vielle and Mallard & Le Chatelier independently discover detonation (l'onde explosive). They find that each explosive mixture has a definite wave speed for "stable" propagation. They studied H_2, C_2H_2, C_2H_6, CH_4, C_2N_2, and O_2 mixtures in lead tubes.

1887 Hugoniot considers the formation of shock waves and independently derives correct jump conditions for shock waves. (Reproduced in Johnson and Chéret, 1998)

1893-1903 Dixon makes photographic observations and velocity measurements of detonation waves. He studied the influence of initial pressure and dilution and does very careful measurements to test detonation theories. Initially unaware of Chapman's work (1899), Berthelot, Vielle, and Dixon all supposed that the wave speed is similar to molecular speed or sound speed of combustion products.

1899 Chapman applies Riemann's theory (modified by Rankine to correctly account for energy conservation) to detonation and postulates that the minimum speed is the correct detonation velocity. Based on

---

[2]Zeldovich, von Neumann, Döering - see Fickett and Davis (1979)

this, he is able to "predict" Dixon's measured detonation velocity dependence on dilution, increase in speed with H_2 dilution, and decrease with increasing O_2 or N_2. However, specific heat data at high temperature is quite uncertain, and agreement with data requires adjustment of specific heats to fit results.

1900 Vielle constructs shock tube, measures shock wave velocities greater than the speed of sound ahead, and notes similarity between shock and detonation. He compares wave speeds with Hugoniot's theory of 1887.

1905 Jouguet independently discovers the shock wave theory of detonation velocity and applies Hugoniot's method to derive detonation velocity. He argues that the CJ condition is correct since sound waves cannot overtake the detonation from behind at this point. He uses $w_2 = a_2$ as condition for determining wave speed. He shows that entropy is a minimum at CJ point.

Both Jouguet and Chapman thought that dissociation was not a significant factor in determining detonation velocities. In their evaluation of the CJ velocity, they used mean values of specific heat capacity that were based on extrapolating low temperature experimental data. This wasn't resolved until thirty years later when better thermochemical data became available and both the variation of specific heat capacity with temperature and effects of chemical equilibrium could be correctly included.

1910 Taylor computes the structure of weak waves using the Navier-Stokes equations and reconciles the overall conservation of energy with the existence of dissipation with a thin layer where entropy is generated. (Reproduced in Johnson and Chéret, 1998)

1922 Becker discusses the jump condition solution for shock waves with variable specific heat and liquids. He derives the relationship between slope of adiabat and isentrope. He discusses the importance of the second derivative for existence of expansion or compression shocks. He introduces an approximate equation of state with an exponential term for treating high explosives. He discusses how the thickness of shock waves can be estimated from transport properties.

1925 Jouguet shows that detonation speeds appear to be reasonably well predicted but in some cases there are significant discrepancies, ie, computed velocities for $2H_2 + O_2$ were higher than the measured velocities.

1930 Lewis and Friauf re-examine the CJ model, carry out new experimental measurements and compute wave speeds using the latest thermochemical data. Most importantly, they include the following dissociation reactions for $2H_2 + O_2$ case.

$$2H_2O \rightleftarrows 2H_2 + O_2$$
$$2H_2O \rightleftarrows H_2 + 2OH$$
$$H_2 \rightleftarrows 2H$$
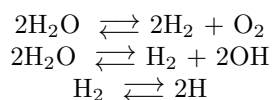
Their formulation of the jump conditions assumes a frozen sound speed and average, but realistic, heat capacity. For case of no dissociation, the solution is obtained by iterating the jump conditions using the temperature at state 2. The method for including dissociation is not described. They recognize the issue of equilibrium vs. frozen sound speeds and make a comparison, finding only 0.4% difference so they use the frozen speed for its simplicity.

Comparing results with and without dissociation, they show that dissociation has a very large effect for $2H_2 + O_2$, $U_{CJ} = 3278$ m/s without dissociation and 2806 m/s with dissociation! Dixon's data was within 1-2% of computations for addition of O_2 or N_2, and within 6% for addition of H_2. Lewis and Friauf examined He and Ar diluted $2H_2 + O_2$ mixtures experimentally, and the comparison was not as good, up to 14% discrepancy. This is attributed to poor accuracy in determining detonation velocity from streak camera records. At this time, the concept of velocity deficit and effect of tube size on detonation velocity was unknown.

1940 Bethe and Teller discuss the effects of vibrational nonequilibrium and chemical reaction on shock waves. They report numerical solution of strong shock waves in air using an iterative technique. This is the first solution of the jump conditions for shock waves to consider chemical reaction and molecular relaxation behind shocks. (See Bethe (1997) for the historical background)

1940 Zel'dovich derives the one-dimensional steady model of detonation structure.

1941 Kistiakowsky and Wilson use a modified version of Becker's equation for computing detonation velocities in high explosives.

1942 von Neumann independently develops the ideal steady detonation structure model.

1943 Döring independently develops the ideal steady detonation structure model.

1942 Bethe develops the theory of shock waves in substances with arbitrary equations of state.

1940-1945 Researchers study underwater explosions at Wood's Hole and in England. They develop experimental and theoretical models of shock waves in water and high explosives. The work is summarized in "Black Books" and Cole (1948).

1947 Brinkley outlines a method for computing the chemical equilibrium of multiple species based on equilibrium constants. This method is formulated as a numerical problem of simultaneous equations in matrix form and solved with the Newton-Raphson method.

1950 Berets et al. compare new experiments with computed of CJ velocities. Computations use a trial and error method similar to that of Lewis & Friauf and Kistiakowsky and Wilson (1941b) (the wartime report) described as "straight forward but laborious" method of successive approximations iterating on temperature. They include more species than Lewis and Friauf but find only a small difference in the computed detonation velocity.

1951 The first National Advisory Committee for Aeronautics (NACA) compiles tables of thermodynamic data valid to 6000 K, which are published by Huff and Gordon. These are the forerunners of the NASA tables that are the basis of most thermodynamic data used today in equilibrium computations.

1953 IBM puts Model 650 on the market. NACA and other groups began to be develop programs to carry out numerical computation of chemical equilibrium.

1954 Cowan and Fickett implement Kistiakowsky and Wilson equation of state for gas species together with chemical equilibrium constraints

$$CO_2 + H_2 \rightleftharpoons CO + H_2O$$
$$H_2O + 1/2\ N_2 \rightleftharpoons H_2 + NO$$
$$2CO \rightleftharpoons CO_2 + C(s)$$
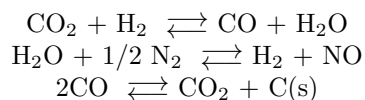
and a solid carbon equation of state. They carry out CJ, overdriven detonation wave, and isentropic expansion computations for TNT, TDX, and HMX mixtures on an IBM 701 at Los Alamos. The minimum velocity method (with a parabolic curve fit similar to the present method) is used to obtain the CJ state.

1957 Fortran released commercially by IBM.

1959 Gordon et al. describe their algorithm and give the machine code for an IBM 650 version of the equilibrium program developed by NASA Lewis.

1960 Zeleznik and Gordon examine several chemical equilibrium computation methods and choose one based on the minimization of Gibbs energy which is substantially more flexible than the older methods based on equilibrium constants. Subsequent methods of chemical equilibrium computation are almost all based on energy minimization algorithms.

1961 Zeleznik and Gordon publish a Newton-Raphson method in T and P with modifications to the pressure jump condition to avoid difficulties with nonphysical values of the density ratio. They discuss how to get a good initial guess and the computation of the derivatives needed for the Jacobian. They also show how derivatives of detonation velocity w.r.t. initial conditions can be used to extrapolate a solution from one set of initial conditions to a slightly different set of initial conditions.

1962 Zeleznik and Gordon publish their theory and Fortran code for NASA Lewis Chemical Equilibrium Code. Gordon and McBride developed this code and implemented it in the CEC71 Fortran IV version (1976), which was widely used, and the thermodynamic database was incorporated into CHEMKIN. The descendant code CEA (Chemical Equilibrium with Applications) is available and in widespread use today. Information about the history, documentation, requests for the code, thermodynamic and transport property databases, and related programs can be found at the NASA CEA website. The most recent versions of the algorithms used in CEA are described in Gordon and McBride (1994) and the program operation in McBride and Gordon (1996).

By the mid 1960s, the development of application software to compute equilibrium in perfect gases has reached a relatively mature state, and subsequent developments focus on refinement and implementation for personal computers. For real gases, solids and liquids – particularly the products of high explosives – further development continues and is currently ongoing. Milestones include TIGER (Cowperthwaite and Zwisler, 1973), its successor CHEETAH (Fried and Howard, 2001), and RUBY developed at Los Alamos (Mader, 1979). Except for RUBY, which is described in Mader's book, the use of this software and the documentation of the algorithms are restricted due to the sensitive nature of the applications to high explosive performance.

1980-1994 Kee et al. develop a gas phase chemical kinetics libraries and application programs at SNL. These are widely distributed and used for gas phase reaction chemistry computations.

1986 Reynolds releases STANJAN which uses a minimization method based on element potentials rather than chemical potentials. The original implementation was written in Fortran and ran as a stand alone PC program with tabulated versions of the JANAF thermodynamic data. Subsequently, STANJAN was modifed by SNL to use the subroutine library of Kee et al. (1980) and the SNL version (Kee et al., 1987) of NASA polynomial fits to the JANAF data.

2001 Goodwin of Caltech develops and releases Cantera, an open source library written in C++ with Python and Matlab interfaces. Cantera contains built-in equilibrium solvers based on a minimization method.

3   Shock and Detonation Waves

We present a brief summary of the shock jump conditions and the standard formulation of the graphical solutions. As discussed in classical texts on gas dynamics, Courant and Friedrichs (1948), Shapiro (1953-54), Liepmann and Roshko (1957), Becker (1968), Thompson (1972), Zel'dovich and Raizer (1966), an ideal shock or detonation wave has no volume and locally can be considered a planar wave if we ignore the structure of the reaction zone.

3.1   Jump Conditions

A wave propagating with speed U into gas at state 1 moving with velocity u_1 is shown in Fig. 1a. This can be transformed into a stationary wave with upstream flow speed w_1 and downstream flow speed w_2, Fig. 1b.

$$w_1 = U_s - u_1 \tag{1}$$
$$w_2 = U_s - u_2 \tag{2}$$

Using a control volume surrounding the wave and any reaction region that we would like to include in our computation, the integral versions of the conservation relations can be used to derive the jump conditions relating properties at the upstream and downstream ends of the control volume. The simplest way to carry
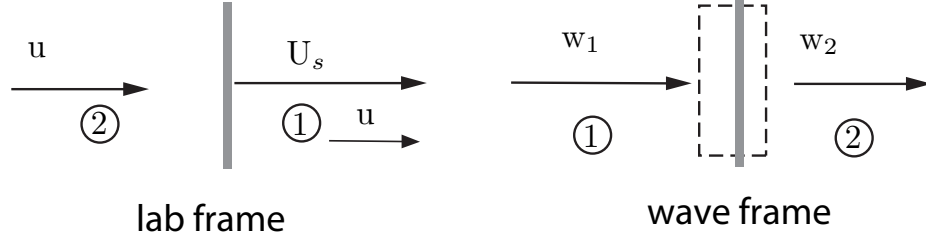
Figure 1: Cartoon depiction of the transformation from the laboratory to the wave fixed reference frame.

out this computation is in a *wave-fixed* coordinate system considering only the velocity components w normal to the wave front. The resulting relationships are the conservation of mass

$$\rho_1 w_1 = \rho_2 w_2 \ , \tag{3}$$

momentum

$$P_1 + \rho_1 w_1^2 = P_2 + \rho_2 w_2^2 \ , \tag{4}$$

and energy

$$h_1 + \frac{w_1^2}{2} = h_2 + \frac{w_2^2}{2} \ . \tag{5}$$

These equations apply equally to moving and stationary waves as well as to oblique waves as long as the appropriate transformations are made to the wave-fixed coordinate system. In addition to the conservation equations (3-5), an entropy condition must also be satisfied.

$$s_2 \geq s_1 \tag{6}$$

For reacting flows in ideal gases, the entropy condition is usually automatically satisfied and no additional constraint on the solution of (3-5) is imposed by this requirement. Considerations about entropy variation as a function of wave speed do enter into the analysis of detonation waves and these are discussed in the subsequent section on detonation analysis.

In general, an equation of state in the form $h = h(P, \rho)$ is required in order to complete the equation set. We will consider the specific case of an ideal gas. The equation of state for this case is given by combining the usual $P(\rho, T)$ relationship with a representation of the enthalpy. The usual $P(\rho, T)$ relationship is

$$P = \rho R T \tag{7}$$

where the gas constant is

$$R = \frac{\mathcal{R}}{\overline{W}} \tag{8}$$

and the average molar mass is

$$\overline{W} = \left(\sum_{i=1}^{K} \frac{Y_i}{W_i} \right)^{-1} \tag{9}$$

11

with the gas compositions specified by the mass fractions Y_i. The enthalpy of an ideal gas can be expressed as

$$h = \sum_{i=1}^{K} Y_i h_i(T) \tag{10}$$

The enthalpy of each species can be expressed as

$$h_i = \Delta_f h_i + \int_{T_\circ}^{T} c_{P,i}(T') \, dT' \tag{11}$$

where $\Delta_f h_i$ is the heat of formation, $c_{P,i}$ is the specific heat capacity, and $T_\circ$ is a reference temperature, usually taken to be 298.15 K. The thermodynamic parameters for each species are specified in the Cantera data input file; the specific heat dependence on temperature is given as a set of polynomial coefficients based on the original NASA format (McBride and Gordon, 1992, McBride et al., 1993). Compilations of this data have been made for many species through the JANAF-NIST project (Chase, 1998) and are available on-line. Coefficients of fits are available from NASA, NIST, BURCAT, and SNL. Cantera provides a utility (`ck2cti`) to convert legacy data sets to its `.cti` file format. The methodology and software for the generation of thermodynamic data and polynomial fits is described in detail in Section E.

Formulation of Jump Conditions in Terms of Density Ratio

An alternate way to look at the jump conditions is to write them as a set of equations for pressure and enthalpy at state 2 in terms of the density ratio ρ_2/ρ_1 and the normal shock speed w_1

$$P_2 = P_1 + \rho_1 w_1^2 \left(1 - \frac{\rho_1}{\rho_2}\right) \tag{12}$$

$$h_2 = h_1 + \frac{1}{2} w_1^2 \left[1 - \left(\frac{\rho_1}{\rho_2}\right)^2\right] \tag{13}$$

The equation of state $h(P,T)$ (10) provides another expression for h_2. This naturally leads to the idea of using functional iteration or implicit solution methods to solve for the downstream state 2. A method based on solving these equations for a given value of w_1 and state 1 is discussed in Section 7.1.

3.2 Chemical Composition

In order to completely determine the state of the gas and solve the jump conditions, we need to know the composition of the gas $(Y_1, Y_2, \ldots, Y_k)$. In the context of jump condition analysis, we only consider two possible cases, either a nonreactive shock wave or complete reaction to an equilibrium state.[3] Although this assumption may seem quite restrictive, these two cases are actually very useful in analyzing many situations. Frozen composition is usually presumed to correspond to the conditions just behind any shock front prior to chemical reaction taking place. Equilibrium composition is usually presumed to occur if the reactions are fast and the reaction zone is thin in comparison with the other lengths of interest in the problem.

The two possibilities for the downstream state 2 are:

1. Nonreactive or frozen composition

$$Y_{2i} = Y_{1i}$$

The frozen composition case assumes that the composition does not change across the shock, which is appropriate for nonreactive flows (moderately strong shocks in inert gases or gas mixtures like air) or the conditions just downstream of a shock that is followed by a reaction zone. In this case, from the equation for enthalpy (10), the state 2 enthalpy will just be a function of temperature

$$h_2 = h(T_2) = \sum_{i=1}^{K} Y_{1i} h_i(T_2) \tag{14}$$

---

[3]The more general problem of finite rate chemical reaction is considered in the companion report Browne et al. (2005) on ZND detonation structure computation.

2. Completely reacted, equilibrium composition.

$$Y_{2i} = Y_i^{eq}(P, T)$$

The case of a completely reacted state 2, the equilibrium mixture is used to treat ideal detonation waves or other reactive waves like bow shocks on re-entry vehicles. In order to determine the equilibrium composition, an iterative technique must be used to solve the system of equations that define chemical equilibrium of a multi-component system. In the present software package, we use the algorithms built into Cantera to determine the equilibrium composition. In this case, the state 2 enthalpy will be a function of both temperature and pressure

$$h_2 = h(T_2, P_2) = \sum_{i=1}^{K} Y_{2i}^{eq}(P_2, T_2) h_i(T_2) \tag{15}$$

3.3 Rayleigh Line and Hugoniot

The jump conditions are often transformed so that they can be represented in P-v thermodynamic coordinates. The *Rayleigh line* is a consequence of combining the mass and momentum conservation relations

$$P_2 = P_1 - \rho_1^2 \mathrm{w}_1^2 (v_2 - v_1) \tag{16}$$

The slope of the Rayleigh line is

$$\frac{P_2 - P_1}{v_2 - v_1} = \frac{\Delta P}{\Delta v} = -\left(\frac{\mathrm{w}_1}{v_1}\right)^2 = -\left(\frac{\mathrm{w}_2}{v_2}\right)^2 \tag{17}$$

where $v = 1/\rho$ and $\Delta P = P_2 - P_1$, etc. The slope of the Rayleigh line is proportional to the square of the shock velocity w_1 for a fixed upstream state 1. The Rayleigh line must pass through both the initial state 1 and final state 2.

If we eliminate the post-shock velocity, energy conservation can be rewritten as a purely thermodynamic relation known as the *Hugoniot* or *shock adiabat*.

$$h_2 - h_1 = (P_2 - P_1)\frac{(v_2 + v_1)}{2} \tag{18}$$

or

$$e_2 - e_1 = \frac{(P_2 + P_1)}{2}(v_1 - v_2) \tag{19}$$

From the previous discussion on chemical composition, we can write the enthalpy as a function of volume and pressure $h_2(v_2, P_2)$ since temperature is related to pressure and volume by

$$v_2 = \frac{R_2 T_2}{P_2} \tag{20}$$

From the definition of internal energy $e = h - Pv$, so $e_2 = e_2(P_2, v_2)$. In principle, this means we can solve either (18) or (19) to obtain the locus of all possible downstream states $P_2(v_2)$ for a fixed upstream state. The result $P(v)$ is referred to as the Hugoniot curve or simply Hugoniot. For a frozen composition or an equilibrium composition in a non-exothermic mixture like air, Fig. 2a, the Hugoniot curve passes through the initial state. For an equilibrium composition in an exothermic mixture like hydrogen-air, Fig. 2b, the chemical energy release displaces the Hugoniot curve from the initial state. The Rayleigh line slope (17) is always negative and dictates that the portion of the Hugoniot curve between the dashed vertical and horizontal lines (Fig. 2b) is nonphysical. The nonphysical region divides the Hugoniot into two branches: the upper branch represents supersonic combustion waves or *detonations*, and the lower branch represents subsonic combustion waves or *deflagrations*. The properties of the detonation and deflagration branches are discussed in more detail in Section 3.5.
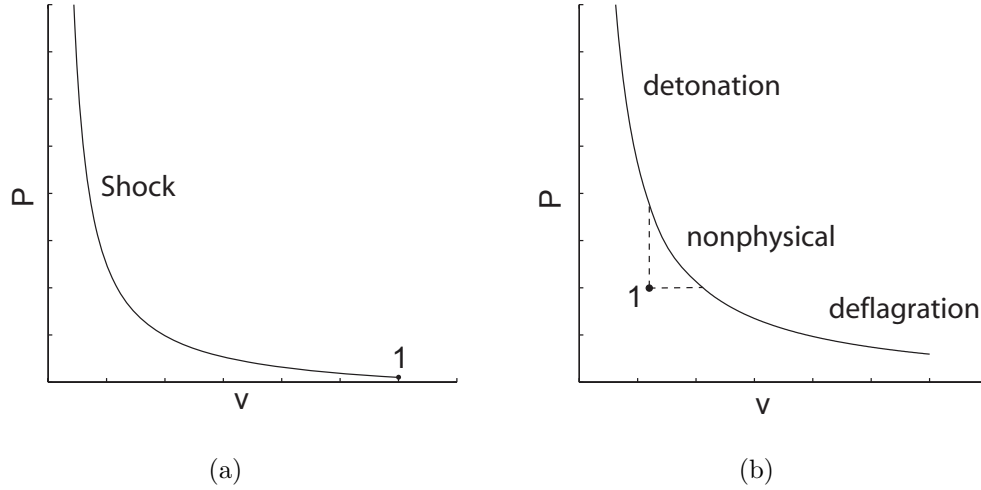
Figure 2: Hugoniots (a) Shock wave propagating in a non-exothermic mixture or a mixture with frozen composition. (b) Shock wave propagating in an exothermic mixture.

The advantage of using the Rayleigh line and Hugoniot formulation is that solutions of the jump conditions for a given shock speed can be graphically interpreted in P-v diagram as the intersection of the Hugoniot and a particular Rayleigh line. This is discussed in the next sections for shock and detonation waves.

See the following examples of Rayleigh and Hugoniot lines:
Matlab Demos:
demo_RH.m, demo_RH_air.m, demo_RH_air_eq.m, demo_RH_air_isentrope.m, and demo_RH_CJ_isentropes.m
Python Demo:
demo_RH.py

3.4   Shock Waves - Frozen and Equilibrium

Examples of the use of the Shock and Detonation Toolbox to find downstream states for shock waves in air are shown in Figure 3. The Rayleigh line and the Hugoniots are shown for two ranges of shock speed. For shock waves less than 1000 m/s[4] (the Rayleigh line shown in Fig. 3a), the frozen and equilibrium Hugoniots are indistinguishable. At these shock speeds, only a very small amount of dissociation occurs behind the shock front so that the composition is effectively frozen. Under these conditions, solutions to the shock jump conditions are only slightly different from the analytical results for constant specific heat ratio (perfect gas approximation) given in Appendix A. Fig. 3a was obtained using the MatLab script `RH_air`.

For shock speeds between 1000 m/s and 3500 m/s, Fig. 3b, the differences between frozen and equilibrium Hugoniot curves becomes increasing apparently with increasing pressure at state 2 corresponding to increasing shock speeds. Fig. 3b was obtained using the MatLab script `RH_air_eq.m`.

3.4.1   Entropy and Sound Speeds

According to (6), the entropy downstream of the shock wave must be greater than or equal to the entropy upstream. For nonreactive flow, this can be verified by computing the isentrope

$$s(P, v, \mathbf{Y}) = \text{constant} \tag{21}$$

---

[4]There is no strict rule about when dissociation begins to be significant and of course, the extent of dissociation changes continuously with shock strength. The choice of 1000 m/s is arbitrary and chosen for convenience for this specific example.
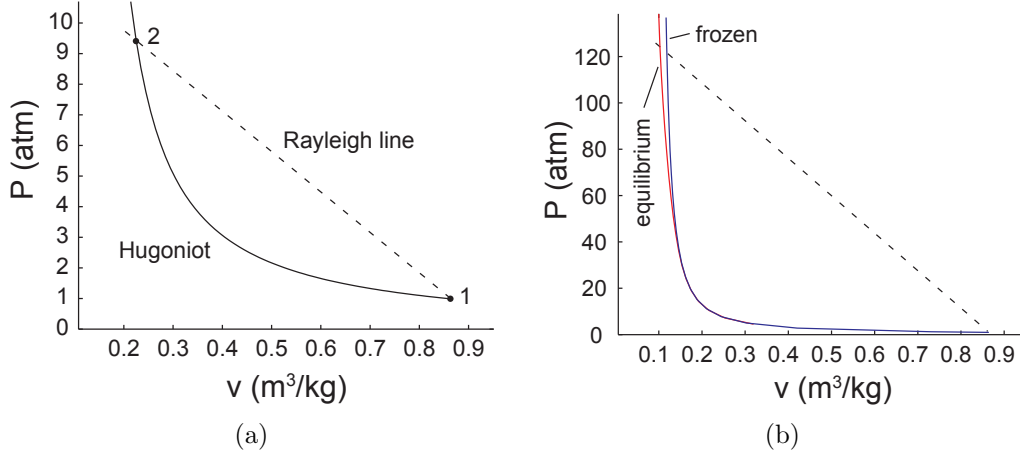
Figure 3: The Rayleigh line and Hugoniot for air with initial pressure of 1 atm and initial temperature of 300 K. `RH_air.m` (a) Frozen composition Hugoniot and Rayleigh line for a shock propagating at 1000 m/s. (b) Comparison of frozen and equilibrium composition Hugoniots and Rayleigh line for a shock propagating at 3500 m/s. `RH_air_eq.m`

with either fixed (frozen) composition $\mathbf{Y}_2 = \mathbf{Y}_1$ or shifting (equilibrium) composition $\mathbf{Y}_2 = \mathbf{Y}^{eq}(P, v)$. The slope of the isentrope can be interpreted in terms of the sound speed a

$$\left.\frac{\partial P}{\partial v}\right|_s = -\left(\frac{a}{v}\right)^2 \tag{22}$$

Both the frozen (see MatLab function `soundspeed_fr`)

$$a_f^2 = -v^2 \left.\frac{\partial P}{\partial v}\right|_{s,\mathbf{Y}} \tag{23}$$

and equilibrium (see MatLab function `soundspeed_eq`)

$$a_e^2 = -v^2 \left.\frac{\partial P}{\partial v}\right|_{s,\mathbf{Y}^{eq}} \tag{24}$$

sound speeds are necessary for reacting flow computations. Frozen sound speeds are always slightly higher than equilibrium sound speeds in chemically reacting mixtures. Acoustic waves in chemically reacting flows are dispersive with the highest frequency waves traveling at the frozen sound speed and the lowest frequency waves traveling at the equilibrium sound speed (Vincenti and Kruger, 1965).

At low temperatures (< 1000 K), there is little dissociation, and the difference between frozen and equilibrium isentropes or sound speeds is negligible. Further, the equilibrium algorithms used in Cantera have difficulty converging when a large number of species have very small mole fractions. This means that at low temperatures, it is often possible and necessary to only compute the frozen isentropes. Examples of the frozen isentropes (see the MatLab script `RH_air_isentrope.m`)

$$P = P(v, s)|_{\mathbf{Y}} \tag{25}$$

are plotted on the P-v plane together with Hugoniot in Fig 4. The entropy for each isentrope is fixed at the value corresponding to the intersection of the isentrope and the Hugoniot. The isentrope labeled s_1 passes through the initial point 1 and the isentrope labeled s_4 passes through the shock state 2. The isentropes entropies are ordered as $s_4 > s_3 > s_2 > s_1$ in agreement with (6). Entropy increases along the Hugoniot.

15
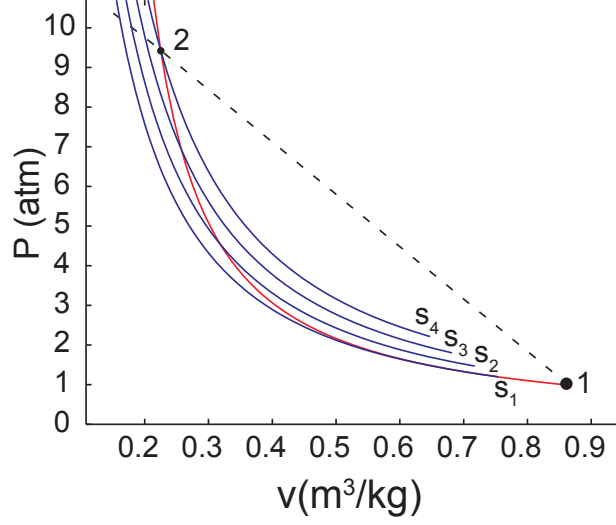
Figure 4: Frozen isentropes, Hugoniot, and a Rayleigh line for a 1000 m/s shock wave in air.
RH_air_isentrope.m

The graphical results for the relationship between Rayleigh lines and the isentropes illustrate a general principle for shock waves: the flow upstream is supersonic, the flow downstream is subsonic. At the initial state 1, the Rayleigh line is steeper than the isentrope

$$\left.\frac{\partial P}{\partial v}\right|_{s,\mathbf{Y}} > \frac{\Delta P}{\Delta v} \tag{26}$$

which from the definition of the slopes of the Rayleigh line (16) and isentrope (23) implies that the flow upstream of the wave is supersonic

$$\mathrm{w}_1 > a_1 \tag{27}$$

At the final state 2, the isentrope is steeper than the Rayleigh line

$$\left.\frac{\partial P}{\partial v}\right|_{s,\mathbf{Y}} < \frac{\Delta P}{\Delta v} \tag{28}$$

which implies that the flow downstream of the shock is subsonic (in the wave-fixed frame)

$$\mathrm{w}_2 < a_2 \tag{29}$$

The isentrope is tangent to the Hugoniot at state 1 and also has the same curvature at this point so that weak shock waves are very close to acoustic waves (Thompson, 1972), with the entropy increasing like the cube of the volume change

$$\delta s \propto \delta v^3 \tag{30}$$

along the Hugoniot near point 1. The isentropes shown in Fig. 4 are frozen isentropes; in general, the correct choice of conditions (frozen vs equilibrium) for evaluating the isentropes depends on the end use.

See the following demos for frozen and equilibrium post shock states:
Matlab: demo_PSfr.m and demo_PSeq.m
Python: demo_PSfr.py and demo_PSeq.py

3.5 Detonation Waves and the Chapman-Jouguet Condition

The Hugoniot for a stoichiometric hydrogen-air mixture and two example Rayleigh lines are shown in Figure 5. The possible solutions to the jump conditions are shown graphically as the intersection points of the Rayleigh lines and Hugoniot. On the upper (U) or detonation branch, the wave speed must be above some minimum value, the upper Chapman-Jouguet (CJ_U) velocity in order for there to be an intersection of the Rayleigh line and the detonation branch of the Hugoniot. On the lower (L) or deflagration branch, the wave speed must be less than some minimum value, the lower Chapman-Jouguet (CJ_L) velocity in order for there to be an intersection of the Rayleigh line and the detonation branch of the Hugoniot. If the perfect gas approximation is used, then it is possible to find analytic solutions (see Appendix B) for the Hugoniot and CJ states. For more general equations of state and realistic thermochemistry, it is necessary to use the numerical methods described in the subsequent sections. The purpose of this section is to present the theoretical background for the CJ state conditions used in those numerical methods.

The minimum pressure point on the detonation branch (CV) corresponds to the final state of a constant volume explosion. The maximum pressure point on the deflagration branch (CP) corresponds to the final state of a constant pressure explosion. Like shock waves, detonation waves are supersonic ($w_1 > a_1$) and a propagating wave will not induce flow upstream but only downstream. However, deflagration waves are subsonic ($w_1 < a_1$) and a propagating wave causes flow both upstream and downstream of the deflagration wave. Examples of deflagration waves in gases are low-speed flames. Since the flow upstream of the flame is subsonic, the flame propagation rate is strongly coupled to the fluid mechanics of the surrounding flow as well as the structure of the flame itself. This makes the deflagration solutions to the jump conditions much less useful than the detonation solutions since flame speeds cannot be determined uniquely by the jump conditions.
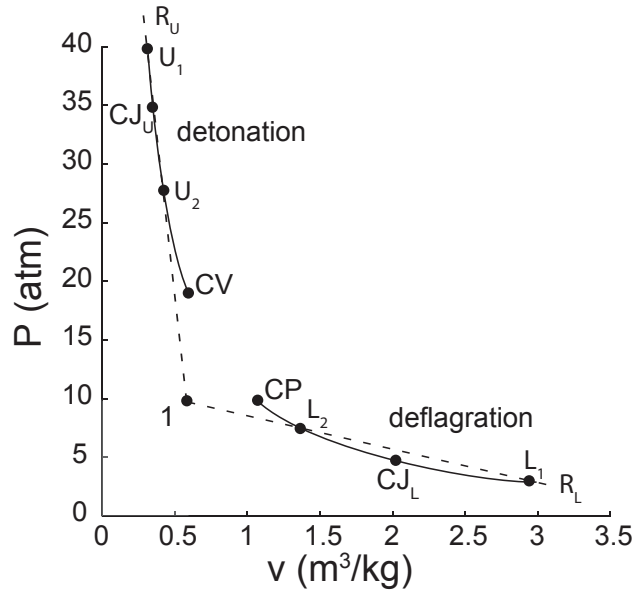
Figure 5: Equilibrium Hugoniot and two Rayleigh lines illustrating detonation and deflagration branches.

In general, there are two solutions (U_1, U_2) possible on the detonation branch for a given wave speed, $\infty > U > U_{CJ_U}$ and two solutions (L_1, L_2) possible on the lower (L) or deflagration branch for for a given wave speed, $0 < U < U_{CJ_L}$. Only one of the two solutions is considered to be physically acceptable. These are the solution (U_1) for the detonation branch and the solution (L_2) for the deflagration branch. According to Jouguet's rule (see Appendix D and Fickett and Davis (1979)), these solutions have subsonic flow behind the wave $w_2 < a_2$ and satisfy the condition of causality, which is that disturbances behind the wave can catch up to the wave and influence its propagation.

As first recognized by Chapman (1899), the geometry (Fig. 6) of the Hugoniot and Rayleigh line impose

restrictions on the possible values of the detonation velocity. Below a minimum wave speed, $w_1 < w_{CJ}$, the Rayleigh line and equilibrium Hugoniot do not intersect and there are no steady solutions. For a wave traveling at the minimum wave speed $w_1 = U_{CJ}$, there is a single intersection with the equilibrium Hugoniot. Above this minimum wave speed $w_1 > U_{CJ}$, the Rayleigh line and equilibrium Hugoniot intersect at two points, usually known as the strong (S) and weak (W) solutions. Based on these observations, Chapman proposed that the measured speed of detonation waves corresponds to that of the minimum wave speed solution, which is unique. A more detailed description for determining the minimum wave speed is given in Appendix C. This leads to the following definition:

Definition I: *The Chapman-Jouguet detonation velocity is the minimum wave speed for which there exists a solution to the jump conditions from reactants to equilibrium products traveling at supersonic velocity.*
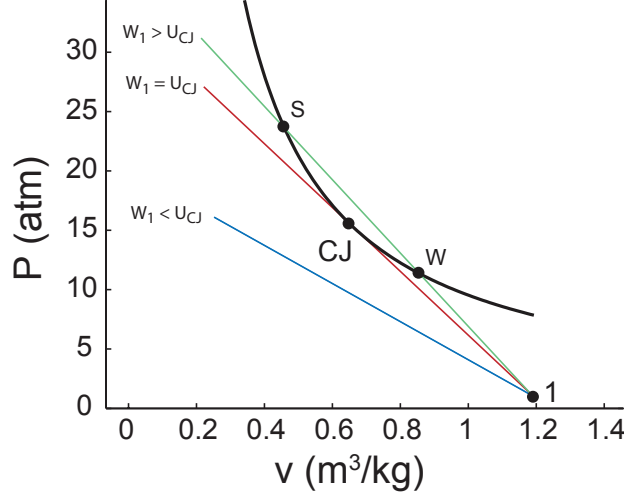
Figure 6: Hugoniot and three representative Rayleigh lines illustrating $w_1 = U_{CJ}$ as the minimum wave speed and tangency of Rayleigh line and Hugoniot at the CJ point.

From the geometry (Fig. 6), it is clear that the minimum wave speed condition occurs when the Rayleigh line is tangent to the Hugoniot. The point of tangency is the solution for the equilibrium downstream state and is referred to as the CJ state, as indicated on Fig. 6. Jouguet (1905) showed that at the CJ point, the entropy is an extreme value and that as a consequence, the isentrope passing through the CJ point is tangent to the Hugoniot and therefore also tangent to the Rayleigh line as indicated in Figure 7 (see the MatLab script RH_CJ_isentropes.m). There are various ways to demonstrate this, e.g. differentiate (19) for a fixed initial state to obtain (dropping the subscript from state 2)

$$de = \frac{1}{2}(\Delta v)dP + \frac{1}{2}(P + P_1)dv \qquad (31)$$

and combine this with the fundamental relation of thermodynamics

$$de = Tds - Pdv \qquad (32)$$

to obtain

$$T\left.\frac{\partial s}{\partial v}\right|_{\mathcal{H}} = -\frac{\Delta v}{2}\left[\left.\frac{\partial P}{\partial v}\right|_{\mathcal{H}} - \frac{\Delta P}{\Delta v}\right] \qquad (33)$$

where $\mathcal{H}$ indicates a derivative evaluated on the Hugoniot. At the point of tangency between Rayleigh line and Hugoniot, the right hand side will vanish so that the entropy is an extremum at the CJ point.

$$\left.\frac{\partial s}{\partial v}\right|_{\mathcal{H},CJ} = 0 \qquad (34)$$

18

This implies that the isentrope passing through the CJ point must be tangent to the Rayleigh line and also the Hugoniot. The nature of the extremum can be determined by either algebraic computation of the curvature of the isentrope or geometric considerations. The entropy variation along the Hugoniot can be determined by inspecting the geometry of the isentropes and the Rayliegh lines. From the slopes shown in Fig. 7, we see that

$$\left.\frac{\partial s}{\partial v}\right|_{\mathcal{H}} < 0 \qquad \text{for} \qquad v < v_{CJ} \tag{35}$$

and

$$\left.\frac{\partial s}{\partial v}\right|_{\mathcal{H}} > 0 \qquad \text{for} \qquad v > v_{CJ} \tag{36}$$

so that the entropy is a local minimum at the CJ point.

$$\left.\frac{\partial^2 s}{\partial v^2}\right|_{\mathcal{H},CJ} > 0 \tag{37}$$

The tangency of the isentrope to the Rayleigh lines at the CJ point

$$\frac{\Delta P}{\Delta v} = -\left(\frac{\mathrm{w}_2}{v_2}\right)^2 = \left.\frac{\partial P}{\partial v}\right|_s = -\left(\frac{a_2}{v_2}\right)^2 \tag{38}$$

implies that

$$\mathrm{w}_2 = a_2 \qquad \text{at the CJ point.} \tag{39}$$

We conclude that at the CJ point, the flow in the products is moving at the speed of sound (termed *sonic* flow) relative to the wave. This leads to the alternative formulation (due to Jouguet) of the definition of the CJ condition.

Definition II: *The Chapman-Jouguet detonation velocity occurs when the flow in the products is sonic relative to the wave. This is equivalent to the tangency of the Rayleigh line, Hugoniot, and equilibrium isentrope at the CJ point.*

The equilibrium isentrope and equilibrium sound speed appear in this formulation because the problem has been approached in a purely thermodynamic fashion with no consideration of time-dependence or detonation structure. In early studies, there was some controversy (see the discussion in Wood and Kirkwood (1959)) about the proper choice of sound speed, equilibrium vs. frozen. However, after careful examination of the equations of time-dependent reacting flow, see papers in Kirkwood (1967) and discussion in Fickett and Davis (1979), it became clear that a truly steady solution to the full reacting flow equations does not exist for most realistic models of reaction that include reversible steps. As a consequence, it is not possible to formulate a truly steady theory of detonation. A consistent thermodynamic theory will use the equilibrium sound speed to define the CJ point and this is what is used in our computations.

See the Following Examples - Matlab: demo_CJ.m Python: demo_CJ.py

3.5.1 Physical Meaning of the CJ condition

The following heuristic argument is due to Jouguet (1905) and a mathematical version was first presented by Brinkley and Kirkwood (1949): Consider a detonation wave traveling faster than the CJ velocity such that the state behind the wave is the upper intersection (S – the strong solution) and the flow behind the wave is subsonic relative to the wave front. In this situation, perturbations from behind the detonation wave can propagate through the flow and interact with the leading shock. In particular, if the perturbations are expansion waves, these perturbations will eventually slow the lead shock to the CJ speed. Once the detonation is propagating at the CJ speed, the flow behind becomes sonic and acoustic perturbations can
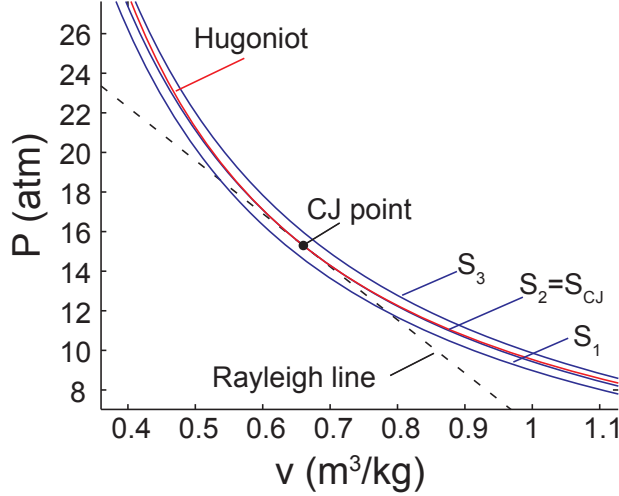
Figure 7: Hugoniot, Rayleigh line, and three representative isentropes (equilibrium) illustrating the tangency conditions at the CJ point. `RH_CJ_isentropes.m`

no longer affect the wave. Thus the CJ condition corresponds a self-sustained wave that is isolated from disturbances from the rear and can propagate indefinitely at the CJ speed. This is why detonation waves that have propagated over sufficiently long distances in tubes are observed to be close to the CJ velocity.

A similar argument cannot be made for the lower (W) or weak solution which has supersonic flow behind the wave relative to the wave front. From a theoretical viewpoint, for steady, planar wave the weak solution is only accessible under very special circumstances that require a specific form of the reaction rate (see Chap. 5 of Fickett and Davis, 1979).

From an experimental viewpoint, the equilibrium CJ model gives reasonable values (within 1-2%) for detonation velocity under ideal conditions of initiation and confinement. However, this does not mean that the actual thermodynamic state corresponds to the CJ point (see Chap. 3 of Fickett and Davis, 1979) since the tangency conditions mean that the thermodynamic state is extremely sensitive to small variations in wave speed. Further, detonations in gases are unstable which leads to a three-dimensional front structure that cannot be eliminated in experimental measurements (see Chap. 7 of Fickett and Davis, 1979).

3.6   Reflected Waves

Assuming a known incident wave speed and upstream state, we can find the gas properties resulting from wave reflection at normal incidence on a rigid surface. We apply the normal shock jump conditions (Section 3.1) across both the incident and reflected waves to find the analog of the Rayleigh and Hugoniot equations. We use a frame of reference where the initial velocity of the reflecting surface has zero velocity. The upstream (1), post-incident-shock region (2), and post-reflected-shock region (3) are as shown in Fig. 8.

Using the velocities in the wave fixed frame relative to the reflected shock for states 2 and 3 as shown in Fig. 8, we obtain the following wave-frame velocities for the reflected wave

$$w_2 = U_R + u_2 \tag{40}$$

$$w_3 = U_R \tag{41}$$
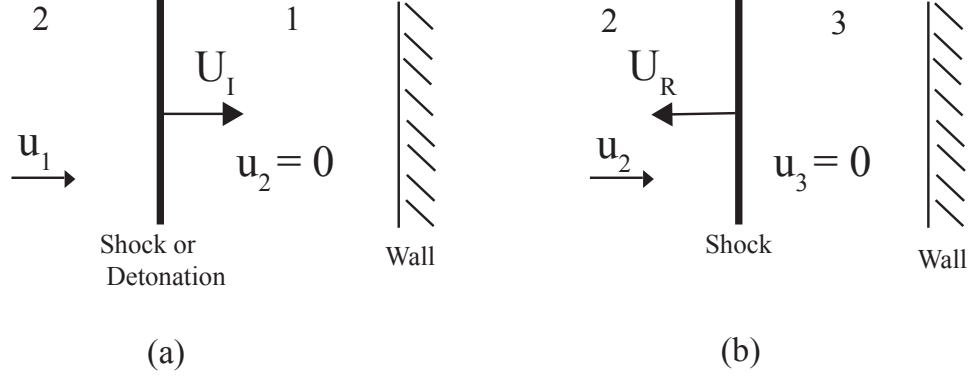
Figure 8: Diagrams showing the incident shock or detonation wave before (a) and after (b) reflection with a wall. States 1, 2, and 3 are shown.

Substituting these into the usual shock jump conditions yields the following relationships across the reflected shock

$$(U_R + u_2)\rho_2 = U_R\,\rho_3 \tag{42}$$

$$P_2 + \rho_2(U_R + u_2)^2 = P_3 + \rho_3 U_R^2 \tag{43}$$

$$h_2 + \frac{1}{2}(U_R + u_2)^2 = h_3 + \frac{1}{2}U_R^2 \tag{44}$$

$$h_3 = h_3(P_3, \rho_3) \tag{45}$$

We combine these relationships in a manner similar to that used for incident shock waves to obtain equations for the shock speed

$$U_R = \frac{u_2}{\dfrac{\rho_3}{\rho_2} - 1}, \tag{46}$$

the pressure P_3 behind reflected shock

$$P_3 = P_2 + \frac{\rho_3 u_2^2}{\dfrac{\rho_3}{\rho_2} - 1}, \tag{47}$$

and the enthalpy h_3 behind reflected shock

$$h_3 = h_2 + \frac{u_2^2}{2}\frac{\dfrac{\rho_3}{\rho_2} + 1}{\dfrac{\rho_3}{\rho_2} - 1}. \tag{48}$$

For substances with realistic equations of state, these equations must be solved using an iterative numerical procedure. The numerical solution methods for reflected shock waves can be taken directly from those used for incident shock waves, which are described in subsequent sections. The post-incident-shock state (2) must be determined before the post-reflected-shock state (3) is found. If the perfect gas approximation is used, then it is possible to find analytic solutions (see Appendix A.2) for the conditions in the reflected region for a specified incident shock wave speed and initial state.

For the detonation wave case, the same procedure is repeated, but instead of an incident shock wave, the incident wave is a detonation and therefore reactive. The post-reflected-shock thermodynamic state (3) can

either be considered in chemical equilibrium or frozen. Experimental, numerical, and approximate analytical solution methods for reflected detonations are compared in Shepherd et al. (1991).

See the following examples for equilibrium and frozen reflected post-shock states:
Matlab: demo_reflected_eq.m and demo_reflected_fr.m Python: demo_reflected_eq.py and demo_reflected_fr.py

4   Relationship of Ideal Model parameters to Real Gas Properties

The two-γ model (Section B) contains six parameters (R_1, γ_1, R_2, γ_2, q, U_{CJ} or M_{CJ}) that have to be determined from computations with a realistic thermochemical model and chemical equilibrium in the combustion products. This can be done with the programs described in the previous sections of this document.

The parameters are computed as follows:

$$R_1 = \frac{\mathcal{R}}{W_1} \tag{49}$$

The universal gas constant (SI units) is

$$\mathcal{R} = 8314. \text{ J} \cdot \text{kmol}^{-1} \cdot \text{K}^{-1} \tag{50}$$

The mean molar mass is computed from the composition of the gas and the mixture formula

$$W = \sum_{i-1}^{K} X_i W_i \tag{51}$$

where X_i is the mole fraction of species i and W_i is the molar mass of species i. The value of γ for the reactants can be interpreted as the ratio of the specific heats

$$\gamma_1 = \frac{C_{p,1}}{C_{v,1}} \tag{52}$$

This is identical to the logarithmic slope of the *frozen* isentrope

$$\gamma_{fr} = -\frac{v}{P} \left. \frac{\partial P}{\partial v} \right)_{s,fr} = \frac{a_{fr}^2}{Pv} \tag{53}$$

where the subscript fr indicates that the composition is held fixed or frozen. In order to compute the downstream state 2, we need to first find the CJ velocity which requires using software like the minimum velocity CJ algorithm implemented in Python or Matlab.

Once the CJ conditions have been computed, the CJ state must be evaluated. This can be done using the jump condition solution algorithm implemented in Python or Matlab. The CJ state includes the mean molar mass W_2 and the value of the parameter γ_2 can be obtained from the logarithmic slope of the *equilibrium* isentrope.

$$\gamma_{eq} = -\frac{v}{P} \left. \frac{\partial P}{\partial v} \right)_{s,eq} \tag{54}$$

where the subscript eq implies that the derivative is carried out with shifting composition to maintain equilibrium. The value of the equilibrium sound speed can be used to find the numerical value of γ_{eq}.

$$\gamma_{eq} = \frac{a_{eq}^2}{Pv} \tag{55}$$

$$\tag{56}$$

Once these parameters have been defined, the value of the parameter q can be obtained by solving the two-γ relationships (194), (195), and (196) to eliminate pressure, volume and temperature.

$$q = a_1^2 \left[\frac{(1 + \gamma_1 M_1^2)^2}{2(\gamma_2^2 - 1)} \left(\frac{\gamma_2}{\gamma_1} \right)^2 \frac{1}{M_1^2} - \frac{1}{\gamma_1 - 1} - \frac{M_1^2}{2} \right] \tag{57}$$

If the one-γ model is used, then this expression simplifies to

$$q = \frac{a_1^2}{2(\gamma^2 - 1)} \left(M_{CJ} - \frac{1}{M_{CJ}} \right)^2 \tag{58}$$

4.1 Example: Ethylene-Oxygen Detonation

A stoichiometric mixture of ethylene and oxygen has the composition

$$C_2H_4 + 3O_2$$
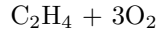
so that $X_{C2H4} = 0.25$ and $X_{O2} = 0.75$. The results of using the Cantera program CJstate_isentrope to compute the CJ velocity and state for initial conditions of 295 K and 1 bar are:

```
Initial pressure 100000 (Pa)
Initial temperature 295 (K)
Initial density 1.2645 (kg/m3)
a1 (frozen) 325.7368 (m/s)
gamma1 (frozen) 1.3417 (m/s)

Computing CJ state and isentrope for C2H4:1 O2:3.01 using gri30_highT.cti
CJ speed 2372.1595 (m/s)
CJ pressure 3369478.0035 (Pa)
CJ temperature 3932.4868 (K)
CJ density 2.3394 (kg/m3)
CJ entropy 11700.9779 (J/kg-K)
w2 (wave frame) 1282.1785 (m/s)
u2 (lab frame) 1089.9809 (m/s)
a2 (frozen) 1334.5233 (m/s)
a2 (equilibrium) 1280.6792 (m/s)
gamma2 (frozen) 1.2365 (m/s)
gamma2 (equilibrium) 1.1388 (m/s)
```

From the program output and gas objects computed by Cantera, we find the following parameters in Table 1

Table 1: Parameters for CJ detonation in stoichiometric ethylene-oxygen computed by the Shock and Detonation Toolbox.

W_1	(kg/kmol)	31.0
a_1	(m/s)	325.7
γ_1		1.342
W_2	(kg/kmol)	23.45
a_2	(m/s)	1280.
γ_2		1.139
U_{cJ}	(m/s)	2372.
M_{CJ}		7.28
q	(MJ/kg)	9.519

5 Detonations in Tubes

The Chapman-Jouguet (CJ) model of an ideal detonation can be combined with the Taylor-Zeldovich (TZ) similarity solution (Taylor, 1950, Zel'dovich and Kompaneets, 1960) to obtain an analytic solution to the flow field behind a steadily-propagating detonation in a tube. The most common situation in laboratory experiments is that the detonation wave starts at the closed end of the tube and the gas in the tube is initially stationary, with flow velocity $u_1 = 0$. This solution can be constructed piecewise by considering the four regions shown on Figure 9; the stationary reactants ahead of the detonation mixture (state 1); the detonation wave between states 1 and 2; the expansion wave behind the detonation (between states 2 and 3); and the stationary products next to the closed end of the tube, state 3.
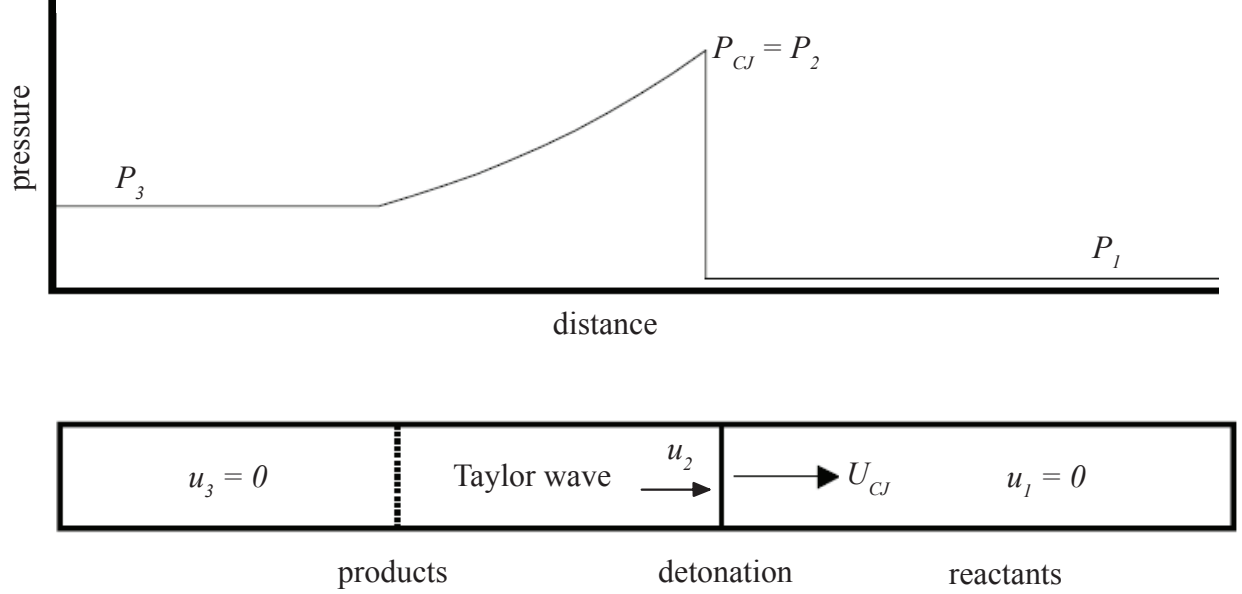
Figure 9: Detonation propagation in tube with a closed end.

In this model, the detonation travels down the tube at a constant speed U, equal to the Chapman-Jouguet velocity U_{CJ}. The corresponding peak pressure, P_2, is the Chapman-Jouguet pressure P_{CJ}. The structure of the reaction zone and the associated property variations such as the Von Neumann pressure spike are neglected in this model. The detonation wave instantaneously accelerates the flow and sets it into motion $u_2 > 0$, then the expansion wave gradually brings the flow back to rest, $u_3 = 0$. As an ideal detonation wave propagates through the tube, the expansion wave increases in width proportionally so that the flow always appears as shown in Fig. 9 with just a change in the scale of the coordinates. This is true only if we neglect non-ideal processes like friction and heat transfer that occur within the expansion wave. If the tube is sufficiently slender (length/diameter ratio sufficiently large), friction and heat transfer will limit the growth of the expansion wave.

5.1 Taylor-Zeldovich Expansion Wave

The properties within the expansion wave can be calculated by assuming a similarity solution with all properties a function $f(x/Ut)$. For a planar flow, the simplest method of finding explicit solutions is with

the method of characteristics . There are two sets of characteristics, C^+ and C^- defined by

$$C^+ \qquad \frac{dx}{dt} = u + a \tag{59}$$

$$C^- \qquad \frac{dx}{dt} = u - a \tag{60}$$

$$\tag{61}$$

On the characteristics the Riemann invariants $J^\pm$ are defined and are constants in the smooth portions of the flow. In an ideal gas, the invariants are:

$$\text{on} \qquad C^+ \qquad J^+ = u + F \tag{62}$$

$$\text{on} \qquad C^- \qquad J^+ = u - F \tag{63}$$

$$\tag{64}$$

The Riemann function F is defined as

$$F = \int_{P_\circ}^{P} \frac{dP'}{\rho a} \tag{65}$$

where $P_\circ$ is a reference pressure and the integrand is computed along the isentrope $s_\circ$ passing through states 2 and 3. For an ideal gas, the integral can carried out and the indefinite integral is equal to

$$F = \frac{2a}{\gamma - 1} \tag{66}$$

In this section, the value of γ is everywhere taken to be the equilibrium value in the detonation products.

The solution proceeds by recognizing that within the expansion fan, $a_3 \geq x/t \geq U_{CJ}$, the C^+ characteristics are simply rays emanating from the origin of the x-t coordinate system and between the end of the expansion fan and the wall, $0 \geq x/t \geq a_3$, the characteristics are straight lines.

$$\frac{dx}{dt} = u + a = \frac{x}{t} \qquad \text{for} \qquad a_3 < \frac{x}{t} < U_{CJ} \tag{67}$$

$$\frac{dx}{dt} = a_3 \qquad \text{for} \qquad 0 < \frac{x}{t} < a_3 \ .$$

The characteristics C^- span the region between the detonation and the stationary gas and on these characteristics the Riemann invariant is constant. Evaluating the value at states 2 and 3 yields the value of the sound speed in region 3 given the state 2, the CJ condition.

$$J^- = u - \frac{2}{\gamma - 1}a = -\frac{2}{\gamma - 1}a_3 = u_2 - \frac{2}{\gamma - 1}a_2 \ . \tag{68}$$

From the CJ condition we have

$$u_2 = U_{CJ} - a_{CJ} \ . \tag{69}$$

and the sound speed in region 3 is

$$a_3 = \frac{\gamma + 1}{2}a_{CJ} - \frac{\gamma - 1}{2}U_{CJ} \ . \tag{70}$$

The variation of properties within the expansion wave can be determined using the similarity properties of the C^+ characteristics and the relationship between velocity and sound speed on the C^- characteristics:

$$\frac{a}{a_3} = 1 - \frac{\gamma - 1}{\gamma + 1}\left(1 - \frac{x}{a_3 t}\right) \tag{71}$$

The other properties within the expansion fan can be found using the fact that the flow is isentropic in this region.

$$\frac{a}{a_3} = \left(\frac{T}{T_3}\right)^{\frac{1}{2}} \quad ; \quad \frac{P}{P_3} = \left(\frac{\rho}{\rho_3}\right)^{\gamma} \quad ; \quad \frac{T}{T_3} = \left(\frac{\rho}{\rho_3}\right)^{\gamma - 1} \tag{72}$$

25

where T is the temperature, ρ is the density and P is the pressure. The subscript $_3$ refers to the conditions at the end of the expansion wave. The pressure P_3 is calculated from

$$P_3 = P_{CJ} \left(\frac{a_3}{a_{CJ}} \right)^{\frac{2\gamma}{\gamma-1}} \quad . \tag{73}$$

This finally gives for the pressure in the expansion wave

$$P = P_3 \left(1 - \left(\frac{\gamma-1}{\gamma+1} \right) \left[1 - \frac{x}{c_3 t} \right] \right)^{\frac{2\gamma}{\gamma-1}} \quad . \tag{74}$$

5.1.1 Determining Realistic TZ parameters

The states on the product isentrope need to be determined numerically, starting at the CJ point and extending to state 3. This is carried out in the program CJstate_isentrope to numerically determine the value of thermodynamic properties such as density, sound speed, and temperature

$$\rho = \rho(P, s = s_{CJ}) \tag{75}$$
$$a = a(P, s = s_{CJ}) \tag{76}$$
$$T = T(P, s = s_{CJ}) \tag{77}$$

and also velocity in the TZ wave

$$u = u_2 + \int_{P_{CJ}}^{P} \frac{dP'}{(\rho a)_{s=s_{CJ}}} \tag{78}$$

parametrically as a function of pressure. The state 3 can be found by numerically solving the integral equation

$$u_2 = \int_{P_{CJ}}^{P_3} \frac{dP}{(\rho a)_{s=s_{CJ}}} \tag{79}$$

obtained by equating the Riemann invariant on the characteristic connecting states 2 and 3. In the program, the integral is carried out by using the trapezoidal rule with on the order of 100-200 increments on the isentrope. Interpolation is used to find state 3.

For the stoichiometric mixture of ethylene and oxygen discussed previously, the computation of state 3 using the Shock and Detonation Toolbox gives the following values.

```
Generating points on isentrope and computing Taylor wave velocity
State 3 pressure 1225686.0898 (Pa)
State 3 temperature 3608.3006 (K)
State 3 volume 1.0434 (m3/kg)
State 3 sound speed (frozen) 1253.7408 (m/s)
State 3 sound speed (equilibrium) 1201.0748 (m/s)
State 3 gamma frozen) 1.2291 (m/s)
State 3 gamma (equilibrium) 1.128 (m/s)
```

We note that there is a small change in γ_2 with the change in pressure on the isentrope and the pressure at state 3 is approximately $0.36 P_{CJ}$.

5.2 Approximating the TZ Wave

The property variations within the ideal detonation wave are now completely specified. For example, the exact solution for the pressure profile is

$$P(x,t) = \begin{cases} P_1 & U_{CJ} < x/t < \infty \\ P_3 \left(1 - \left(\frac{\gamma-1}{\gamma+1} \right) \left[1 - \frac{x}{a_3 t} \right] \right)^{\frac{2\gamma}{\gamma-1}} & a_3 < x/t < U_{CJ} \\ P_3 & 0 < x/t < a_3 \end{cases} \tag{80}$$

26

In analytical studies, it is useful to approximate the dependence of the pressure within the expansion wave with a simpler function. Experimenting with several functional forms (Beltman and Shepherd, 2002) shows that an exponential can be used to represent this variation. At a fixed point in space, the variation of pressure with time can be represented by

$$P(x,t) = \begin{cases} P_1 & 0 < t < t_{CJ} \\ (P_2 - P_3)\exp\left(-(t - t_{CJ})/T\right) + P_3 & t_{CJ} < t < \infty \end{cases} \tag{81}$$

Where $t_{CJ} = x/U_{CJ}$ is the time it takes for a detonation to travel from the origin to the measurement location x. The time constant T can be determined by fitting the exponential relationship to the exact expression. The exact expression for pressure in the expansion wave can be rewritten as

$$P(x,t) = P_3 \left[1 - \frac{\gamma - 1}{\gamma + 1}\left(\frac{U_{CJ}/c_3 - 1 - \tau/t_{CJ}}{1 + \tau/t_{CJ}}\right) \right]^{\frac{2\gamma}{\gamma - 1}} \tag{82}$$

where $\tau = t$ - t_{CJ}. By inspection of the argument in the exact expression, we see that the time constant should have the form

$$T = \alpha_T t_{CJ} \tag{83}$$

The constant α_T is a function of the ratio of specific heats γ and the parameter U_{CJ}/a_3. Computations of these parameters using the one-γ model shows that $1.9 < a_3/U_{CJ} < 2$ for a wide range of values of γ and detonation Mach numbers $5 < M_{CJ} < 10$. Fitting the exponential function to the pressure variation in the expansion wave for this range of parameters yields a $0.31 < \alpha_T < 0.34$. A useful approximation is

$$T \approx \frac{t_{CJ}}{3} \tag{84}$$

In actual practice, if we are trying to represent the variation of pressure over a limited portion of a detonation tube, it is sufficient to take T to be a constant and this can be evaluated at some intermediate location within the portion of the tube that is of interest. For example, the middle of the center section of the Caltech 280-mm diameter detonation tube is about 4 m from the initiator. A detonation traveling 1500 m/s takes approximately 2.7 ms to reach this point and the characteristic decay time $T \approx 0.9$ ms.

5.2.1 Comparison of Two-Gamma and Real gas models

For the stoichiometric ethylene-oxygen example discussed in the text, the two-γ and real gas results are compared in detail in Table 2.

Table 2: Comparison of real gas and two-γ results for a CJ detonation in stoichiometric ethylene-oxygen.

Parameter	SD Toolbox Value	2-γ Model
M_{CJ}	7.282	7.287
P_2/P_1	33.69	33.78
ρ_2/ρ_1	1.850	1.852
T_2/T_1	13.33	13.80
a_3 (m/s)	1201.1	1206.2
P_3 (MPa)	1.225	1.242
T_3 (K)	3608.3	3603.0
ρ_3	0.9584	0.9726

6 Miscellaneous Applications

The functions in the toolbox can be combined and used together with other Cantera functions to solve a number of problems in shock and detonation physics. The following applications are written in MATLAB for Windows but can readily be adapted to Python.

6.1 Isentropic Expansion Following Shock Wave

The interaction of shock waves with material interfaces can generate a reflected expansion wave (Meyers, 1994, Glass and Sislian, 1994). In order to calculate the strength of this wave, it is necessary to find the states on the isentrope passing through the post-shock state and values of the Riemann function. The program shock_state_isentrope computes the shock state for a specified shock speed and calculates states on the isentrope. The output is a file shock_isentrope.plt containing the v, T, P, a_{eq}, u evaluated at fixed intervals on the isentrope. The example is for a shock wave in air with a speed of 1633 m/s. The initial conditions are:

```
# Shock State Isentrope
# Calculation run on 29-Jan-2008 05:47:49
# Initial conditions
# Shock speed  (m/s) 1633.0
# Temperature (K) 295.0
# Pressure (Pa) 100000.0
# Density (kg/m^3) 1.1763e+000
# Initial species mole fractions: N2:3.76 O2:1.0
# Reaction mechanism: gri30_highT.cti
```

and the results are shown in Fig. 10.
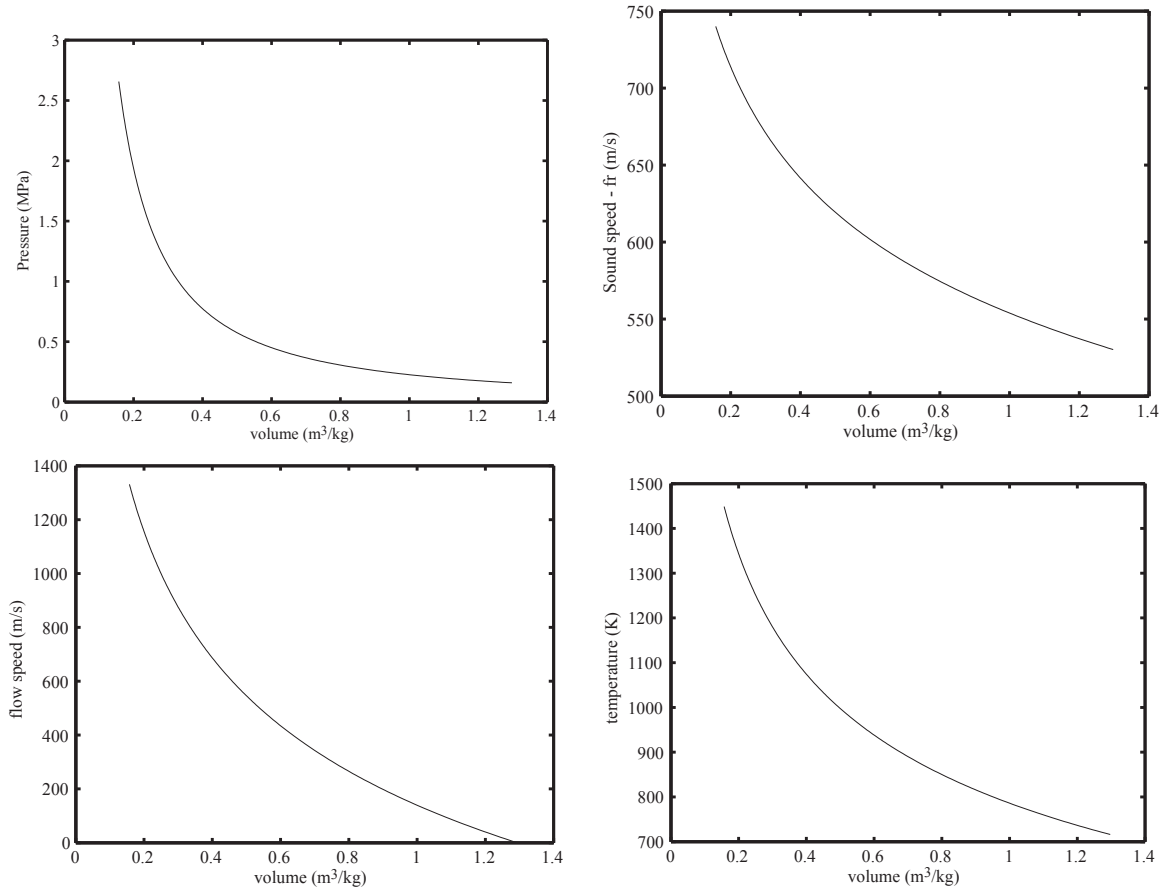
Figure 10: Property variation on an isentrope (frozen) passing through the postshock state of a 1633 m/s shock wave in air.

28

6.2 Reflection of overdriven detonation waves

Detonation waves emerging from a deflagration-to-detonation transition event (Ciccarelli and Dorofeev, 2008, OECD, 2000) are often observed to have a velocity in excess of the Chapman-Jouguet speed for that mixture, $U > U_{CJ}$. Such waves are referred to as overdriven and the peak pressure produced by wave reflection from a closed end is of interest in estimating structural loads. The estimation of peak pressure behind both incident and reflected waves is straightforward using the programs described in Section 3.4 and 3.6. An example program in MATLAB is given in overdriven which computes the states behind incident and reflected waves in H_2-N_2O mixtures as a function of wave speed and prints a summary output file. A plot of the incident and reflected pressures from the output file is shown in Fig. 11. The ratio of reflected-to-incident pressure (Fig. 12) varies from about 2.4 for the CJ detonation up to 6.5 for a highly overdriven wave. The increase in pressure ratio with wave speed is shows that as the wave speed increases, the combustion energy release becomes less important than the kinetic energy in the flow
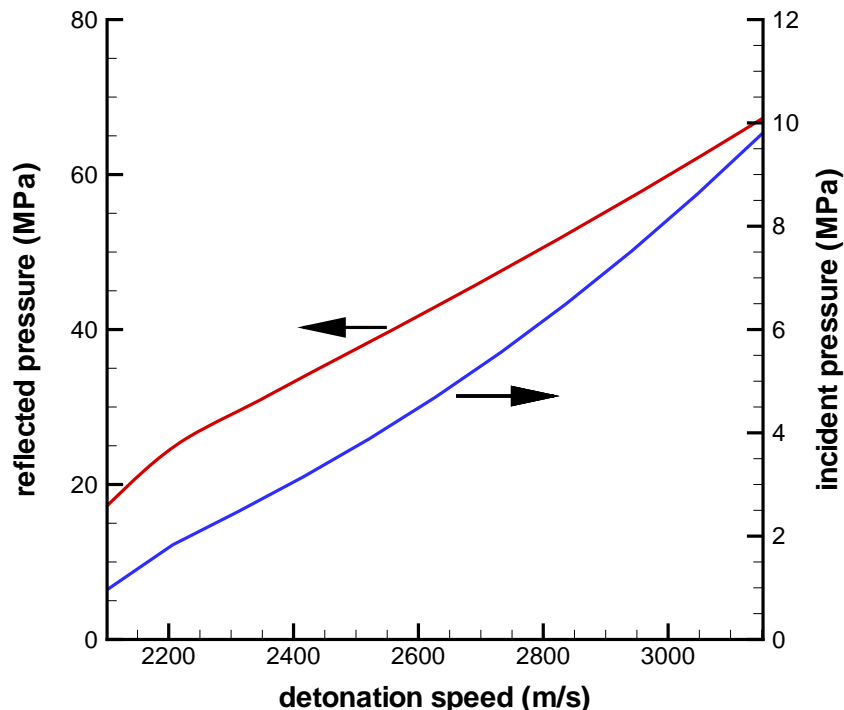
Figure 11: Incident and reflected pressures for a detonation in H_2-N_2O (31% H_2, 1 bar , 300 K) mixtures.

6.3 Detonation in a compressed gas region and subsequent reflection

Detonation in a closed vessel or pipe can occur after a deflagration (flame) is ignited, then accelerates to high speed and transitions to detonation near the vessel surface or the closed end of the pipe (Shepherd, 1992). The initial deflagration propagates quite slowly and results in the compression of the unburned gas ahead of the wave as the pressure increases inside the vessel. As a consequence, the detonation occurs in compressed gas region which has higher pressure and temperature than the initial gas within the vessel. In addition, the detonation may emerge from the transition region with a much higher velocity and pressure than the CJ values. The results in much higher detonation pressures and pressures behind the reflected shock wave that is created when the detonation reaches the vessel wall or pipe end. The MATLAB script precompression_detonation. computes the conditions behind a CJ detonation wave and associated reflected shocks in an isentropically compressed gas for a range of compression ratios. The pressures behind overdriven
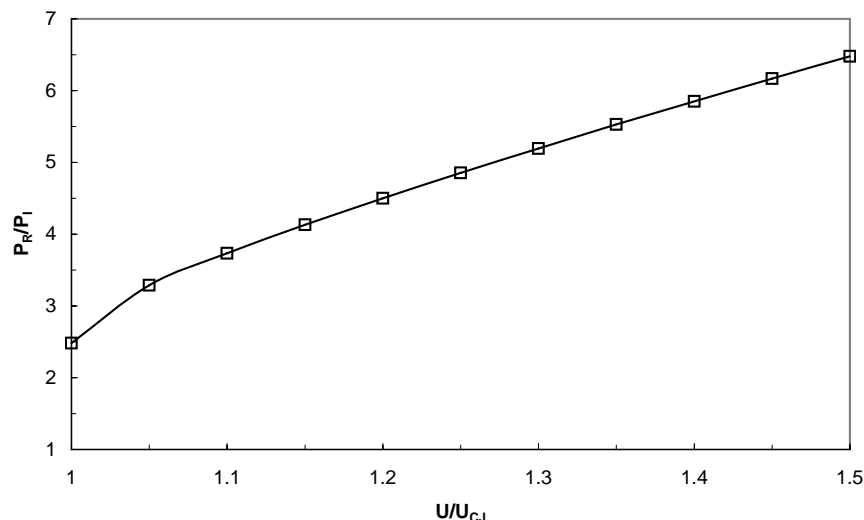
Figure 12: Ratio of reflected-to-incident pressures for data in Fig. 11.

detonation waves and associated reflected shocks is then computed for each isentropic compression condition. The results are given in an output file.

6.4 Pressure-velocity relationship behind a detonation

Interaction of a detonation wave or a shock with a contact surface will result in reflected and transmitted waves (Meyers, 1994, Glass and Sislian, 1994). The computation of these wave amplitudes (for a one-dimensional interaction) requires matching pressure and velocity at the contact surface. This requires computing the locus of shock and expansion wave states "centered" on the state behind the incident detonation wave or shock. This can be carried out by combining the methods that have been previously developed to compute the conditions behind the incident shock and then the subsequent shock or expansion moving into that state. A MATLAB script detonation_pu. computes the conditions behind a CJ detonation wave and the pressure-velocity relationship for a shock wave moving back into the detonation products. The output from the script is in a file that can be used to construct a pressure-velocity diagram. An example for a detonation in H_2-N_2O is shown in Fig. 13a. The case of a shock wave is appropriate for a reflection from "hard" material, that is, one that has a higher acoustic impedance than the material in the post-shock or post-detonation state. The solution to the interface matching condition requires constructing the pressure-velocity relationship for the "hard" material and finding the intersection. An example for a detonation wave incident on water is shown in Fig. 13b. Water is quite stiff and dense in comparison to the detonation products so that the interface pressure is very close to that found for rigid reflection ($u = 0$) and only a small velocity (4 m/s) is induced.

6.5 Ideal Rocket motor performance

The performance of an ideal rocket motor can be described by the quasi-one dimensional steady flow relationships. In general, accurate estimates of performance require consideration of the kinetics of the reactions in the gases in order to predict the extent of recombination and exhaust velocity at the exit of the nozzle. In realistic engineering design we need to also consider two- and three-dimensional flow, boundary layers, heat transfer, and most importantly, off-design operation with shock waves inside the nozzle that result in flow separation and recirculation. These effects are all outside the scope of quasi-one dimensional flow and the present discussion is only considered with ideal nozzle performance, which can be bounded by considering the simple limiting cases of either *frozen* or *equilibrium* isentropic expansion within an inviscid stream tube of specified area.
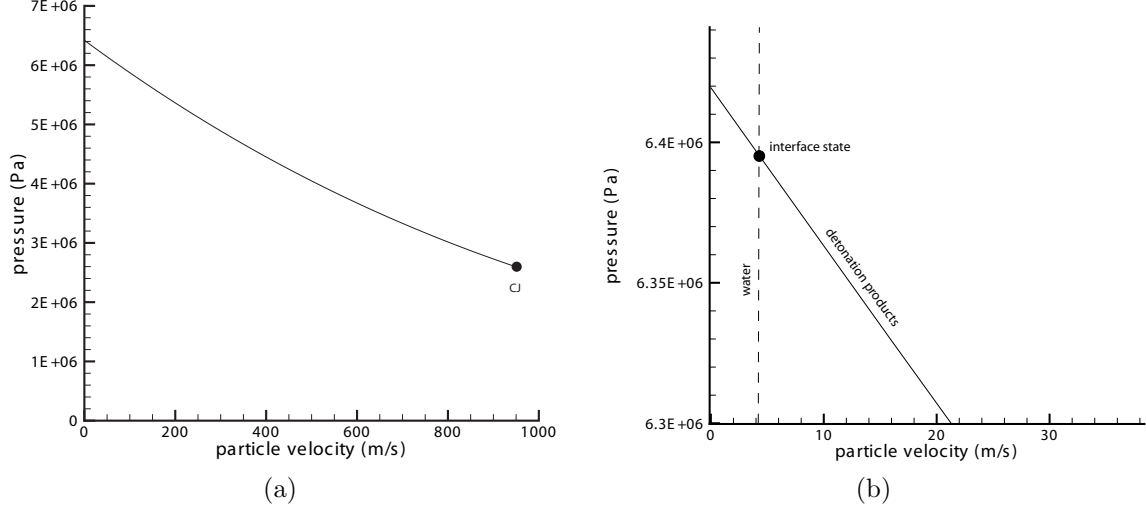
Figure 13: a) CJ state and pressure velocity-relationship on reflected shock wave for H_2-N_2O mixtures initially at 300 K and 1 bar. b) Matching pressure and velocity for transmitting a shock wave into water.

The conditions inside the combustion chamber are estimated by carrying out a constant-pressure equilibrium computation using the specified inlet conditions and mixture of fuel and oxidizer to determine the initial enthalpy. Neglecting the velocity of the bulk flow within the chamber, the enthalpy of the combustion products is taken to be the total (ideal stagnation) enthalpy and the chamber pressure is the total pressure. With these as initial conditions, the flow in the nozzle is computed using the ideal quasi-one dimensional model.

In steady, quasi-one dimensional flow, the mass flow rate is constant

$$\rho u A = \dot{M} \tag{85}$$
$$= \text{constant} , \tag{86}$$

and equal to the values at the sonic point which is the location of the ideal throat in the converging-diverging nozzle downstream of the combustion chamber.

$$= \rho^* u^* A^* \quad \text{where} \quad u^* = a . \tag{87}$$

The total enthalpy is constant

$$h_t = h + \frac{u^2}{2} \tag{88}$$

so that the velocity can be computed from the thermodynamic state as

$$u = \sqrt{2(h_t - h)} . \tag{89}$$

The enthalpy is considered to be a function of pressure, entropy, and composition

$$h = h(P, s, \mathbf{Y}) \tag{90}$$

The entropy fixed at the value of the products in the combustion chamber and the composition is either specified to the values in the combustion chamber (frozen flow)

$$Y_{i,fr} = Y_i \quad \text{combustion products in chamber} \tag{91}$$

31

or computed to be the equilibrium values consistent with the given pressure at fixed entropy

$$Y_{i,eq} = Y_i(P, s = s_{chamber}) \quad \text{equilibrium at specified } P, s \,. \tag{92}$$

The ideal thrust for expansion to a given area, velocity, and pressure is

$$F = \dot{M}u + A(P - P_a) \tag{93}$$

which is traditionally expressed as the specific impulse, defined as

$$I_{sp} = \frac{F}{\dot{M}g_e} \tag{94}$$

$$= \frac{u}{g_e} + \frac{P - P_a}{\rho u g_e} \tag{95}$$

where P_a is the ambient pressure and $g_e = 9.81$ m·s^{-2} is the acceleration of gravity on the earth's surface. The vacuum performance is obtained when $P_a \to 0$. In practice, the lowest pressure that can be used in the computation is limited by the temperature range of the thermodynamic fitting polynomials (usually valid only to 200 K) and the convergence of the numerical solution to the isentrope.

An example of the computation of flow in a nozzle is given in the Matlab program quasi_1d for a hydrogen-oxygen-helium mixture with varying amounts of helium. This program uses interpolation to find the throat conditions and recalculates the streamtube area as the nondimensional value A/A^*. A modification of this program rocket_impulse computes and plots (Fig. 14) an estimate of the vacuum I_{sp} for both frozen and equilibrium conditions.
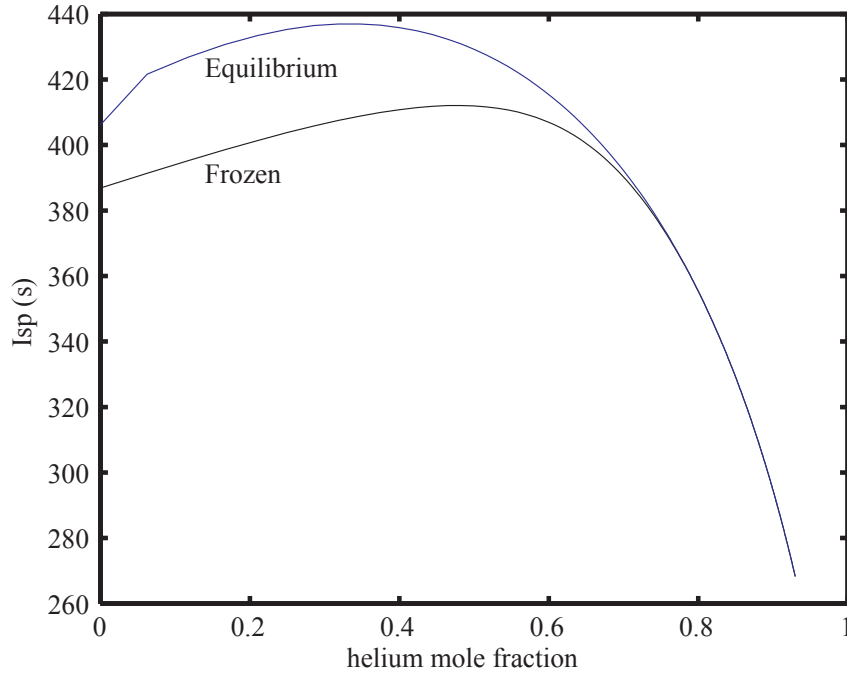
Figure 14: Vacuum specific impulse for an ideal hydrogen-oxygen-helium rocket motor

7 Numerical Methods for the Jump Equations

The most common predictive problem in shock physics is to numerically determine the post-shock state 2 given an initial state 1 and shock velocity $U_s = w_1$. There are many methods to accomplish this task, two of

which are given below. The first method is based on functional iteration in a single variable (density ratio). The second method is based on a two-variable (temperature and volume) implicit solution using Newton's method. The second method is more robust than the first and is used in the numerical algorithms in our software package.

In order to use these methods, an equation of state in the form $e(P, \rho)$ or equivalently $h(p, \rho)$ is required. This can be either an analytic formula, a set of tabulated data, or an algorithmic procedure.

7.1 Iterative Solution with Density

One convenient way to approach this problem is to rewrite the momentum and energy jump relationships as a function of density ρ_2

$$P_2 = P_1 + \rho_1 \mathrm{w}_1^2 \left(1 - \frac{\rho_1}{\rho_2} \right) \tag{96}$$

$$h_2 = h_1 + \frac{1}{2} \mathrm{w}_1^2 \left[1 - \left(\frac{\rho_1}{\rho_2} \right)^2 \right] \tag{97}$$

Using an assumed value of $\rho_2 = \rho_2^*$ and the initial state $(P_1, \rho_1, h_1, \mathrm{w}_1)$, Equations (96) and (97) are used to predict interim values of pressure and enthalpy, P_2^* and h_2^*. The enthalpy from (97) is then compared with the value obtained from the equation of state

$$h = h(P_2^*, \rho_2^*) \tag{98}$$

to obtain an error

$$Err = h(98) - h(97) \tag{99}$$

Depending on the sign of Err, a new value for $\rho_2 = \rho_2^*$ that will reduce the magnitude of Err is selected. Through repeated[5] trials (iterations), Err can be reduced to less than a desired tolerance ϵ. This formulation of the problem can be used with any equation of state that can be evaluated to yield $h(P, \rho)$; *Mollier* charts and tables (Reynolds, 1979) that are widely available for many substances are well suited for this approach. This method is the basis of the post-shock state solution in the original detonation structure program ZND developed by Shepherd (1986).

7.1.1 Algorithm

The details of the solution algorithm are as follows:

1. Define known quantities: Upstream State $(P_1, \rho_1, T_1, h_1, \mathrm{w}_1, \overline{W})$, $\mathcal{R}$, error tolerances

2. Seek unknown quantities: Downstream State (P_2, ρ_2, T_2, h_2)

3. Define the unknown specific volume ratio to be X

$$X = \left(\frac{\rho_1}{\rho_2} \right) \tag{100}$$

4. Guess a value for X within assumed upper and lower bounds $X_{min} < X < X_{max}$.

$$X_{min} = \frac{1}{40} \tag{101}$$

$$X_{max} = \frac{1}{1.005} \tag{102}$$

---

[5]This is most conveniently carried out using one of the "canned" nonlinear root solvers available in standard libraries of numerical subroutines (Press et al., 1986).

5. Compute the tentative value for pressure from momentum jump

$$P_2^* = P_1 \rho_1 w_1^2 (1 - X) \tag{103}$$

6. Compute density, temperature, and enthalpy from the equation of state

$$\rho_2^* = \frac{\rho_1}{X} \tag{104}$$

$$T_2^* = \frac{P_2 \overline{W}}{\mathcal{R} \rho_2} \tag{105}$$

$$h_2^* = h(T_2^*, P_2^*) \tag{106}$$

7. Compute the enthalpy using the energy jump equation

$$h_2 = h_1 + \frac{w_1^2}{2} \left(1 - X^2\right) \tag{107}$$

8. Find the error as the difference between the two enthalpies

$$Err = h_2 - h_2^* \tag{108}$$

In (106), $h(T, P)$ is the thermodynamic equation of state of the products. If the products are in chemical equilibrium, in step 6, first determine the equilibrium composition corresponding to P^* and ρ^*. Then compute T^* and h^* for the new composition.

9. Iterate until Err (108) is less than the specified value.

10. Return final values of P_2, ρ_2, and composition $\mathbf{Y}_2$ as the post-shock state.

The program ZEROIN (Shampine and Watts, 1970) was used in Shepherd (1986) to carry out the iteration.

7.1.2 Algorithm Analysis

This algorithm has difficulty converging with strong shock waves such as the leading shock of a highly overdriven detonation, i.e., a wave speed significantly exceeding the Chapman-Jouguet value. This is due to the vertical asymptote of the Hugoniot at high pressures (Fig. 15). Small changes in density correspond to large changes in pressure, and if the bounds on the density are not chosen carefully, the algorithm will pick values that fall to the left of the asymptote which may cause the root-solving routine to fail. In order to use this method, we need find a good approximation to the lower bound on the specific volume ratio X_{min}. An approximate asymptote (110) can be determined from the constant c_P analytic solution to the jump conditions (see Appendix A).

$$\frac{\rho_2}{\rho_1} = \frac{\gamma + 1}{\gamma - 1 + \dfrac{2}{M_1^2}} \tag{109}$$

where γ is the ratio of specific heats, c_P/c_v. As $M \to \infty$, this expression becomes

$$\frac{\rho_2}{\rho_1} = \frac{\gamma + 1}{\gamma - 1} \tag{110}$$

In general, particularly when considering a wide range of shock speeds, the value of $\gamma(T)$ shown (Fig. 16) varies with postshock temperature (and pressure for reacting cases) since $c_P(T)$. In order for this estimate to be useful, we need a value for γ. This will depend on the postshock temperature and pressure. A typical
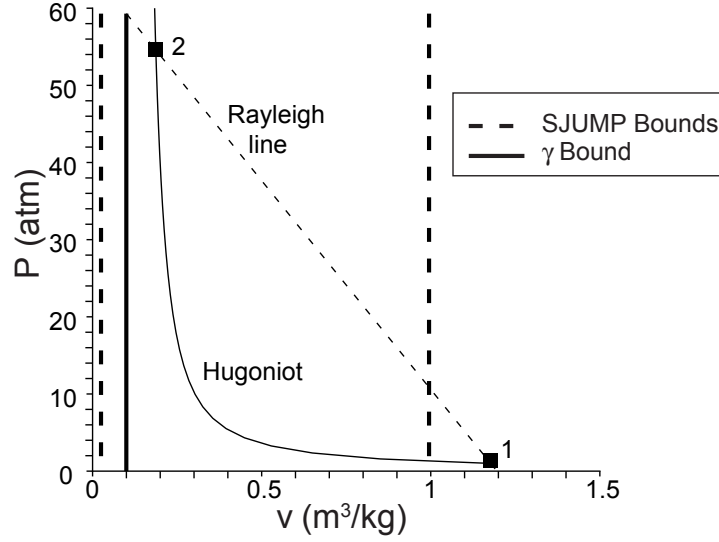
Figure 15: The Rayleigh line and reactant (frozen) Hugoniot with the minimum (101) and maximum (102) density ratios superimposed for stoichiometric hydrogen-air with the same initial conditions as Fig. 3 and a shock speed of $1.4u_{CJ}$. The proposed asymptote (110), γ bound, is also shown. `demo_RH.m`
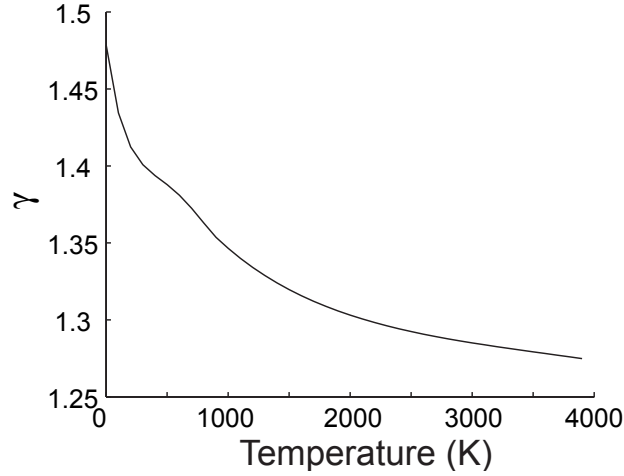
Figure 16: γ as a function of temperature for stoichiometric hydrogen-air at 1 atm (frozen composition).

maximum leading shock velocity in unstable detonations (Eckett et al., 2000) is about $1.4U_{CJ}$, where U_{CJ} is the Chapman-Jouguet value. The value of γ for a shock of this strength in air is about 1.3. Figure 15 shows the typical bounds on the density ratio for this case and we see that the simple estimate falls to the left[6] of the actual solution, which means that considerable trial and error is needed to get appropriate bounds on the trial value of the density. For this reason, functional iteration on density is not a very robust method for a wide range of problems, and a more reliable technique is needed.

---

[6]When the specific heat is a function of temperature, even if the composition is fixed, (110) is incorrect.

7.2 Newton-Raphson Method in Temperature and Volume

The iterative solution with density requires a good initial guess for the density and care must be taken not to exceed the maximum density. The steep slope of the Hugoniot for strong shocks makes this method unsuitable in those cases. We have found that a more robust method is to use a two-variable Newton-Raphson scheme with the variables temperature and specific volume. The scheme presented below is an extension of the method used by Reynolds (1986a) to solve the jump conditions for a Chapman-Jouguet detonation.

The momentum and energy jump conditions can be expressed as

$$\mathcal{H} = \left(h_2 + \frac{1}{2} \mathrm{w}_2^2 \right) - \left(h_1 + \frac{1}{2} \mathrm{w}_1^2 \right) \tag{111}$$

$$\mathcal{P} = \left(P_2 + \rho_2 \mathrm{w}_2^2 \right) - \left(P_1 + \rho_1 \mathrm{w}_1^2 \right) \tag{112}$$

The exact solution to the jump conditions then occurs when both $\mathcal{H}$ and $\mathcal{P}$ are identically zero. We can construct an approximate solution by simultaneously iterating these two equations until $\mathcal{H}$ and $\mathcal{P}$ are less than a specified tolerance. An iteration algorithm can be developed by considering trial values of (T, v) for the downstream thermodynamic state 2 that are close to but not equal to the exact solution, (T_2, v_2). The expansion of (112) and (111) to first order in a Taylor series about the exact solution,

$$\mathcal{H}(T, v) = \mathcal{H}(T_2, v_2) + \frac{\partial \mathcal{H}}{\partial T}(T - T_2) + \frac{\partial \mathcal{H}}{\partial v}(v - v_2) + \dots \tag{113}$$

$$\mathcal{P}(T, v) = \mathcal{P}(T_2, v_2) + \frac{\partial \mathcal{P}}{\partial T}(T - T_2) + \frac{\partial \mathcal{P}}{\partial v}(v - v_2) + \dots \tag{114}$$

can be written this as a matrix equation

$$\left(\begin{array}{c} \mathcal{H} \\ \mathcal{P} \end{array} \right) = \left(\begin{array}{cc} \frac{\partial \mathcal{H}}{\partial T} & \frac{\partial \mathcal{H}}{\partial v} \\ \frac{\partial \mathcal{P}}{\partial T} & \frac{\partial \mathcal{P}}{\partial v} \end{array} \right) \left(\begin{array}{c} \delta T \\ \delta v \end{array} \right) \tag{115}$$

where $\delta T = T - T_2$ and $\delta v = v - v_2$. This equation is used to compute corrections, δT and δv, to the current values of (T, v) and through successive applications, approach the true solution to within a specified error tolerance. At step i, we have values (T^i, v^i) which we use to evaluate (111) and (112) and obtain $\mathcal{H}^i$ and $\mathcal{P}^i$; then we solve (115) for δT^i and δv^i and compute the next approximation to the solution as

$$T^{i+1} = T^i - \delta T^i \tag{116}$$

$$v^{i+1} = v^i - \delta v^i \tag{117}$$

The corrections can be formally obtained by inverting the Jacobian

$$J = \left(\begin{array}{cc} \frac{\partial \mathcal{H}}{\partial T} & \frac{\partial \mathcal{H}}{\partial v} \\ \frac{\partial \mathcal{P}}{\partial T} & \frac{\partial \mathcal{P}}{\partial v} \end{array} \right) \tag{118}$$

and carrying out the matrix multiplication operation.

$$\left(\begin{array}{c} \delta T \\ \delta v \end{array} \right) = J^{-1} \left(\begin{array}{c} \mathcal{H} \\ \mathcal{P} \end{array} \right) \tag{119}$$

This is equivalent to the Newton-Raphson method (Press et al., 1986) of solving systems of nonlinear equations. The derivatives needed for the Jacobian might be computed analytically although it is often simpler to compute these numerically for complex equations of state or problems that involve chemical equilibrium. This is the approach used by Reynolds (1986a) in his implementation of this method for finding CJ states for detonations and the basis for the method used in the present software.

Subfunctions `shk_calc` **and** `shk_eq_calc`

1. Define known quantities: Upstream State $(P_1, \rho_1, T_1, h_1, \mathrm{w}_1, \overline{W})$, $\mathcal{R}$, error tolerances, increment values $(\Delta T, \Delta v)$

2. Seek unknown quantities: Downstream State (P_2, ρ_2, T_2, h_2)

3. Establish preliminary guess $(i = 1)$

$$\rho_2^i = 5\rho_1$$
$$v_2^i = \frac{1}{\rho_2^i}$$
$$P_2^i = P_1 + \rho_1 \mathrm{w}_1^2 \left(1 - \frac{\rho_1}{\rho_2^i}\right)$$
$$T_2^i = T_1 \frac{P_1}{P_2^i} \frac{\rho_2^i}{\rho_1}$$

4. Call Subfunction `FHFP_fr` to get $\mathcal{H}(T_2^i)$ and $\mathcal{P}(T_2^i)$

5. Perturb temperature holding volume fixed and call Subfunction `FHFP_fr` to get $\mathcal{H}(T_2^i + \Delta T)$ and $\mathcal{P}(T_2^i + \Delta T)$

6. Perturb specific volume holding temperature fixed and call Subfunction `FHFP_fr` to get $\mathcal{H}(v_2^i + \Delta v)$ and $\mathcal{P}(v_2^i + \Delta v)$

7. Evaluate the elements of the Jacobian by first order differences

$$\frac{\partial \mathcal{H}}{\partial T} = \frac{\mathcal{H}(T_2^i + \Delta T) - \mathcal{H}(T_2^i)}{\Delta T}$$
$$\frac{\partial \mathcal{P}}{\partial T} = \frac{\mathcal{P}(T_2^i + \Delta T) - \mathcal{P}(T_2^i)}{\Delta T}$$
$$\frac{\partial \mathcal{H}}{\partial v} = \frac{\mathcal{H}(v_2^i + \Delta v) - \mathcal{H}(v_2^i)}{\Delta v}$$
$$\frac{\partial \mathcal{P}}{\partial v} = \frac{\mathcal{P}(v_2^i + \Delta v) - \mathcal{P}(v_2^i)}{\Delta v}$$

8. Solve the linear system given in (115) to find δT and δv

9. Update post-shock state

$$T_2^{i+1} = T_2^i + \delta T$$
$$v_2^{i+1} = v_2^i + \delta v$$

10. Check convergence

$$T_2^{i+1} - T_2^i < T_{error}$$
$$v_2^{i+1} - v_2^i < v_{error}$$

11. Repeat 4-10 as needed

12. Return final values of T_2 and v_2 as the post-shock state.

Subfunction FHFP_fr

1. Define known quantities: Upstream State (P_1, ρ_1, T_1, h_1, w_1, $\overline{W}$), $\mathcal{R}$, Current Guess State (P_2^i, ρ_2^i, T_2^i, h_2^i)

2. Seek unknown quantities: Error in jump conditions ($\mathcal{H}$, $\mathcal{P}$)

3. Determine $\mathcal{H}$ and $\mathcal{P}$ from

$$\mathrm{w}_2^2 = \mathrm{w}_1^2 \left(\frac{\rho_1}{\rho_2^i} \right)^2 \tag{120}$$

$$\mathcal{H} = \left(h_2^i + \frac{1}{2}\mathrm{w}_2^2 \right) - \left(h_1 + \frac{1}{2}\mathrm{w}_1^2 \right) \tag{121}$$

$$\mathcal{P} = \left(P_2^i + \rho_2^i \mathrm{w}_2^2 \right) - \left(P_1 + \rho_1 \mathrm{w}_1^2 \right) \tag{122}$$

7.3 Chapman-Jouguet Detonation Velocity

As discussed previously, the (upper) Chapman-Jouguet detonation velocity, U_{CJ}, can be determined either by finding the minimum speed solution of the jump conditions or the downstream sonic flow solution in the wave-fixed frame. The minimum wave speed method is more robust since it does not require an additional iteration to compute the equilibrium sound speed. However, obtaining an accurate solution requires careful treatment of the iteration convergence. If a robust method of computing the equilibrium sound speed is available as a standard routine, then the sonic flow method is easier to implement and test convergence. We describe and implement both methods.

7.3.1 Sonic Flow Algorithm

This algorithm (CJSpeed2) finds the solution of the shock jump conditions (111) and (112) where w_1 is unknown and w_2 is the equilibrium sound speed. The equilibrium sound speed is calculated according the the following equation

$$a_{eq}^2 = \left(\frac{\partial P}{\partial \rho} \right)_{s\mathbf{Y}^{eq}}$$

This algorithm is implemented in a similar way to the specified shock problem. The only difference is the structure of the subfunction which we called FHFP_CJ2 for this case. This new subfunction executes the following scheme and uses subfunction soundspeed_eq to calculate a_{eq}.

Subfunction FHFP_CJ2

1. Define known quantities: Upstream State (P_1, ρ_1, T_1, h_1, w_1, $\overline{W}$), $\mathcal{R}$, Current Guess State (P_2^i, ρ_2^i, T_2^i, h_2^i)

2. Seek unknown quantities: Error in jump conditions ($\mathcal{H}$, $\mathcal{P}$)

3. Determine $\mathcal{H}$ and $\mathcal{P}$ from

$$\mathrm{w}_2 = a_{2eq} \tag{123}$$

$$\mathrm{w}_1^2 = \mathrm{w}_2^2 \left(\frac{\rho_2^i}{\rho_1} \right)^2 \tag{124}$$

$$\mathcal{H} = \left(h_2^i + \frac{1}{2}\mathrm{w}_2^2 \right) - \left(h_1 + \frac{1}{2}\mathrm{w}_1^2 \right) \tag{125}$$

$$\mathcal{P} = \left(P_2^i + \rho_2^i \mathrm{w}_2^2 \right) - \left(P_1 + \rho_1 \mathrm{w}_1^2 \right) \tag{126}$$

Subfunction `soundspeed_eq`

1. Define known quantities: Upstream State (P_1, ρ_1)

2. Seek unknown quantities: Equilibrium Sound Speed (a_{eq})

3. Perturb density

4. Equilibrate with constant s and ρ

5. $a_{2eq}^2 = \dfrac{P_2 - P_1}{\rho_2 - \rho_2}$

Note: This function works well for hydrogen-air mixtures, however, there are still difficulties with the highly complex mechanism files of mixtures such as isopropyl nitrate (IPN, 2-propyl nitrate). Most likely, due to the large number of chemical reactions and species of the mechanism, the equilibrate function in Cantera (Goodwin) has problems converging to an equilibrium sound speed. To remedy these problems, we chose to develop an alternate more robust (but slower) algorithm to find the CJ speed.

7.3.2 Minimum Wave Speed Algorithm

As discussed previously, the minimum wave speed solution uniquely determines the (upper) Chapman-Jouguet point. We implement this by determining w_1 as a function of $\frac{\rho_2}{\rho_1}$ at discrete points and then using a combination of analysis near the CJ point and statistical methods, find an approximation to the minimum value of w_1. The solution of the jump conditions for a given density uses the same Newton-Raphson method previously discussed but with a key difference that instead of solving a system of equations in volume and temperature (115), we used initial velocity and temperature as variables.

$$
\left(\begin{array}{c} \delta\mathcal{H} \\ \delta\mathcal{P} \end{array} \right) = \left(\begin{array}{cc} \dfrac{\partial\mathcal{H}}{\partial T} & \dfrac{\partial\mathcal{H}}{\partial w_1} \\ \dfrac{\partial\mathcal{P}}{\partial T} & \dfrac{\partial\mathcal{P}}{\partial w_1} \end{array} \right) \left(\begin{array}{c} \delta T \\ \delta w_1 \end{array} \right)
\tag{127}
$$

Subfunction `CJ_calc`

1. Define known quantities: Upstream State (P_1, ρ_1, T_1, h_1, ρ_2, $\overline{W}$), $\mathcal{R}$, error tolerances, increment values (ΔT, Δw_1)

2. Seek unknown quantities: Downstream State (P_2, T_2, h_2)

3. Establish preliminary guess: ($i = 1$)

$$
w_1^i = 2000
$$
$$
T_2^i = 2000
$$

4. Equilibrate the system with constant temperature and specific volume to find P_2^i and h_2^i

5. Call Subfunction `FHFP_CJ` to get $\mathcal{H}(T_2^i)$ and $\mathcal{P}(T_2^i)$

6. Perturb temperature holding initial velocity constant and call Subfunction `FHFP_CJ` to get $\mathcal{H}(T_2^i + \Delta T)$ and $\mathcal{P}(T_2^i + \Delta T)$

7. Perturb initial velocity holding temperature constant and call Subfunction `FHFP_CJ` to get $\mathcal{H}(w_1^i + \Delta w_1)$ and $\mathcal{P}(w_1^i + \Delta w_1)$

8. Evaluate the elements of the Jacobian by first order differences

$$\frac{\partial \mathcal{H}}{\partial T} \approx \frac{\mathcal{H}(T_2^i + \Delta T) - \mathcal{H}(T_2^i)}{\Delta T}$$
$$\frac{\partial \mathcal{P}}{\partial T} \approx \frac{\mathcal{P}(T_2^i + \Delta T) - \mathcal{P}(T_2^i)}{\Delta T}$$
$$\frac{\partial \mathcal{H}}{\partial \mathrm{w}_1} \approx \frac{\mathcal{H}(\mathrm{w}_1^i + \Delta \mathrm{w}_1) - \mathcal{H}(\mathrm{w}_1^i)}{\Delta \mathrm{w}_1}$$
$$\frac{\partial \mathcal{P}}{\partial \mathrm{w}_1} \approx \frac{\mathcal{P}(\mathrm{w}_1^i + \Delta \mathrm{w}_1) - \mathcal{P}(\mathrm{w}_1^i)}{\Delta \mathrm{w}_1}$$

9. Solve the linear system given in (127) to find δT and $\delta \mathrm{w}_1$

10. Update values

$$T_2^{i+1} = T_2^i + \delta T$$
$$\mathrm{w}_1^{i+1} = \mathrm{w}_1^i + \delta \mathrm{w}_1$$

11. Equilibrate the system with constant temperature and specific volume to find P_2^{i+1} and h_2^{i+1}

12. Check convergence

$$T_2^{i+1} - T_2^i < T_{error}$$
$$\mathrm{w}_1^{i+1} - \mathrm{w}_1^i < \mathrm{w}_{1error}$$

13. Repeat 4-12 as needed

14. Return final values of T_2 and w_1.

Subfunction `FHFP_CJ`

1. Define known quantities: Upstream State (P_1, ρ_1, T_1, h_1, ρ_2, $\overline{W}$), $\mathcal{R}$, Current Guess State (P_2^i, w_1^i, T_2^i, h_2^i)

2. Seek unknown quantities: Error in jump conditions ($\mathcal{H}$, $\mathcal{P}$)

3. Determine $\mathcal{H}$ and $\mathcal{P}$ from

$$\mathrm{w}_2 = \mathrm{w}_1^i \left(\frac{\rho_1}{\rho_2} \right) \tag{128}$$

$$\mathcal{H} = \left(h_2^i + \frac{1}{2}\mathrm{w}_2^2 \right) - \left(h_1 + \frac{1}{2}\mathrm{w}_1^{i2} \right) \tag{129}$$

$$\mathcal{P} = \left(P_2^i + \rho_2\mathrm{w}_2^2 \right) - \left(P_1 + \rho_1\mathrm{w}_1^{i2} \right) \tag{130}$$

7.3.3   Minimizing Initial Velocity

Following the algorithm outlined above, we are able to find how the initial velocity varies with the final density. Analytically, we have found that the initial velocity varies quadratically with density close to the CJ point (see Appendix C). In order to find the minimum w_1, the CJ speed, we used the Matlab `cfit` toolbox to apply a quadratic least squares fit to the data points that we gathered from the above algorithm. We used the R-squared value to quantify the precision of our fit and simultaneous new observation predicition bounds to quantify the uncertainty in our minimum wave speed.

Subfunction `CJSpeed`

1. Define known quantities: Upstream State (P_1, ρ_1, T_1, h_1, $\overline{W}$), $\mathcal{R}$, initial ($i = 1$) density ratio range ($min^i = 1.5$, $max^i = 2.0$), number of density ratios of interest (numstep)

2. Seek unknown quantities: CJ speed

3. Call `CJ_calc` for each density ratio, X ($X^i = min^i + i \cdot step^i \quad i \in (0, \text{numsteps})$)

4. Fit data to a quadratic equation ($aX^2 + bX + c$)

5. Find minimum of fit $\left(X_{min} = -\dfrac{b}{2a} \right)$

6. Narrow density ratio range

$$min^{i+1} = X_{min} - 0.001 X_{min} \tag{131}$$
$$max^{i+1} = X_{min} + 0.001 X_{min} \tag{132}$$

7. Check convergence

$$R^2 > 0.99999 \tag{133}$$

8. Repeat 3-7 as needed

9. Return

$$\text{w}_{1min} = \frac{b^2}{4a} - \frac{b^2}{2a} + c \tag{134}$$

of the fitted curve and the prediction bounds on this minimum

Figures 17 and 18 depict the results that we obtain from the method described in this section.
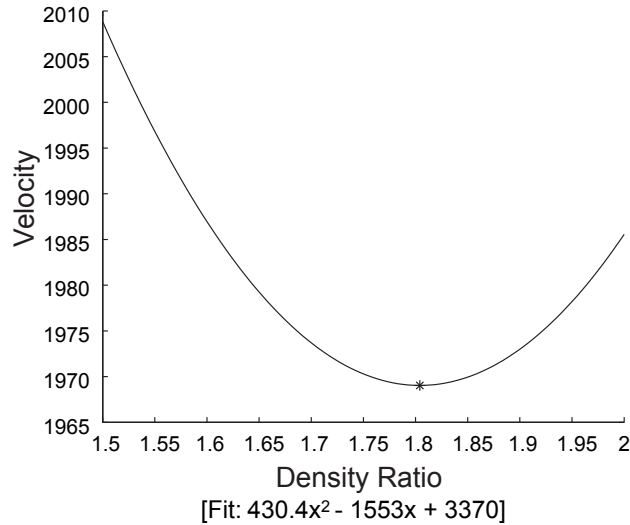
Figure 17: Initial velocity as a function of density ratio for stoichiometric hydrogen-air with intial temperature 300 K and initial pressure 1 atm. Chapman-Jouguet velocity is 1969.03 m/s $\pm$ 1.65×10^{-6} corresponding to a density ratio of 1.80. `demo_CJ.m`
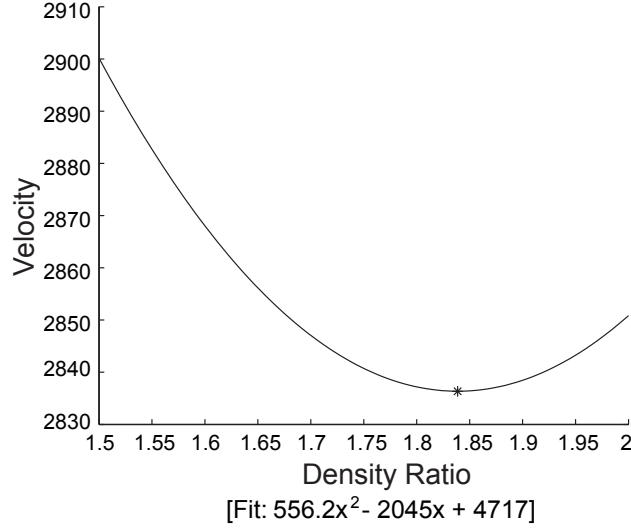
Figure 18: Initial velocity as a function of density ratio for stoichiometric hydrogen-oxygen with intial temperature 300 K and initial pressure 1 atm. Chapman-Jouguet velocity is 2836.36 m/s $\pm$ 2.37$\times 10^{-6}$ corresponding to a density ratio of 1.84. demo_CJ.m

7.3.4   Statistical Analysis of CJ Speed Solution

As discussed above, we have used the R-squared value to quantify the precision of the fit and simultaneous new observation prediction bounds to quantify the uncertainty in the computed value of the CJ speed. In this section these quantities will be discussed more thoroughly.

If $y(x)$, the R-squared value is defined by the following equation

$$R^2 = \frac{\sum_{i=1}^n (\hat{y}_i - \overline{y})^2}{\sum_{i=1}^n (y_i - \overline{y})^2} \tag{135}$$

If this value is very close to unity then the curve is a good fit.

Simultaneous prediction bounds according to Matlab measure the confidence that a new observation lies within the interval regardless of the predictor value. Matlab offers two main measures of confidence: confidence bounds and prediction bounds. The confidence bounds give the uncertainty in the least square coefficients. These uncertainties are correlated, and the prediction bounds account for this correlation. In our particular problem we have uncertainty in both the x value of the minimum as well as the y value of the minimum. This is because we choose

$$x_{min} = -\frac{b}{2a} \tag{136}$$

$$y_{min} = ax_{min}^2 + bx_{min} + c \tag{137}$$

and there is uncertainty in a, b, and c. We choose simultaneous prediction bounds because that will account for the uncertainty in x. Non-simultaneous prediction bounds assume that there is no uncertainty in x. Matlab defines simultaneous new observation prediction bounds with the following expression.

$$P_{s,o} = \hat{y} \pm f \sqrt{\sigma_{sample}^2 + xSx'} \tag{138}$$

42

In this expression f is the inverse of the cumulative distribution function F (Fig. 19), σ^2_{sample} is the mean squared error (139), x is the predictor value for the new observation, and S is the covariance matrix of the coefficient estimates (140).

$$\sigma^2_{sample} = \frac{1}{\nu} \sum_{i=0}^{n} (y_i - \hat{y}_i)^2 \tag{139}$$

$$S = (X^T X)^{-1} \sigma^2_{sample} \tag{140}$$
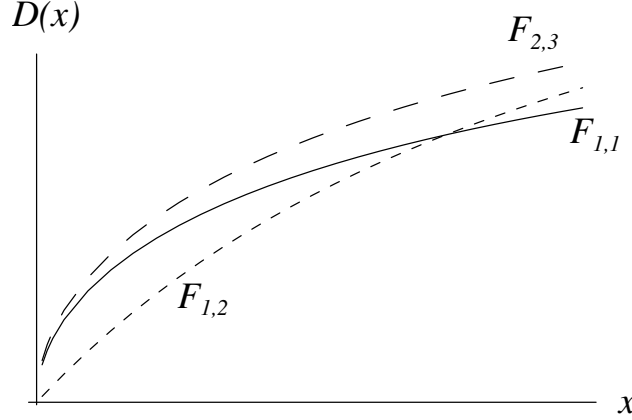
Figure 19: Cumulative distribution function F for error in fitted parameters.

8 Verification and Validation

As depicted in Fig. 3, for a Chapman-Jouguet detonation in stoichiometric hydrogen-air with standard intial conditions, there is a unique post-shock state. Our experience is that unique results are obtained for all cases of equilibrium reacting gas mixtures described by ideal gas thermodynamics.[7] Theoretical support for the uniqueness of the post-shock state is given by Menikoff and Plohr (1989a). They have determined that the Bethe-Weyl theorem assures that the Hugoniot is well-behaved when Γ, the fundamental derivative of gas dynamics, is positive. We note that our algorithms may not be appropriate for cases when $\Gamma < 0$. We do not plan to explore systems like these at this time.

We can verify the correctness of the software by comparing with perfect gas analytic solutions and validating it against results from legacy software. First, we can compare `PostShock_fr` results with the exact solution to the jump conditions for a perfect gas (see Thompson (1988) or Appendix A).

$$P_2 = P_1 \left(1 + \frac{2\gamma}{\gamma + 1} \left(M_1^2 - 1 \right) \right) \tag{141}$$

$$v_2 = v_1 \left(1 - \frac{2}{\gamma + 1} \left(1 - \frac{1}{M_1^2} \right) \right) \tag{142}$$

In the case of a perfect gas, the specific heat is constant and the enthalpy can be expressed as $h = c_P T$. Figure 20 shows the error in pressure, density, temperature, and enthalpy between the exact solution and `PostShock_fr`'s results for shock speeds ranging from 500 to 5000 m/s. The system for these simulations was one mole of Argon at 1 atmosphere and 300 Kelvin.

---

[7]This does not mean that the ideal post-shock state or CJ condition always correctly describes the physical situation. We are only referring to the mathematical uniqueness of our solution methods.
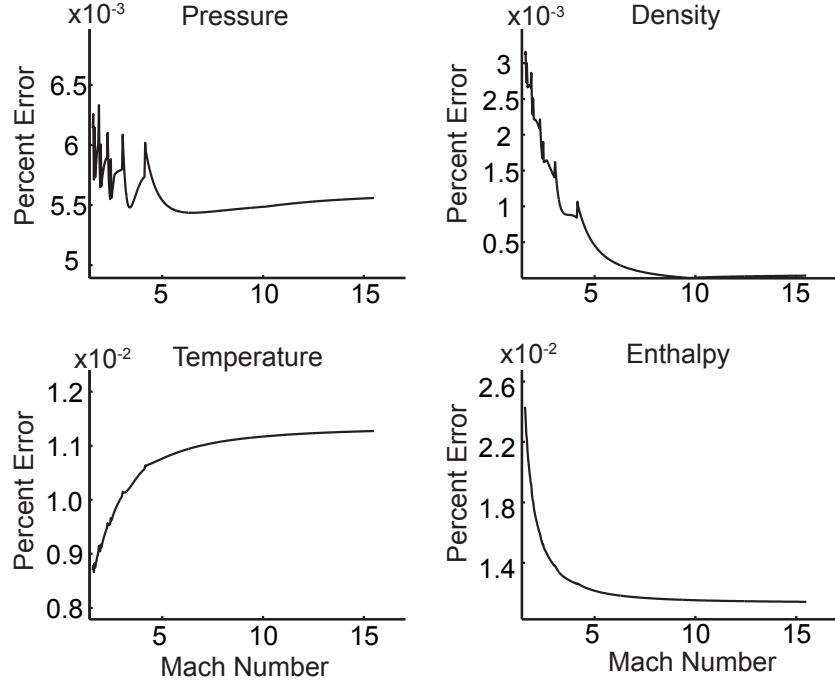
Figure 20: The percent error in the exact solution and the results of `PostShock_fr` for one mole of Argon with initial temperature 300 K and initial pressure 1 atm.

For mixtures with non-constant specific heat, we can compare the results of `PostShock_fr` with STAN-JAN (Reynolds, 1986b) results. Figure 21 shows the percent difference in post-shock pressure and temperature for stoichiometric hydrogen air with varying shock speed.
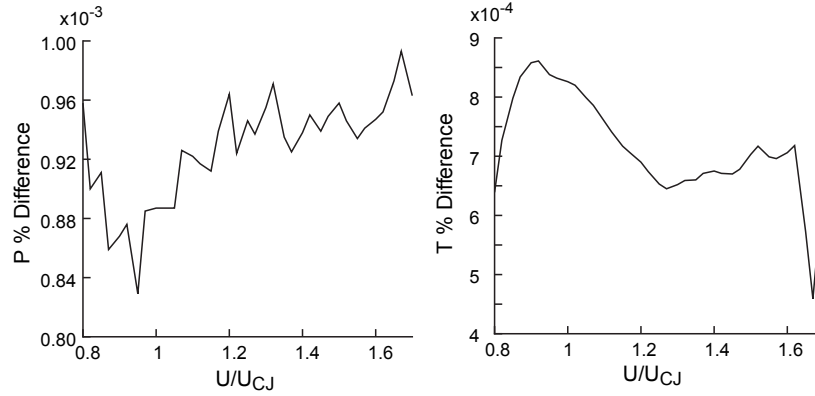
Figure 21: The percent difference in the solutions of STANJAN and `PostShock_fr` for hydrogen-air at an equivalence ratio of 0.5 for varying shock speed with initial temperature 300 K and initial pressure 1 atm.

We have also investigated the shape of the $\mathcal{H}$ and $\mathcal{P}$ surfaces resulting from `PostShock_fr`. Figure 22 shows that the surface generated by calculating the RMS of $\mathcal{H}$ and $\mathcal{P}$ according to (143) has a distinct

minimum, and that the minimum corresponds to the valid solution.

$$RMSCJ = \sqrt{\left(\frac{\mathcal{H}}{h_{CJ}}\right)^2 + \left(\frac{\mathcal{P}}{P_{CJ}}\right)^2} \tag{143}$$
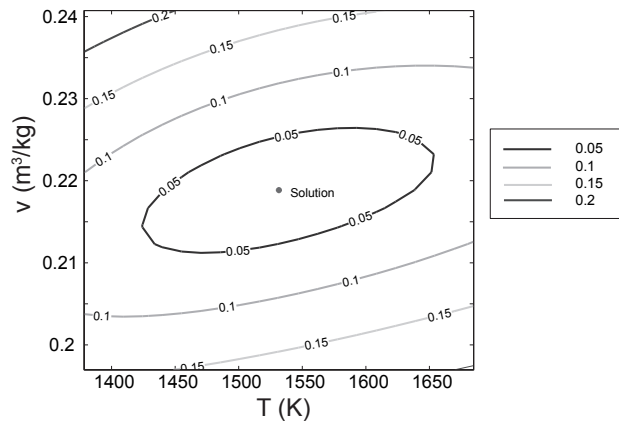
Figure 22: A contour plot of the RMS surface with the solution indicated at the minimum.

The concave shape of the RMS surface implies that the solution should converge to the minimum. Figure 23 shows the absolute value of the differential values at each step and demonstrates this convergence.
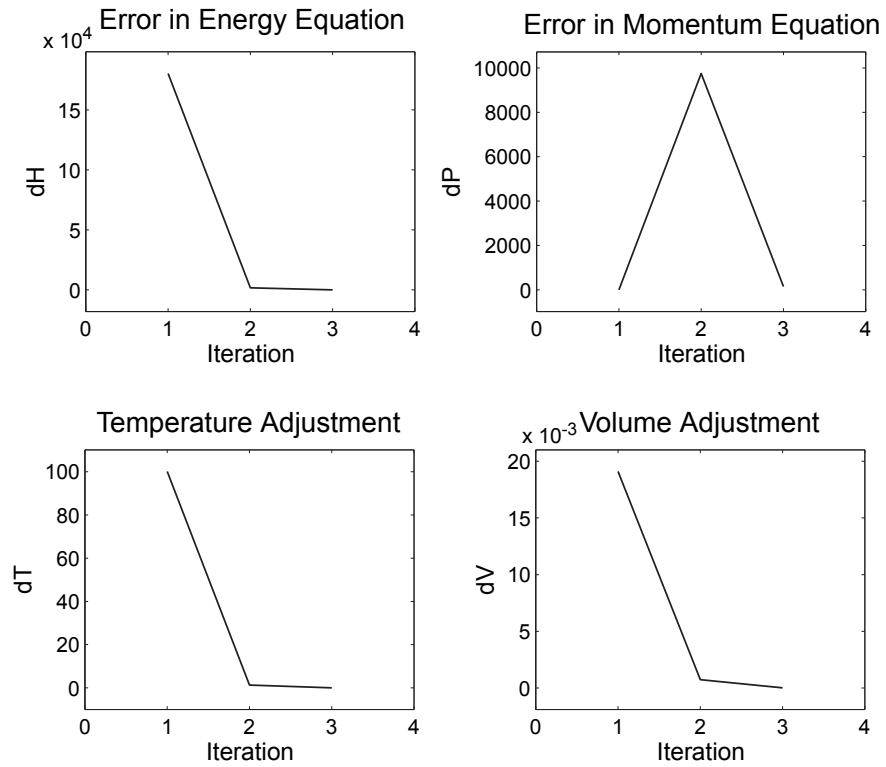
Figure 23: Convergence study for stoichiometric hydrogen-air with initial temperature 300 K and initial pressure 1 atm using PostShock_fr.

9   Summary

We have derived and implemented algorithms for computing shock and detonation wave properties that researchers and students commonly encounter in studying wave propagation in reacting gases. The scripts and functions that we have written can be used as provided or, more logically, combined to perform a sequence of computations to analyze more complex problems in the gas dynamics of explosions. By using the full functionality of Cantera, the user can extend the basic functionality of our scripts and tailor the methods to specific problems. A number of demonstration programs (see the Shock and Detonation Toolbox website) have been written to illustrate how to apply the basic software. These are a useful starting point for learning how to use the Shock and Detonation Toolbox and developing new applications.

References

E. Becker. *Gas Dynamics*. Academic Press, 1968. QC168 .B4313 (Out of print). 10

R. Becker. Impact waves and detonation. *Zeitschrift für Physik*, VIII:321–, 1922. Available in translation as NACA TM-505 and TM-506. 8, 70

W.M. Beltman and J.E. Shepherd. Linear elastic response of tubes to internal detonation loading. *Journal of Sound and Vibration*, 252(4):617–655, 2002. 27

S. W. Benson. *Thermochemical Kinetics*. John Wiley, NY, 1976. 74

D. J. Berets, E. F. Greene, and G. B. Kistiakowsky. Gaseous detonation waves: Stationary waves in the hydrogen-oxygen system. *J. Am. Chem. Soc.*, 72:1080, 1950. 9

H. A. Bethe. *Deviations from Thermal Equilibrium in Shock Waves*, volume 18 of *World Scientific series in 20th century physics*. World Scientific, Singapore, 1997. 9, 47

H.A. Bethe. The theory of shock waves for an arbitrary equation of state. Technical Report 545, Office of Scientific Research and Development, Washington DC, 1942. Wartime report of National Defense Research Committee. 9

H.A. Bethe and E. Teller. Deviations from thermal equilibrium in shock waves. Technical Report X-117, Ballistics Research Lab, Aberdeen Proving Grounds, MD, 1945. This report was actually written in 1940 or 1941. Some historical background and the first two sections are given in Bethe (1997). 9

W. A. Bone and D. T. Townend. *Flame and Combustion in Gases*. Longmans, Green, and Co, 1927. 7

S. R. Brinkley, Jr. Calculation of the equilibrium composition of systems of many constituents. *J. Chem. Phys.*, 12:107–110, 1947. 9

S. R. Brinkley, Jr and J. G. Kirkwood. On the condition of stability of the plane detonation wave. In *3rd Sympposium on Combustion, Flame, and Explosion Phenomena*, page 586, 1949. see Kirkwood (1967) for a reprint and erratum. 19

S. Browne, J. Ziegler, and J. E. Shepherd. Numerical solution methods for control volume explosions and znd detonation structure. Technical Report FM2006.007, GALCIT, 2005. 7, 12, 83

D. L. Chapman. On the rate of explosion in gases. *Philos. Mag.*, 14:1091–1094, 1899. 7, 17

M.W. Chase, Jr. NIST-JANAF thermochemical tables. *Journal of Physical and Chemical Reference Data, Monograph 9*, 1998. Update of 3rd Edition. 12, 74, 75

G. Ciccarelli and S. B. Dorofeev. Flame acceleration and transition to detonation in ducts. *Progress in Energy and Combustion Science*, 2008. in press. 29

J.F. Clarke and M. McChesney. *The Dynamics of Real Gases*. Butterworths, 1964. QC168 .C56 (Out of print). 6

R. H. Cole. *Underwater Explosions*. Princeton Univ. Press, 1948. QC151 .C6 1948. 9

R. Courant and K. O. Friedrichs. *Supersonic Flow and Shock Waves*. Interscience, 1948. QA930 .C6. 10

R. D. Cowan and W. Fickett. Equations of state for high explosives based on the kistiakowsky-wilson equation of state for product gases. Technical Report LA-1865, Los Alamos National Laboratory, 1954. 9

M. Cowperthwaite and W.H. Zwisler. TIGER computer program documentation. Technical Report Z106, SRI, 1973. 10

H.B. Dixon. On the movements of flames in the explosion of gases. *Phil. Trans. A*, 200:315–352, 1903. 7

W. Döring. On detonation processes in gases. *Ann. Phys.*, 43:421–436, 1943. 9

C. A. Eckett, J. J. Quirk, , and J. E. Shepherd. The role of unsteadiness in direct initiation of gaseous detonations. *Journal of Fluid Mechanics*, 421:147–183, 2000. 35

W. Fickett and W. C. Davis. *Detonation*. University of California Press, Berkerely, CA, 1979. 7, 17, 19, 20

L.E. Fried and W.M. Howard. CHEETAH 3.0 users manual. Technical Report UCRL-MA-117541, Lawrence Livermore National Laboratory, Livermore, CA, 2001. 10

I.I. Glass and J. P. Sislian. *Nonstationary flows and shock waves*. Oxford University Press, 1994. 28, 30

D. Goodwin. Cantera: Object-oriented software for reacting flows. http://www.cantera.org. 7, 10, 39

S. Gordon, F. J. Zeleznik, and V. N. Huff. A general method for automatic computation of equilibrium composition and theoretical rocket performance of propellants. Technical Note TN-132, NASA, 1959. 9

Sanford Gordon and Bonnie J. McBride. Computer program for calculation of complex chemical equilibrium compositions and applications. I. analysis. Reference Publication RP-1311, NASA, 1994. Describes theory and numerical algorithms behind CEA computer program. 10

W. D. Hayes. *Gasdynamic Discontinuities*. Princeton, 1960. TL571 H35. 68

V. N. Huff and S. Gordon. Tables of thermodynamic functions for analysis of aircraft-propulsion systems. Technical Note TN-2161, NACA, 1950. 9

K.K. Irikura and D.J. Frurip, editors. *Computational thermochemistry: prediction amd estimation of molecular thermodynamics.* American Chemical Society, 1998. 76

J. N. Johnson and R. Chéret, editors. *Classic Papers in Shock Compression Science.* Springer, 1998. 7, 8

W. Jost. *Explosion and Combustion Processes in Gases.* McGraw-Hill, NY, 1946. Translation of Explosions-und Verbrennungsvorgänge in Gasen - published in 1935. 7

E. Jouguet. On the propagation of chemical reactions in gases. *J. de Mathematiques Pures et Appliquees*, 1: 347–425, 1905. continued in 2:5-85, 1906. 8, 18, 19

R. J. Kee, J. A. Miller, and T. H. Jefferson. CHEMKIN: A general–purpose, problem–independent, transportable, fortran chemical kinetics code package. Technical Report SAND80-8003, Sandia National Laboratories, 1980. 10

R. J. Kee, F. M. Rupley, and J. A. Miller. The CHEMKIN thermodynamic data base. Technical Report SAND87-8215, Sandia National Laboratories, 1987. 10

R. J. Kee, M. E. Coltrin, and P. Glarborg. *Chemically Reacting Flow: Theory and Practice.* Wiley-Interscience, NJ, 2003. 75

J. G. Kirkwood. *Shock and Detonation Waves.* Gordon and Breach, 1967. QC168 K55. 19, 48, 51

G.B. Kistiakowsky and E.B. Wilson. Final report on the hydrodynamic theory of detonation and shock waves. Technical Report OSRD-114, Office of Scientific Research and Development, 1941a. 9, 70

G.B. Kistiakowsky and E.B. Wilson. Report on the prediction of detonation velocities of solid explosives. Technical Report OSRD-69, Office of Scientific Research and Development, 1941b. 9

B. Lewis and J. B. Friauf. Explosions in detonating gas mixtures. I. calculations of rates of explosions in mixtures of hydrogen and oxyen and the influence of rare gases. *J. Am. Chem. Soc.*, 52:3905–3920, 1930. 8

H. W. Liepmann and A. Roshko. *Elements of Gasynamics.* Wiley, New York, 1957. 10

A. Maczek. *Statistical mechanics.* Oxford Science Publications, 2004. 75

C.L. Mader. *Numerical Modeling of Explosives and Propellants.* University of California Press, 1979. 10

B. J. McBride and S. Gordon. Computer program for calculating and fitting thermodynamic functions. Reference Publication RP-1271, NASA, 1992. This describes how statistical mechanics and molecular data are used to compute the thermodynamic functions needed for chemical equilibrium analysis. 12, 72, 75, 80

Bonnie J. McBride and Sanford Gordon. Computer program for calculation of complex chemical equilibrium compositions and applications. II. User's manual and program description. Reference Publication RP-1311-P2, NASA, 1996. 10

Bonnie J. McBride, Sanford Gordon, and Martin A. Reno. Coefficients for calculating thermodynamic and transport properties of individual species. Technical Memorandum TM-4513, NASA, 1993. This describes the pre-1994 7-coefficient fit, which is used in Cantera. 12, 72, 75

D. A. McQuarrie. *Statistical mechanics.* University Science Books, CA, 2000. 75

R. Menikoff and B. Plohr. The riemann problem for fluid-flow of real materials. *Reviews of Modern Physics*, 61(1):75–130, 1989a. 43

R. Menikoff and B.J. Plohr. The riemann problem for fluid-flow of real materials. *Reviews Of Modern Physics*, 61(1):75–130, 1989b. 68, 71

M. A. Meyers. *Dynamic behavior of materials.* John Wiley & Sons, 1994. 28, 30

OECD. Flame acceleration and deflagration to detonation transition in nuclear safety. Technical Report NEA/CSNI/R(2000)7, OECD Nuclear Energy Agency, 2000. State-of-the-Art Report by a Group of Experts, http://www.galcit.caltech.edu/~jeshep/SOAR/index.html. 29

W. H. Press, B. P. Flannery, S. A. Teukolsky, and W. T. Vetterling. *Numerical Recipes - The art of scientific computing*. Cambridge University Press, 1986. 33, 36

W. C. Reynolds. *Thermodynamic properties in SI: Graphs, tables, and computational equations for forty substances*. Dept Mechanical Engineering, Stanford University, 1979. 33

W. C. Reynolds. The element potential method for chemical equilibrium analysis: Implementation in the interactive program STANJAN, version 3. Technical report, Mechanical Engineering, Stanford University, Stanford, CA, January 1986a. 36

W. C. Reynolds. The element potential method for chemical equilibrium analysis: Implementation in the interactive program STANJAN. Technical report, Stanford University, Dept of Mech. Eng., 1986b. 10, 44

M. D. Salas. The curious events leading to the theory of shock waves. *Shock Waves*, 16:477–487, 2007. 7

L. F. Shampine and H. A. Watts. ZEROIN, A root-solving code. Technical Report SAND SC-TM-70-631, Sandia National Laboratories, 1970. 34

A. H. Shapiro. *The Dynamics and Thermodynamics of Compressible Fluid Flow*. Ronald Press Co., NY, 1953-54. QA911 .S497 (Out of print). 10

J. Shepherd. Chemical kinetics of hydrogen-air-diluent detonations. In *International Colloquium on Dynamics of Explosions and Reactive Systems (10th : 1985 : Berkeley, Calif.)*, volume 106 of *Progress in Astronautics and Aeronautics*, pages 263–293. AIAA, 1986. 7, 33, 34

J. E. Shepherd. Pressure loads and structural response of the BNL high-temperature detonation tube. Technical Report A-3991, Brookhaven National Laboratory, January 1992. 72 pp. 29

J.E. Shepherd. Detonation waves and propulsion. In J. Buckmaster, T.L. Jackson, and A. Kumar, editors, *Combustion in High-Speed Flows*, pages 373–420. Kluwer, 1994. 6

J.E. Shepherd, A. Teodorcyzk, R. Knystautas, and J.H. Lee. Shock waves produced by reflected detonations. *Progress in Astronautics and Aeronautics*, 134:244–264, 1991. 22, 59

Ames Research Staff. Equations, tables, and charts for compressible flow. Technical Report TR 1135, NACA, 1953. 52

K. I. Stanyukovich. *Unsteady motion of continuous media*. Pergamon Press, 1960. QC168 .S813 1960. 59

G. I. Taylor. The dynamics of the combustion products behind plane and spherical detonation fronts in explosives. *Proc. Roy. Soc.*, A200:235–247, 1950. 24

P. A. Thompson. *Compressible Fluid Dynamics*. McGraw-Hill, New York, 1972. Out of print from McGraw-Hill, but reprinted privately and available from the Rensselaer Union Bookstore, RPI, Troy, NY. TEL 518 276 6555. 6, 7, 10, 16

P. A. Thompson. *Compressible–Fluid Dynamics*. Rensselaer Polytechnic Institute, 1988. 43

Philip A. Thompson. A fundamental derivative in gasdynamics. *The Physics of Fluids*, 14(9):1843–1849, 1971. 71

V. G. Vincenti and C. H. Kruger. *Introduction to Physical Gas Dynamics*. Wiley, 1965. QC168 .V55 (Reprinted by R.E. Kreiger). 6, 15

J. von Neumann. Theory of detonation waves. In A. J. Taub, editor, *John von Neumann, Collected Works*. Macmillan, New York, 1942. 9

E. Wintenberger and J. E. Shepherd. The stagnation hugoniot analysis for steady combustion waves in propulsion systems. *Journal of Propulsion and Power*, 22(4):835–844, 2006. 71

W. W. Wood and J. G. Kirkwood. Present status of detonation theory. *J. Chem. Phys.*, 29:957, 1959. see Kirkwood (1967) for a reprint. 19

Ya. B. Zel'dovich. On the theory of the propagation of detonation in gaseous systems. *Zhurnal Experimentalnoi i Teoreticheskoi Fiziki*, 10:542–568, 1940. Available in translation as NACA TM-1261. 9

Ya. B. Zel'dovich and A. S. Kompaneets. *Theory of Detonation*. Academic Press, NY, 1960. English translation of original Russian. 24

Ya. B. Zel'dovich and Yu. P. Raizer. *Physics of Shock Waves and High-Temperature Hydrodynamic Phenomena*, volume 1 and 2. Wiley, NY, 1966. 10

F. J. Zeleznik and S. Gordon. An analytical investigation of three general methods for of calculating chemical equilibrium compositions. Technical Note TN-473, NASA, 1960. 9

F. J. Zeleznik and S. Gordon. Calculation of detonation parameters and the effect of independent parameters on gaseous detonation. *ARS Journal*, pages 606–615, 1961. 10

F. J. Zeleznik and S. Gordon. A general IBM 704 or 7090 computer program for computation of chemical equilibrium compositions, rocket performance and chapman-jouguet detonations. Technical Note TN-1454, NASA, 1962. 10

A Shock Jump Conditions for a Perfect Gas

The perfect gas has a constant heat capacity and we assume a fixed composition across the shock, so that for both upstream and downstream states, the equation of state is given by

$$P = \rho R T \tag{144}$$

$$h = c_P T \tag{145}$$

The classical studies of gas dynamics use this model extensively since the jump conditions and many other problems can be solved exactly. A compendium of exact solutions for perfect gases is given in Staff (1953).

A.1 Incident Shock Waves

The standard approach in classical gas dynamics is to express the solutions in terms of nondimensional variables and parameters. Instead of the specific heat capacity, the gas is characterized by the nondimensional parameter $\gamma = c_P/c_v$, the ratio of specific heats. Instead of velocities, the Mach number is used

$$M = \text{w}/a \tag{146}$$

For a perfect gas, because the specific heat is constant, there is a single sound speed.

$$a = \sqrt{\gamma R T} \tag{147}$$

The conservation relationships can be analytically solved in terms of the jump or change in properties,

$$[F] = F_2 - F_1 \,, \tag{148}$$

across the wave

$$\frac{[P]}{P_1} = \frac{2\gamma}{\gamma + 1} \left(M_1^2 - 1 \right) \tag{149}$$

$$\frac{[\text{w}]}{a_1} = -\frac{2}{\gamma + 1} \left(M_1 - \frac{1}{M_1} \right) \tag{150}$$

$$\frac{[v]}{v_1} = -\frac{2}{\gamma + 1} \left(1 - \frac{1}{M_1^2} \right) \tag{151}$$

$$\frac{[s]}{R} = -\ln \left(\frac{P_{t2}}{P_{t1}} \right) \tag{152}$$

$$\frac{P_{t2}}{P_{t1}} = \frac{1}{\left(\dfrac{2\gamma}{\gamma + 1} M_1^2 - \dfrac{\gamma - 1}{\gamma + 1} \right)^{\frac{1}{\gamma - 1}}} \left(\frac{\dfrac{\gamma + 1}{2} M_1^2}{1 + \dfrac{\gamma - 1}{2} M_1^2} \right)^{\frac{\gamma}{\gamma - 1}} \tag{153}$$

Using the transformation from wave-fixed to laboratory frame, we have

$$[\text{w}] = -[\text{u}] \tag{154}$$

so that

$$\frac{[\text{u}]}{a_1} = \frac{2}{\gamma + 1} \left(M_1 - \frac{1}{M_1} \right) \tag{155}$$

$$\tag{156}$$

We can also analytically express the shock adiabat or Hugoniot

$$\frac{P_2}{P_1} = \frac{\dfrac{\gamma+1}{\gamma-1} - \dfrac{v_2}{v_1}}{\dfrac{\gamma+1}{\gamma-1}\dfrac{v_2}{v_1} - 1} \tag{157}$$

or alternatively

$$\frac{P_2}{P_1} = 1 + \frac{2\gamma}{\gamma+1}\left(M_1^2 - 1\right) \tag{158}$$

$$= \frac{2\gamma}{\gamma+1}M_1^2 - \frac{\gamma-1}{\gamma+1} \tag{159}$$

$$\frac{\rho_2}{\rho_1} = \frac{\gamma+1}{\gamma-1+\dfrac{2}{M_1^2}} \tag{160}$$

$$M_2^2 = \frac{M_1^2 + \dfrac{2}{\gamma-1}}{\dfrac{2\gamma}{\gamma-1}M_1^2 - 1} \tag{161}$$

Another useful equation is *Prandtl's relation*,

$$\mathrm{w}_1 \mathrm{w}_2 = a^{*2}, \tag{162}$$

where a^* is the sound speed at a sonic point obtained in a fictitious isentropic process in the upstream flow.

$$a^* = \sqrt{2\frac{\gamma-1}{\gamma+1}h_t}, \qquad h_t = h + \frac{\mathrm{w}^2}{2} \tag{163}$$

A.2 Reflected Shock Waves

Several relationships for reflected waves can be derived by based on the fact that fluid adjacent to a stationary surface must be stationary. Figure 8 (Section 3.6) illustrates a possible geometry for wave reflection. The above condition requires that

$$\mathrm{u}_1 = \mathrm{u}_3 = 0 . \tag{164}$$

Therefore, the jump in velocity across the reflected wave,

$$[\mathrm{u}]_R = \mathrm{u}_3 - \mathrm{u}_2 = -\mathrm{u}_2 \tag{165}$$

is the exact opposite of the jump in velocity across the incident wave,

$$[\mathrm{u}]_I = \mathrm{u}_2 - \mathrm{u}_1 = \mathrm{u}_2 , \tag{166}$$

or

$$[\mathrm{u}]_I = -[\mathrm{u}]_R \tag{167}$$

The Rayleigh line equation (16) can be expressed in terms of jumps in properties, i.e.

$$[\mathrm{u}]^2 = -[P][v] \tag{168}$$

Now we relate the Rayleigh line of each wave

$$[P]_R[v]_R = [P]_I[v]_I . \tag{169}$$

53

Pressure Jump

Using the perfect gas Hugoniot relationship (157) for both the incident and reflected waves, we can eliminate the volume jumps and find a relationship between the pressure ratios across the incident and reflected waves. Using the notation in Section 3.6,

$$\frac{P_3}{P_2} = \frac{(3\gamma - 1)\dfrac{P_2}{P_1} - (\gamma - 1)}{(\gamma - 1)\dfrac{P_2}{P_1} + (\gamma + 1)} \tag{170}$$

The pressure ratio across the reflected shock is always less than across the incident shock and has a limiting value for large incident shock speeds of

$$\frac{P_3}{P_2} \to \frac{3\gamma - 1}{\gamma - 1} \quad \text{as} \quad \frac{P_2}{P_1} \to \infty \tag{171}$$

On the other hand, for small incident shock speeds, the pressure ratio across the reflected and incident shock waves approaches 1. In this limit, if we expand about the initial state,

$$\frac{P_3}{P_2} - 1 = \frac{P_2}{P_1} - 1 - \frac{\gamma - 1}{2\gamma}\left(\frac{P_2}{P_1} - 1\right)^2 + \left(\frac{\gamma - 1}{2\gamma}\right)^2 \left(\frac{P_2}{P_1} - 1\right)^3 + \dots , \tag{172}$$

and retain only the first order terms of the series, we obtain the acoustic result, i.e. the pressure rise across the reflected shock is equal to the rise across the incident shock. In other words, the total pressure rise $(P_3 - P_1)$ is twice the pressure rise due to the incident wave $(P_2 - P_1)$.

$$P_3 - P_1 \approx 2\,(P_2 - P_1) \quad \text{for acoustic waves} \tag{173}$$

Mach Number

Similarly, we can determine an expression for the reflected shock Mach number. First, we define the incident and reflected shock Mach numbers.

$$M_I = \frac{\mathrm{U}_I}{a_1} \tag{174}$$

$$M_R = \frac{\mathrm{U}_R + \mathrm{u}_2}{a_2} . \tag{175}$$

Then, using the velocity jump relation (155) and recalling (164), we relate the two Mach numbers

$$M_R - \frac{1}{M_R} = \frac{a_1}{a_2}\left(M_I - \frac{1}{M_I}\right) . \tag{176}$$

The left-hand side is a function α of the incident shock speed

$$\alpha = \frac{a_1}{a_2}\left(M_I - \frac{1}{M_I}\right) . \tag{177}$$

For a specified incident shock Mach number, we can compute α and find the reflected shock Mach number by solving the resulting quadratic equation

$$M_R = \frac{\alpha + \sqrt{\alpha^2 + 4}}{2} . \tag{178}$$

From the incident shock jump conditions, α ranges between zero and a maximum value which is only a function of γ. Taking the limit as $M_I \to \infty$, we find that

$$\alpha_{max} = \frac{\gamma + 1}{\sqrt{2\gamma(\gamma - 1)}} \tag{179}$$

which means that the reflected shock Mach number ranges betweem one and a maximum value of

$$M_{R,max} = \sqrt{\frac{2\gamma}{\gamma - 1}} \ . \tag{180}$$

Enthalpy

For strong incident shock waves, we can derive from the reflected shock relationships (46)-(48), the approximate results

$$h_2 \approx h_1 + \frac{1}{2}U_I^2 \tag{181}$$

$$h_3 \approx h_2 + \frac{1}{2}U_I^2 \tag{182}$$

so that the enthalpy behind a strong reflected shock wave is

$$h_3 \approx h_1 + U_I^2 \tag{183}$$

which is very useful in estimations of the reservoir enthalpy in the reflected shock tunnels.

B   Detonation Waves in Perfect Gases

The jump conditions given in Section 3.1 are

$$\rho_1 w_1 = \rho_2 w_2 \tag{184}$$

$$P_1 + \rho_1 w_1^2 = P_2 + \rho_2 w_2^2 \tag{185}$$

$$h_1 + \frac{w_1^2}{2} = h_2 + \frac{w_2^2}{2} \tag{186}$$

$$s_2 \geq s_1 \tag{187}$$

Perfect-Gas, 2-γ Model

For a detonation, we assume two perfect gases, reactant (1) and product (2), with different specific heats and molecular weights. In this case, there will be two gas constants. We also assume an energy release, q, due to exothermic chemistry. Now our thermodynamic relations are

$$h_1 = c_{P1} T \tag{188}$$

$$h_2 = c_{P2} T - q \tag{189}$$

$$P_1 = \rho_1 R_1 T_1 \tag{190}$$

$$P_2 = \rho_2 R_2 T_2 \tag{191}$$

$$c_{P1} = \frac{\gamma_1 R_1}{\gamma_1 - 1} \tag{192}$$

$$c_{P2} = \frac{\gamma_2 R_2}{\gamma_2 - 1} \tag{193}$$

We substitute these into the jump conditions to yield:

$$\frac{P_2}{P_1} = \frac{1 + \gamma_1 M_1^2}{1 + \gamma_2 M_2^2} \tag{194}$$

$$\frac{v_2}{v_1} = \frac{\gamma_2 M_2^2}{\gamma_1 M_1^2} \frac{1 + \gamma_1 M_1^2}{1 + \gamma_2 M_2^2} \tag{195}$$

$$\frac{T_2}{T_1} = \frac{\gamma_1 R_1}{\gamma_2 R_2} \frac{\dfrac{1}{\gamma_1 - 1} + \dfrac{1}{2} M_1^2 + \dfrac{q}{a_1^2}}{\dfrac{1}{\gamma_2 - 1} + \dfrac{1}{2} M_2^2} \tag{196}$$

Additionally, the entropy variation along adiabat is

$$ds = \frac{1}{2T} (v_1 - v)^2 \, d(\rho w)^2 \tag{197}$$

B.1   Chapman-Jouguet Conditions

At the CJ point, the isentrope, and Hugoniot and Rayleigh line are all tangent.

$$\frac{P_{CJ} - P_1}{v_{CJ} - v_1} = \left. \frac{\partial P}{\partial v} \right)_{\mathcal{H}} = \left. \frac{\partial P}{\partial v} \right)_s \tag{198}$$

which implies that the product velocity is *sonic relative to the wave*

$$w_{2,CJ} = a_2 \tag{199}$$

Jouguet's Rule

$$\frac{w^2 - a^2}{v^2} = \left[1 - \frac{G}{2v}(v_1 - v)\right]\left[\left(\frac{\partial P}{\partial v}\right)_{Hug} - \frac{\Delta P}{\Delta v}\right] \tag{200}$$

where G is the Grúniesen coefficient.

The flow downstream of a detonation is subsonic relative to the wave for points above the CJ state and supersonic for states below.

Using these conditions and the perfect-gas, 2-γ model, and the Mach number for the upper CJ (detonation) point

$$M_{CJ} = \sqrt{\mathcal{H} + \frac{(\gamma_1 + \gamma_2)(\gamma_2 - 1)}{2\gamma_1(\gamma_1 - 1)}} + \sqrt{\mathcal{H} + \frac{(\gamma_2 - \gamma_1)(\gamma_2 + 1)}{2\gamma_1(\gamma_1 - 1)}} \tag{201}$$

where the parameter $\mathcal{H}$ is the nondimensional energy release

$$\mathcal{H} = \frac{(\gamma_2 - 1)(\gamma_2 + 1)q}{2\gamma_1 R_1 T_1} \tag{202}$$

Other quantities of interest include

- CJ pressure

$$\frac{P_{CJ}}{P_1} = \frac{\gamma_1 M_{CJ}^2 + 1}{\gamma_2 + 1} \tag{203}$$

- CJ density

$$\frac{\rho_{CJ}}{\rho_1} = \frac{\gamma_1(\gamma_2 + 1)M_{CJ}^2}{\gamma_2(1 + \gamma_1 M_{CJ}^2)} \tag{204}$$

- CJ temperature

$$\frac{T_{CJ}}{T_1} = \frac{P_{CJ}}{P_1}\frac{R_1 \rho_1}{R_2 \rho_{CJ}} \tag{205}$$

B.2 Strong detonation approximation

A useful limit for approximate analysis is $M_{CJ} \gg 1$. This simplifies the expressions for the CJ properties (203)-(205).

$$U_{CJ} \approx \sqrt{2(\gamma_2^2 - 1)q} \tag{206}$$

$$\rho_{CJ} \approx \frac{\gamma_2 + 1}{\gamma_2}\rho_1 \tag{207}$$

$$P_{CJ} \approx \frac{1}{\gamma_2 + 1}\rho_1 U_{CJ}^2 \tag{208}$$

$$a_{CJ} \approx \frac{\gamma_2 U_{CJ}}{\gamma_2 + 1} \tag{209}$$

$$u_{CJ} \approx \frac{U_{CJ}}{\gamma_2 + 1} \tag{210}$$

B.3 Reflection of Detonation

A detonation wave incident on a rigid surface will reflect as a shock wave which propagates into the detonation products. The computation of the properties behind the reflected wave proceed in the same fashion as with the previous discussion for shock waves (Appendix A.2). When we compare the reflection of a detonation wave (traveling at CJ velocity) with a nonreactive shock wave of the same speed, we find that the pressure behind the resulting reflected shock wave is much higher in the case of the incident shock than the detonation.

This is because the momentum flux behind the shock wave is higher than that behind the detonation. The chemical energy release in the detonation increases the equilibrium post-incident-wave temperature and lowers the post-incident-wave pressure, density, and particle velocity compared to a shock wave of the same speed.

demo_CJ_and_shock_state.m demonstrates how to compute the following four states.

- CJ state: equilibrium behind a CJ detonation

- Frozen post-reflected-shock state resulting from reflection of a CJ detonation

- Frozen post-incident-shock state behind a shock traveling at the CJ speed

- Frozen post-reflected-shock state resulting from reflection of a frozen shock wave

for stoichiometric hydrogen-air mixtures.

CJ state

```
CJ speed 1968. (m/s)
CJ pressure 1.54 (MPa)
CJ temperature 2940. (K)
CJ density 1.511 (kg/m3)
w2 (wave frame) 1092. (m/s)
u2 (lab frame) 875.7 (m/s)
a2 (frozen) 1127. (m/s)
a2 (equilibrium) 1091. (m/s)
gamma2 (frozen) 1.242 (m/s)
gamma2 (equilibrium) 1.163 (m/s)
```

Reflected shock (equilibrium) from CJ detonation

```
Reflected wave speed 782.9 (m/s)
Reflected shock pressure 3.74 (MPa)
Reflected shock temperature 3297. (K)
Reflected shock density 3.200 (kg/m3)
```

Incident Shock (frozen) at CJ speed

```
shock speed 1968. (m/s)
shock pressure 2.74 (MPa)
shock temperature 1530. (K)
shock density 4.506 (kg/m3)
w2 (wave frame) 366.1 (m/s)
u2 (lab frame) 1602. (m/s)
a2 (frozen) 895.8 (m/s)
gamma2 (frozen) 1.319 (m/s)
```

Reflected shock (frozen)

```
Shock speed 1968. (m/s)
Reflected wave speed 599.4 (m/s)
Reflected shock pressure 18.63 (MPa)
Reflected shock temperature 2832. (K)
Reflected shock density 16.55 (kg/m3)
```

In this example, the pressure behind the reflection of a frozen shock wave is 18.6 MPa as compared with 3.74 MPa behind the reflection of the detonation. The ratio of reflected to incident post-wave pressure is 6.97 for the frozen incident shock wave and only 2.46 for the detonation case. The ratio computed for the detonation is found to be very insensitive to the mixture composition with both computed and measured values being close to 2.5 (see Shepherd et al., 1991).

Following the derivation of Stanyucovich and Zel'dovich (Stanyukovich, 1960, p. 372-372), the ratio of post-reflected to post-incident pressure can be approximately computed for detonations using ideas similar to those for incident shock waves together with the strong detonation approximation (Appendix B.2). Using the notation of Section 3.6, the Rayleigh line for the detonation can be written:

$$\mathrm{u}_2^2 = (P_2 - P_1)(v_1 - v_2) \tag{211}$$

and applying the strong detonation approximation (210), this is

$$\mathrm{u}_2^2 \approx \frac{P_2 v_1}{\gamma + 1} \tag{212}$$

where we have dropped the subscripts on γ and assumed it has the same value for state 2 and 3. For the reflected shock wave, the Rayleigh line is

$$\mathrm{u}_2^2 = (P_3 - P_2)(v_2 - v_3) \ . \tag{213}$$

We can eliminate v_3 by using the following form of the Hugoniot relation

$$\frac{v_3}{v_2} = \frac{(\gamma + 1)P_3 + (\gamma - 1)P_2}{(\gamma - 1)P_3 + (\gamma + 1)P_2} \ . \tag{214}$$

The volumes v_2 and v_1 can be eliminated by using the strong detonation relation (207)

$$v_2 \approx \frac{\gamma v_1}{\gamma + 1} \tag{215}$$

which results in a quadratic for the pressure ratio P_3/P_2. The solution to the quadratic is

$$\frac{P_3}{P_2} = \frac{5\gamma + 1 + \sqrt{17\gamma^2 + 2\gamma + 1}}{4\gamma} \ . \tag{216}$$

For values of γ between 1 and 5/3 (realistic for gases), this approximate formula give values of the pressure ratio between 2.4 and 2.5. Despite the very rough nature of the strong detonation approximation, the resulting values are in reasonable agreement with detailed computations and experimental data as discussed in Shepherd et al. (1991).

C Initial Velocity as a Function of Density Ratio

C.1 Derivation

We will use the following notation for partial derivatives evaluated at a specific state.

$$\left(\frac{\partial f}{\partial x}\right)_1 = f_{1,x} \tag{217}$$

$$\left(\frac{\partial^2 f}{x^2}\right)_1 = f_{1,xx} \tag{218}$$

where f is a function of x and 1 is the state where we evaluate the derivative. Also if we are holding y constant, where f is also a function of y, we will express that as

$$\left(\frac{\partial f}{\partial x}\right)_y = (f_{,x})_y \tag{219}$$

Recall

- Rayleigh Line

$$P - P_1 = -\left(\frac{w_1}{v_1}\right)^2 (v - v_1) \tag{220}$$

- Hugoniot

$$h - h_1 = (P - P_1)\frac{(v + v_1)}{2} \tag{221}$$

Now we find the Taylor expansion of P about P_2 along the Hugoniot.

$$P = P_2 + P_{2\mathcal{H},v}\delta v + \frac{1}{2}P_{2\mathcal{H},vv}(\delta v)^2 + ... \tag{222}$$

We want an equation of the form

$$\delta w_1 = C(\delta v)^n \tag{223}$$

that explains how the curve $w_1(v_2/v_1)$ behaves near the post-shock state, so we perturb the system from this state, state 2, where w_1^* is the specific value of w_1 that produces the chosen state 2.

$$v = v_2 + \delta v \tag{224}$$
$$w_1 = w_1^* + \delta w_1 \tag{225}$$

The equation of the Rayleigh line (220) becomes

$$P - P_1 = -\frac{1}{v_1^2}(w_1 + \delta w_1)^2((v_2 + \delta v) - v_1) \tag{226}$$

and combined with the Hugoniot pressure expansion (222)

$$(P_2 - P_1) + P_{2\mathcal{H},v}\delta v + \frac{1}{2}P_{2\mathcal{H},vv}(\delta v)^2 + ...$$
$$= -\frac{1}{v_1^2}(w_1^{*2} + 2w_1^*\delta w_1 + (\delta w_1)^2)(v_2 + \delta v - v_1) \tag{227}$$

Now we can group terms in powers of δv

- Zero Order

$$(P_2 - P_1) = -\frac{\text{w}_1^{*2}}{v_1^2}(v_2 - v_1) \tag{228}$$

Because this is (220) evaluated at state 2, these terms cancel.

- Higher Order

$$P_{2\mathcal{H},v} + \frac{1}{2}P_{2\mathcal{H},vv}(\delta v)^2 + ... = -\frac{\text{w}_1^{*2}}{v_1^2} - \frac{1}{v_1^2}(2\text{w}_1^*\delta\text{w}_1 + (\delta\text{w}_1)^2)(v_2 + \delta v - v_1) \tag{229}$$

It is important to remember that the derivatives of pressure are evaluated along the Hugoniot so $P_{2\mathcal{H},v}$ is the slope of the equilibrium Hugoniot.

C.2   CJ Point Analysis

From (220), the slope of the Rayleigh line is

$$-\frac{\text{w}_1^2}{v_1^2} \tag{230}$$

which is

$$-\frac{U_{CJ}^2}{v_1^2} \tag{231}$$

in the CJ case. At the CJ point, the Rayleigh line and the Hugoniot are tangent (i.e. have the same slope) so the slope of the Hugoniot, $P_{2\mathcal{H},v}$, is the equal to the slope of the Rayleigh line. Now it is clear that the first order terms of (229)

$$P_{2\mathcal{H},v} = -\frac{\text{w}_1^{*2}}{v_1^2} = -\frac{U_{CJ}^2}{v_1^2} \tag{232}$$

also cancel. The remaining higher order terms equation is

$$\frac{1}{2}P_{2\mathcal{H},vv}(\delta v)^2 + ... = -\frac{1}{v_1^2}(2\text{w}_1^*\delta\text{w}_1 + (\delta\text{w}_1)^2)(v_2 + \delta v - v_1) \tag{233}$$

and if we only retain the lowest order term on each side, the equation simplifies to

$$\frac{v_1^2}{2}P_{2\mathcal{H},vv}(\delta v)^2 = -\delta\text{w}_1[2\text{w}_1^*(v_2 - v_1)] \tag{234}$$

Therefore in the CJ case, (227) reduces to the form (223) we want

$$\delta\text{w}_1 = \frac{\text{w}_1^*}{4(P_2 - P_1)}P_{2\mathcal{H},vv}(\delta v)^2 \tag{235}$$

C.3   Derivatives of Pressure

It would be convenient if we could express $P_{2\mathcal{H},vv}$ in terms of quantities that we can measure. We can use (221) to accomplish this. We would like to express enthalpy as a function of pressure and specific volume: $h(P, v)$

$$h(P, v) = h_2 + [h_{2,P}dP + h_{2,v}dv] + \frac{1}{2}\left[h_{2,PP}dP^2 + 2h_{2,Pv}dPdv + h_{2,vv}dv^2\right] \tag{236}$$

To evaluate $P_{2\mathcal{H},vv}$, we will look again at states near state 2. Equation 236 close to state 2 is

$$h(P,v) = h_2 + [h_{2,P}(P - P_2) + h_{2,v}(v - v_2)] +$$
$$\frac{1}{2}\left[h_{2,PP}(P - P_2)^2 + 2h_{2,Pv}(P - P_2)(v - v_2) + h_{2,vv}(v - v_2)^2\right]$$

(237)

To simplify this equation, substitute $v - v_2 = \delta v$.

$$h(P,v) = h_2 + [h_{2,P}(P - P_2) + h_{2,v}\delta v] +$$
$$\frac{1}{2}\left[h_{2,PP}(P - P_2)^2 + 2h_{2,Pv}(P - P_2)\delta v + h_{2,vv}(\delta v)^2\right]$$

(238)

Now we can group terms

$$h(P,v) = [h_2] + \delta v\,[h_{2,v}] + (\delta v)^2\left[\frac{h_{2,vv}}{2}\right] + (P - P_2)\,[h_{2,P} + \delta v(h_{2,Pv})] + (P - P_2)^2\left[\frac{h_{2,PP}}{2}\right]$$

(239)

Substituting (239) the Hugoniot equation 221 gives

$$[h_2 - h_1] + \delta v\,[h_{2,v}] + (\delta v)^2\left[\frac{h_{2,vv}}{2}\right] + (P - P_2)\,[h_{2,P} + \delta v(h_{2,Pv})] + (P - P_2)^2\left[\frac{h_{2,PP}}{2}\right]$$
$$= [(P - P_2) + (P_2 - P_1)]\left(\frac{v_1 + v_2}{2} + \frac{\delta v}{2}\right)$$

(240)

If we substitute the Taylor expansion for Hugoniot pressure (222 this equation becomes

$$\left[(h_2 - h_1) - (P_2 - P_1)\frac{v_2 + v_1}{2}\right] + \delta v\left[h_{2,v} - \frac{P_2 - P_1}{2}\right] + (\delta v)^2\left[\frac{h_{2,vv}}{2}\right]$$
$$= \left(P_{2\mathcal{H},v}\delta v + \frac{1}{2}P_{2\mathcal{H},vv}(\delta v)^2\right)\left[\frac{v_2 + v_1}{2} - h_{2,P} + \delta v\left(\frac{1}{2} - h_{2,Pv}\right)\right] -$$
$$\left(P_{2\mathcal{H},v}^2(\delta v)^2 + P_{2\mathcal{H},v}P_{2\mathcal{H},vv}(\delta v)^3 + \frac{1}{4}P_{2\mathcal{H},vv}^2(\delta v)^4\right)\left[\frac{h_{2,PP}}{2}\right]$$

(241)

As before we can group powers of δv

- Zero Order
$$(h_2 - h_1) - (P_2 - P_1)\frac{v_2 + v_1}{2} = 0$$

(242)

This is exactly the Hugoniot curve expression (221) evaluated at state 2. Therefore, these terms cancel.

- First Order
$$h_{2,v} - \frac{P_2 - P_1}{2} = P_{2\mathcal{H},v}\left(\frac{v_2 + v_1}{2} - h_{2,P}\right)$$

(243)

so

$$P_{2\mathcal{H},v} = \left[h_{2,v} - \frac{P_2 - P_1}{2}\right]\left[\frac{2}{v_2 + v_1 - 2h_{2,P}}\right]$$

(244)

- Higher Order

$$(\delta v)^2 \frac{h_{2,vv}}{2} = (\delta v)^2 P_{2\mathcal{H},v} \left(\frac{1}{2} - h_{2,Pv}\right) + \frac{(\delta v)^2}{2} P_{2\mathcal{H},vv} \left[\frac{v_2 + v_1}{2} - h_{2,P} + \delta v \left(\frac{1}{2} - h_{2,Pv}\right)\right]$$
$$- \left(P_{2\mathcal{H},v}^2 (\delta v)^2 + P_{2\mathcal{H},v} P_{2\mathcal{H},vv} (\delta v)^3 + \frac{1}{4} P_{2\mathcal{H},vv}^2 (\delta v)^4\right) \left[\frac{h_{2,PP}}{2}\right] \tag{245}$$

If we only keep the lowest order term on each side, the equation simplifies to

$$\frac{h_{2,vv}}{2} = P_{2\mathcal{H},v} \left(\frac{1}{2} - h_{2,Pv}\right) + \frac{1}{2} P_{2\mathcal{H},vv} \left[\frac{v_2 + v_1}{2} - h_{2,P}\right] - P_{2\mathcal{H},v}^2 \left[\frac{h_{2,PP}}{2}\right] \tag{246}$$

Solving for $P_{2\mathcal{H},vv}$, we get

$$P_{2\mathcal{H},vv} = \left[h_{2,vv} + P_{2\mathcal{H},v}^2 (h_{2,PP}) + P_{2\mathcal{H},v} (2h_{2,Pv} - 1)\right] \left[\frac{2}{v_2 + v_1 - 2h_{2,P}}\right] \tag{247}$$

C.4 Thermodynamic Analysis

We would like to express the derivatives of enthalpy as functions of quantities that we can determine so that we can evaluate the derivatives of pressure. To determine these derivatives of enthalpy we need two fundamental equations as well as the definitions of the Grüneisen Coefficient, G, and the equilibrium sound speed, a_{eq}.

$$dh = Tds + vdP \tag{248}$$
$$Tds = de + Pdv \tag{249}$$
$$G = v\,(P_{,e})_v \tag{250}$$
$$a_{eq}^2 = -v^2\,(P_{,v})_s \tag{251}$$

First we will evaluate the first order partial derivatives of enthalpy

$$(h_{,P})_v = (e_{,P} + (Pv)_{,P})_v \tag{252}$$
$$= (e_{,P})_v + v \tag{253}$$
$$= \frac{v}{G} + v \tag{254}$$
$$(h_{,P})_v = v\frac{G + 1}{G} \tag{255}$$

Similarly

$$(h_{,v})_P = (Ts_{,v} + vP_{,v})_P \tag{256}$$
$$= (Ts_{,v})_P \tag{257}$$
$$= -(Ts_{,P})_v\,(P_{,v})_s \tag{258}$$
$$= -(e_{,P})_v\,(P_{,v})_s \tag{259}$$
$$= -\left(\frac{v}{G}\right)\left(\frac{-a_{eq}^2}{v^2}\right) \tag{260}$$
$$(h_{,v})_P = \frac{a_{eq}^2}{v}\frac{1}{G} \tag{261}$$

To evaluate the second order partial derivatives of enthalpy, we need to take derivatives of the above expressions

$$(h_{,PP})_v = (v_{,P})_v \left(1 + \frac{1}{G}\right) - \frac{v}{G^2} (G_{,P})_v \tag{262}$$

$$(h_{,vv})_P = \frac{a_{eq}}{vG} \left(2 (a_{eq,v})_P - \frac{a_{eq}}{vG} (G + v (G_{,v})_P)\right) \tag{263}$$

$$\left([(h_{,P})_v]_{,v}\right)_P = (v_{,v})_P \left(1 + \frac{1}{G}\right) - \frac{v}{G^2} (G_{,v})_P \tag{264}$$

$$\left([(h_{,v})_P]_{,P}\right)_v = \frac{a_{eq}}{vG} \left(2 (a_{eq,P})_v - \frac{a_{eq}}{vG} (G (v_{,P})_v + v (G_{,P})_v)\right) \tag{265}$$

The mixed partials should be equivalent so

$$G + 1 + \left(\frac{a_{eq}^2}{vG} - \frac{v}{G}\right) (G_{,P})_v = -\frac{a_{eq}^2}{v^2} (v_{,P})_v + \frac{2a_{eq}}{v} (a_{eq,P})_v \tag{266}$$

Plugging in these expressions for derivatives of enthalpy into the derivatives of pressure gives

$$P_{2\mathcal{H},v} = \left[\frac{a_{2eq}^2}{v_2} \frac{1}{G_2} - \frac{P_2 - P_1}{2}\right] \left[\frac{2G_2}{G_2(v_1 - v_2) - 2v_2}\right] \tag{267}$$

$$\begin{aligned} P_{2\mathcal{H},vv} = &\frac{a_{2eq}}{v_2 G_2} \left[\frac{2G_2}{G_2(v_1 - v_2) - 2v_2}\right] \left[2 (a_{2eq,v})_P - \frac{a_{2eq}}{v_2 G_2} (G_2 (v_{2,P})_v + v_2 (G_{2,v})_P)\right] \\ &+ P_{2\mathcal{H},v}^2 \left[\frac{2G_2}{G_2(v_1 - v_2) - 2v_2}\right] \left[(v_{2,P})_v \left(1 + \frac{1}{G_2}\right) - \frac{v_2}{G_2^2} (G_{2,P})_v\right] \\ &+ P_{2\mathcal{H},v} \left[\frac{2G_2}{G_2(v_1 - v_2) - 2v_2}\right] [2h_{2,Pv} - 1] \end{aligned} \tag{268}$$

C.5   Perfect Gas Analysis

For a perfect gas, the specific heat is constant and the equation of state is given by

$$P = \rho RT \tag{269}$$
$$h = c_P T \tag{270}$$

The derivatives of enthalpy are

$$h_{,P} = \frac{\gamma}{\gamma - 1} v \tag{271}$$
$$h_{,v} = \frac{\gamma}{\gamma - 1} P \tag{272}$$
$$h_{,PP} = 0 \tag{273}$$
$$h_{,vv} = 0 \tag{274}$$
$$h_{,Pv} = \frac{\gamma}{\gamma - 1} \tag{275}$$

Plugging these derivatives of enthalpy into the derivatives of pressure (267)-(268), we get

$$P_{2\mathcal{H},v} = \left[\frac{\gamma}{\gamma-1} P_2 - \frac{P_2 - P_1}{2} \right] \left[\frac{2}{v_1 + v_2 - 2\frac{\gamma}{\gamma-1}v_2} \right] \tag{276}$$

$$= \left[P_1 + P_2 \frac{\gamma+1}{\gamma-1} \right] \left[\frac{\gamma-1}{v_1(\gamma-1) + v_2(\gamma+1)} \right]$$

$$P_{2\mathcal{H},vv} = \left[0 + 0 + P_{2\mathcal{H},v}\left(2\frac{\gamma}{\gamma-1} - 1 \right) \right] \left[\frac{2}{v_1 + v_2 - 2\frac{\gamma}{\gamma-1}v_2} \right] \tag{277}$$

$$= 2P_{2\mathcal{H},v}\left[\frac{\gamma+1}{\gamma-1} \right] \left[\frac{\gamma-1}{v_1(\gamma-1) + v_2(\gamma+1)} \right]^2$$

We can check the validity of (276)-(277) if we use the perfect gas expressions in the Hugoniot equation (221) directly, i.e.

$$\frac{\gamma}{\gamma-1}(Pv - P_1 v_1) = (P - P_1)\frac{(v + v_1)}{2} \tag{278}$$

which simplifies as follows

$$P_1 \left[\frac{(v + v_1)}{2} - v_1 \frac{\gamma}{\gamma-1} \right] = P \left[\frac{(v + v_1)}{2} - v \frac{\gamma}{\gamma-1} \right] \tag{279}$$

$$(P_1 v - P v_1) = (P_1 v_1 - P v)\left(\frac{\gamma+1}{\gamma-1} \right) \tag{280}$$

Now, we perturb the system as before and look at terms of the same order

$$P_1 \left[\frac{(v_2 + \delta v + v_1)}{2} - v_1 \frac{\gamma}{\gamma-1} \right] = \left(P_2 + P_{2\mathcal{H},v}\delta v + \frac{1}{2}P_{2\mathcal{H},vv}(\delta v)^2 \right) \tag{281}$$

$$\left[\frac{(v_2 + \delta v + v_1)}{2} - (v_2 + \delta v)\frac{\gamma}{\gamma-1} \right]$$

$$\left[P_1 \left(v_2 - v_1 \frac{\gamma+1}{\gamma-1} \right) \right] + \delta v = \left(P_2 + P_{2\mathcal{H},v}\delta v + \frac{1}{2}P_{2\mathcal{H},vv}(\delta v)^2 \right) \tag{282}$$

$$\left[\left(v_1 - v_2 \frac{\gamma+1}{\gamma-1} \right) - \delta v \left(\frac{\gamma+1}{\gamma-1} \right) \right]$$

- Zero Order

$$P_1 \left(v_2 - v_1 \frac{\gamma+1}{\gamma-1} \right) = P_2 \left(v_1 - v_2 \frac{\gamma+1}{\gamma-1} \right) \tag{283}$$

- First Order

$$1 = -P_2 \left(\frac{\gamma+1}{\gamma-1} \right) + P_{2\mathcal{H},v}\left(v_1 - v_2 \frac{\gamma+1}{\gamma-1} \right) \tag{284}$$

so

$$P_{2\mathcal{H},v} = \left[1 + P_2 \left(\frac{\gamma+1}{\gamma-1} \right) \right] \left[\frac{\gamma-1}{v_1(\gamma-1) - v_2(\gamma+1)} \right] \tag{285}$$

This is exactly (276).

65

- Higher Order

$$0 = -(\delta v)^2 P_{2\mathcal{H},v} \left(\frac{\gamma + 1}{\gamma - 1} \right) +$$
$$\frac{(\delta v)^2}{2} P_{2\mathcal{H},vv} \left[\left(v_1 - v_2 \frac{\gamma + 1}{\gamma - 1} \right) - \delta v \left(\frac{\gamma + 1}{\gamma - 1} \right) \right] \tag{286}$$

If we only keep the lowest order term on each side, the equation simplifies to

$$0 = -P_{2\mathcal{H},v} \left(\frac{\gamma + 1}{\gamma - 1} \right) + \frac{P_{2\mathcal{H},vv}}{2} \left(v_1 - v_2 \frac{\gamma + 1}{\gamma - 1} \right) \tag{287}$$

Solving for $P_{2\mathcal{H},vv}$

$$P_{2\mathcal{H},vv} = 2 P_{2\mathcal{H},v} \left[\frac{\gamma + 1}{\gamma - 1} \right] \left[\frac{\gamma - 1}{v_1(\gamma - 1) - v_2(\gamma + 1)} \right] \tag{288}$$

We see that this expression for $P_{2\mathcal{H},vv}$ is identical to (277) which verifies that the general solution reduces correctly to the perfect gas model solution.

D Thermodynamics of the Hugoniot

Using thermodynamics, the jump conditions, and the Hugoniot equation, we can determine if the flow is subsonic or supersonic behind the wave and also the nature of the entropy extremum at the CJ points.

D.1 Jouguet's rule

The starting point of this discussion is the variation of entropy on the Hugoniot that was derived from the Fundamental Relation of Thermodynamics and the energy version of the Hugoniot equation 19.

$$\left(\frac{\partial s}{\partial v}\right)_{\mathcal{H}} = \frac{\Delta v}{2T}\left[\frac{\Delta P}{\Delta v} - \left(\frac{\partial P}{\partial v}\right)_{\mathcal{H}}\right] \tag{289}$$

This expression gives the entropy change in terms of the difference between the slope of the Hugoniot and Rayleigh line. In order to draw conclusions about the flow Mach number, we need to reformulate this in terms of the slope of the isentropes and the Rayleigh line. The relationship of the Hugoniot to the isentropes requires determining the slope of the Hugoniot. This can be accomplished by expanding internal energy $e(P,v)$ as a function of pressure and volume.

$$de = \left(\frac{\partial e}{\partial P}\right)_v dP + \left(\frac{\partial e}{\partial v}\right)_P dv \tag{290}$$

Using thermodynamic relationships, we can write the coefficients in terms of the Grüniesen coefficient G

$$G = v\left(\frac{\partial P}{\partial e}\right)_v \tag{291}$$

$$= -\frac{v}{T}\left(\frac{\partial T}{\partial v}\right)_s \tag{292}$$

$$de = \frac{v}{G}dP - \left[\frac{v}{G}\left(\frac{\partial P}{\partial v}\right)_s + P\right]dv \tag{293}$$

Equating this to the expression obtained by differentiating the Hugoniot and solving for the slope, we have

$$\left(\frac{\partial P}{\partial v}\right)_{\mathcal{H}} = \frac{\left(\frac{\partial P}{\partial v}\right)_s + \frac{G}{2v}\Delta P}{1 + \frac{G}{2v}\Delta v} \tag{294}$$

An independent relationship between the Hugoniot and isentrope slopes can be obtained by expanding $P(v,s)$ on the Hugoniot

$$\left(\frac{\partial P}{\partial v}\right)_{\mathcal{H}} = \left(\frac{\partial P}{\partial v}\right)_s + \left(\frac{\partial P}{\partial s}\right)_v\left(\frac{\partial s}{\partial v}\right)_{\mathcal{H}} \tag{295}$$

This can be simplified by using the thermodynamic relations to read

$$\left(\frac{\partial P}{\partial v}\right)_{\mathcal{H}} = \left(\frac{\partial P}{\partial v}\right)_s + G\frac{T}{v}\left(\frac{\partial s}{\partial v}\right)_{\mathcal{H}} \tag{296}$$

Note that the unsubscripted variable v, G, and the slope of the isentrope are to be evaluated at the downstream conditions (2) in this equation. Equation (296) indicates how the sign of G and the rate of change of entropy along the isentrope determines if the slope of the isentrope is larger or smaller than the slope of the Hugoniot. For substances with $G > 0$, the slope of the Hugoniot will be smaller (larger) than the slope of the

isentrope when the entropy derivative $(ds/dv)_{\mathcal{H}} < 0 \; (> 0)$. Shock waves in usual substances (see Menikoff and Plohr, 1989b) are compression waves

$$\Delta P > 0 \tag{297}$$

and have $G > 0$ and $(ds/dv)_{\mathcal{H}} < 0$, so that

$$\infty < \left(\frac{\partial P}{\partial v}\right)_{\mathcal{H}} < \left(\frac{\partial P}{\partial v}\right)_s < 0 \tag{298}$$

and there are no vertical asymptotes (see Hayes, 1960) so that the denominator does not vanish

$$1 + G\frac{\Delta v}{2v} > 0 \tag{299}$$

Combining (294) and (289) gives

$$\left(\frac{\partial s}{\partial v}\right)_{\mathcal{H}} = \frac{\Delta v}{2T}\left[\frac{\dfrac{\Delta P}{\Delta v} - \left(\dfrac{\partial P}{\partial v}\right)_s}{1 + G\dfrac{\Delta v}{2v}}\right] \tag{300}$$

which can also be written as

$$\left(\frac{\partial s}{\partial v}\right)_{\mathcal{H}} = \frac{\Delta v}{2Tv^2}\left[\frac{a^2 - \mathrm{w}^2}{1 + G\dfrac{\Delta v}{2v}}\right] \tag{301}$$

This illuminates out a crucial connection between the flow speed (subsonic vs supersonic) downstream of the shock, the Grüniesen parameter, and the variation of entropy along the Hugoniot. The denominator is positive for most substances since the slope of a realistic Hugoniot (294) is negative and is a continuous function of the volume. Equating the two expressions for the variation of entropy along the Hugoniot (289) and (301), we find

$$\frac{\Delta P}{\Delta v} - \left(\frac{\partial P}{\partial v}\right)_{\mathcal{H}} = \frac{1}{v^2}\frac{a^2 - \mathrm{w}^2}{1 + G\dfrac{\Delta v}{2v}} \tag{302}$$

This equation can be applied to the downstream state at any intersection point between the Rayleigh line and the Hugoniot. From the geometry of the Hugoniot and Rayleigh line shown in Fig. 4, we conclude that if the denominator of (302) is positive, the flow downstream (state 1) of a shock wave is subsonic.

The flow upstream of a shock is supersonic, $\mathrm{w}_1 > a_1$, since the isentrope and Hugoniot are tangent at the initial state (294) and from the geometry shown in Fig. 4, we have

$$\frac{\Delta P}{\Delta v} < \left(\frac{\partial P}{\partial v}\right)_{\mathcal{H}} = \left(\frac{\partial P}{\partial v}\right)_s \tag{303}$$

or

$$-\frac{\mathrm{w}_1^2}{v_1^2} < -\frac{a_1^2}{v_1^2} \tag{304}$$

which proves that the flow is superonic upstream of the wave

$$\mathrm{w}_1 > a_1 \tag{305}$$

For detonation waves, we can apply (302) at the downstream state 2 to determine the nature of the flow there. Assuming that the denominator of the r.h.s. is positive, we obtain **Jouguet's rule**: *The flow*

Table 3: Jouguet's rule for detonations and deflagrations

Case	$a^2 - w^2$	$\partial s/\partial v)_{\mathcal{H}}$	Note
detonation, U_1	< 0	< 0	strong detonation
detonation, U_2	> 0	> 0	weak detonation
detonation, L_2	< 0	< 0	strong deflagration
detonation, L_1	> 0	> 0	weak deflagration

downstream is subsonic or supersonic if the slope of the Hugoniot is smaller or larger than the slope of the Rayleigh line. Referring to Fig. 5, there are four cases to consider, given in Table 3. The physically reasonable solutions for both detonations and deflagrations have subsonic states (strong solution) downstream of the wave.

We can show that the denominator of (302) is positive for a shock wave in a perfect gas. The Grüneisen parameter for a perfect gas is a constant and is equal to

$$G = \gamma - 1 \ . \tag{306}$$

From the perfect gas shock jump conditions (Section A), the jump in volume normalized by state 2 is

$$\frac{\Delta v}{v_2} = \frac{-2 + \dfrac{2}{M_1^2}}{\gamma + 1 + \dfrac{2}{M_1^2}} \tag{307}$$

so that

$$1 + G\frac{\Delta v}{2v_2} = \frac{2 + \dfrac{\gamma + 1}{M_1^2}}{\gamma + 1 + \dfrac{2}{M_1^2}} \tag{308}$$

$$> 0 \tag{309}$$

For large shock speeds, $M_1 \to \infty$, a limiting value is reached

$$\to \frac{2}{\gamma + 1} \tag{310}$$

For reacting gases with realistic thermodynamic properties, the Grüneisen parameter has to be computed numerically. The simplest way to do this is to use finite differences to approximate

$$G = -\frac{v}{T}\left(\frac{\partial T}{\partial v}\right)_s \tag{311}$$

The evaluation can be carried out either at frozen composition (gruneisen_fr.m) or equilibrium composition (gruneisen_eq.m). An example of an evaluation of G and the denominator of (294) is shown in Fig. 24 for states on the Hugoniot near the CJ point of hydrogen-air detonation (see RH_CJ_isentropes.m). The values of both G and the denominator are approximated by the perfect gas expressions for strong shock waves

$$G \approx \gamma_s - 1 \tag{312}$$

$$\frac{2}{\gamma_s + 1} < 1 + \frac{G}{2v}\Delta v < 1 \tag{313}$$

and the equilibrium value of the isentropic exponent γ_s

$$\gamma_s = -\frac{v}{P}\left(\frac{\partial P}{\partial v}\right)_{s,eq} \tag{314}$$
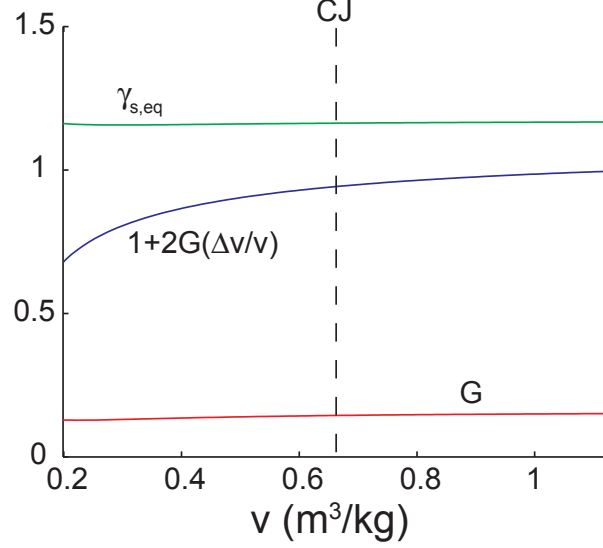
Figure 24: Grüneisen parameter, denominator of (294), and isentropic exponent (314) for the example shown in Fig. 7.

D.2 Entropy Extremum

The nature of the entropy extremum at the CJ points can be determined by computing the second derivative of entropy along the Hugoniot. This argument is apparently due to Becker (1922) and an alternate presentation is given by Kistiakowsky and Wilson (1941a). Proceed by differentiating (289) and evaluating at the CJ point, where

$$\left(\frac{\partial s}{\partial v}\right)_{\mathcal{H}} = 0 \quad \text{at the CJ point} \tag{315}$$

to obtain

$$\left(\frac{\partial^2 s}{\partial v^2}\right)_{\mathcal{H}} = -\frac{\Delta v}{2T}\left(\frac{\partial^2 p}{\partial v^2}\right)_{\mathcal{H}} \quad \text{at the CJ point} \tag{316}$$

Now consider using the differentiation rule embodied by (296)

$$\left(\frac{\partial}{\partial v}\right)_{\mathcal{H}} = \left(\frac{\partial}{\partial v}\right)_{s} + \left(\frac{\partial s}{\partial v}\right)_{\mathcal{H}}\left(\frac{\partial}{\partial s}\right)_{v} \tag{317}$$

twice to compute the derivative

$$\left(\frac{\partial^2 P}{\partial v^2}\right)_{\mathcal{H}} = \left(\frac{\partial}{\partial v}\right)_{\mathcal{H}}\left(\frac{\partial P}{\partial v}\right)_{\mathcal{H}} \tag{318}$$

$$= \left[\left(\frac{\partial}{\partial v}\right)_{s} + \left(\frac{\partial s}{\partial v}\right)_{\mathcal{H}}\left(\frac{\partial}{\partial s}\right)_{v}\right]\left(\frac{\partial P}{\partial v}\right)_{s} + \left(\frac{\partial}{\partial v}\right)_{\mathcal{H}}\left[\left(\frac{\partial P}{\partial s}\right)_{v}\left(\frac{\partial s}{\partial v}\right)_{\mathcal{H}}\right] \tag{319}$$

Carrying out the differentiation and evaluating at the CJ point, the only remaining non-zero terms are

$$\left(\frac{\partial^2 P}{\partial v^2}\right)_{\mathcal{H}} = \left(\frac{\partial^2 P}{\partial v^2}\right)_{s} + \left(\frac{\partial P}{\partial s}\right)_{v}\left(\frac{\partial^2 s}{\partial v^2}\right)_{\mathcal{H}} \quad \text{at the CJ point} \tag{320}$$

70

Combining this with the result of (316), we have that

$$\left(\frac{\partial^2 P}{\partial v^2}\right)_{\mathcal{H}} = \frac{1}{1+\dfrac{G}{2v}\Delta v}\left(\frac{\partial^2 P}{\partial v^2}\right)_s \quad \text{at the CJ point} \tag{321}$$

the curvatures of the isentrope and Hugoniot have the same sign as long as the denominator is positive. Define the *Fundamental Derivative of Gasdynamics* Thompson (1971) as

$$\Gamma = \frac{v^3}{2a^2}\left(\frac{\partial^2 P}{\partial v^2}\right)_s \tag{322}$$

we can write (316) to clearly show the sign and verify the dimensional correctness

$$\left(\frac{\partial^2 s}{\partial v^2}\right)_{\mathcal{H}} = \left(\frac{-\Delta v}{v}\right)\cdot\left(\frac{a^2}{Tv^2}\right)\cdot\left(\frac{1}{1+G\dfrac{\Delta v}{2v}}\right)\cdot\Gamma \quad \text{at the CJ point.} \tag{323}$$

For normal fluids Menikoff and Plohr (1989b), the curvature of the isentropes will be positive, $\Gamma > 0$, so that the entropy is a relative minimum at the upper CJ point

$$\left(\frac{\partial^2 s}{\partial v^2}\right)_{\mathcal{H}} > 0 \quad \text{at the upper CJ point} \quad \Delta v < 0 \tag{324}$$

and a relative maximum at the lower CJ point

$$\left(\frac{\partial^2 s}{\partial v^2}\right)_{\mathcal{H}} < 0 \quad \text{at the lower CJ point} \quad \Delta v > 0 \tag{325}$$

The entropy extremum property has been the source of a great deal of confused speculation and led to the misconception that detonation-based combustors are the most efficient for propulsion. There is a very substantial irreversible entropy rise associated with detonation compared to the modest irreversibility for deflagration. The variation of entropy on the Hugoniot and the implications for propulsion systems are discussed in detail by Wintenberger and Shepherd (2006). From their Abstract, we quote the results:

> "For a given stagnation enthalpy, we find that stationary detonation waves generate a higher entropy rise than deflagration waves. The combustion process generating the lowest entropy increment is found to be constant-pressure combustion. These results clearly demonstrate that the minimum entropy property of detonations derived from the conventional Hugoniot analysis does not imply superior performance in all propulsion systems. This finding reconciles previous analysis of flow path performance analysis of detonation-based ramjets with the thermodynamic cycle analysis of detonation-based propulsion systems. We conclude that the thermodynamic analysis of propulsion systems based on stationary detonation waves must be formulated differently than for propagating waves, and the two situations lead to very different results."

71

E Thermodynamic Property Polynomial Representation

This appendix describes how the ideal gas thermodynamic properties are represented as a function of temperature in the Cantera program and procedures for deriving polynomial fits from tabulated data. For ideal gas mixtures, only three functions for each species are needed for deriving all other thermodynamic properties. The functions are conventionally chosen to be the specific heat $c_{Pi} = c_{Pi}(T)$, specific enthalpy $h_i = h_i(T)$, and the pressure independent portion of the entropy $s_{\circ i} = s_{\circ i}(T)$. Using a known composition, the ideal gas mixture $P(\rho, T)$ relationship is

$$P = \rho R T \tag{326}$$

with the mixture gas constant defined by

$$R = \frac{\mathcal{R}}{\overline{W}} \tag{327}$$

where $\mathcal{R} = N_A k_B$ is the universal gas constant, k_B is the Boltzmann constant, and N_A is Avogadro's number. The average molar mass (kg per mol), $\overline{W}$, the mass fractions, Y_i, and enthalpy, h, of an ideal gas mixture are given by

$$\overline{W} = \left(\sum_{i=1}^{K} \frac{Y_i}{W_i} \right)^{-1} \tag{328}$$

$$h = \sum_{i=1}^{K} Y_i h_i(T) \tag{329}$$

It must be emphasized that all the derivations and formulas in this section apply only to *ideal gases*. *Real gases* have enthalpies and specific heats that are functions of both pressure and temperature; however, for *ideal gases*, they are functions of only temperature. The ideal gas properties are defined as

$$c_P^{IG}(T) = \lim_{P \to 0} c_P(T, P) \tag{330}$$

$$h^{IG}(T) = \lim_{P \to 0} h(T, P) \tag{331}$$

$$s_\circ^{IG}(T) = \lim_{P \to 0} [s(T, P) - R \ln (P^\circ / P)] \tag{332}$$

where IG signifies an ideal gas property. Our convention in this document will be to drop this superscript. The superscript, $\circ$ indicates the standard state condition of $T^\circ = 298.15$ K and $P^\circ = 1$ bar. Our convention is different from that used in the CHEMKIN and Cantera documents which use $c_P^\circ = c_P^{IG}$, $h^\circ = h^{IG}$, and $s^\circ = s_\circ^{IG}$, for the constant pressure (one bar), ideal gas properties.

The Cantera software uses a piecewise polynomial representation for the specific heat at constant pressure. In non-dimensional form, the specific heat at constant pressure is

$$\frac{c_{Pi}}{R_i} = \begin{cases} \sum_{n=0}^{4} a_{ni} T^n & T_{min} \leq T \leq T_{mid} \\ \\ \sum_{n=0}^{4} b_{ni} T^n & T_{mid} \leq T \leq T_{max} \end{cases} \tag{333}$$

where $R_i = \mathcal{R}/W_i$ is the gas constant for species i. The constants a_{ni} and b_{ni} have to be determined by fitting the polynomial representation to tabular data that is either determined by experiment or as described below, computed from statistical mechanics. The values of the coefficients also have to be adjusted so that the specific heat is continuous at the midpoint temperature T_{mid}. This representation of the specific heat dependence on temperature and the method used to derive the other properties was first used in the NASA chemical equilibrium computer program (McBride and Gordon, 1992, McBride et al., 1993) and widely used by other researchers for representing ideal gas thermodynamic properties. For this reason, these are usually known as NASA-style polynomial representations of thermodynamic data.

The ideal gas enthalpy can be found by integrating the specific heat since $dh = c_P dT$ for an ideal gas, which for a single species results in

$$h_i = \int_{T^\circ}^{T} c_{Pi}(T') dT' + \Delta_f h_i^\circ \tag{334}$$

where the constant of integration is the heat of formation $\Delta_f h_i^\circ$ at the standard thermochemical state of T° = 298.15 K, $P^\circ = 1$ bar (one atm in older data sets) for the ith species. Inserting the functional form of (333) and integrating the polynomial term-by-term, the nondimensional enthalpy is

$$\frac{h_i}{R_i T} = \begin{cases} \sum_{n=0}^{4} \dfrac{a_{ni} T^n}{n+1} + \dfrac{a_{5i}}{T} & T_{min} \leq T \leq T_{mid} \\[2ex] \sum_{n=0}^{4} \dfrac{b_{ni} T^n}{n+1} + \dfrac{b_{5i}}{T} & T_{mid} \leq T \leq T_{max} \end{cases} \tag{335}$$

The constant a_{i5} is determined by evaluating the enthalpy at the standard state to obtain

$$\Delta_f h_i^\circ = h_i(T^\circ) \tag{336}$$

so that

$$a_{i5} = \frac{\Delta_f h_i^\circ}{R_i} - \sum_{n=0}^{4} \frac{a_{ni}}{n+1} (T^\circ)^{n+1} \tag{337}$$

The constant b_{i5} is determined by requiring continuity of the two representations at the midpoint temperature.

The entropy can be determined by using the fundamental relation of thermodynamics

$$dh = T ds - v dP \tag{338}$$

This be written for an ideal gas as

$$ds = \frac{c_p dT}{T} - R \frac{dP}{P} \tag{339}$$

For a single species in a gas mixture, the pressure is interpreted as the partial pressure of that species $P_i = X_i P$, and the entropy differential is integrated to obtain

$$s_i(T, P_i) = s_{oi}(T) - R_i \ln\left(\frac{P_i}{P^\circ}\right) \tag{340}$$

The pressure-independent portion of the entropy is

$$s_{oi} = \int_{T^\circ}^{T} \frac{c_{Pi}(T')}{T'} dT' + s_{oi}(T^\circ) \tag{341}$$

Using the polynomial representation of the specific heats and integrating term by term, we have

$$\frac{s_{oi}}{R_i} = \begin{cases} a_{0i} \ln(T) + \sum_{n=1}^{4} \dfrac{a_{ni} T^n}{n} + a_{6i} & T_{min} \leq T \leq T_{mid} \\[2ex] b_{0i} \ln(T) + \sum_{n=1}^{4} \dfrac{b_{ni} T^n}{n} + b_{6i} & T_{mid} \leq T \leq T_{max} \end{cases} \tag{342}$$

where a_{6i} is determined from the species entropy evaluated at the standard state.

$$s_i(T^\circ, P^\circ) = s_{\circ i}(T^\circ) \tag{343}$$

$$a_{6i} = \frac{s_{\circ i}(T^\circ)}{R_i} - \left(a_{0i} \ln(T^\circ) + \sum_{n=1}^{4} \frac{a_{ni}(T^\circ)^n}{n} \right) \tag{344}$$

The constant b_{6i} is determined by requiring continuity at the midpoint temperature.

Using the definitions of the thermodynamic potentials, all other properties and potentials can be found. Specific heat at constant volume:

$$c_{vi} = c_{Pi} - R_i \tag{345}$$

Internal energy:

$$e_i = h_i - R_i T \tag{346}$$

Gibbs energy:

$$g_i = h_i - T s_i \tag{347}$$

Helmholtz energy:

$$a_i = e_i - T s_i \tag{348}$$

Thermodynamic properties of various species have to be defined in a self-consistent fashion to reproduce the known experimental relationships for enthalpy and chemical equilibrium; see Chase (1998) for a complete exposition of the methods used to do this. For example, suppose we need to the enthalpy of formation of a species A and no measurement is available. The heat of formation can be computed using Hess's law which is simply a form of the conservation of energy. Given the heat of formation values for the compounds B-C and A-B-C and the heat of reaction for

$$\text{A} + \text{B-C} \longrightarrow \text{A-B-C}$$
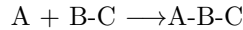
at standard conditions, then the enthalpy of formation of A can be determined using conservation of energy

$$\Delta_r H = \Delta_f H_A^\circ + \Delta_f H_{BC}^\circ - \Delta_f H_{ABC}^\circ \tag{349}$$

Therefore, solving for the heat of formation of species A yields

$$\Delta_f H_A^\circ = \Delta_r H - \Delta_f H_{BC}^\circ + \Delta_f H_{ABC}^\circ \tag{350}$$

Note that we have carried out the computation using the *molar enthalpy* which is consistent with the standard chemical practice and can be simply related to the stoichiometry of the reaction. The relationship to mass-specific enthalpy is simply $h_i = H_i/W_i$. Consistent values for the standard state enthalpy and entropy have been evaluated from experimental data for a number of substances and are available in the JANAF compilation (Chase, 1998). However, in some cases experimentally-based values are not available, and the standard state enthalpy and entropy must be estimated using theoretical or empirical methods. The most common empirical method is known as the group additivity method, which is discussed in detail by Benson (1976).

E.1 Specification for Cantera input

The thermodynamic properties c_{Pi}/R, h_i/RT, and s_i/R for each species are specified in the Cantera mechanism (.cti file). For each species in the .cti file that uses the NASA-style polynomials, Cantera requires

```
species( name = "CH3CHCHCHO",
    atoms = " C:4  H:6  O:1 ",
    thermo = (
       NASA( [  200.00,  2500.00], [ -2.696365560E-01,   4.341252850E-02,
                -3.073846170E-05,   1.115698570E-08,  -1.581997240E-12,
                -1.483378370E+04,   2.817336550E+01] ),
       NASA( [ 2500.00,  5000.00], [  8.318851910E+01,  -6.599805600E-02,
                 2.896794850E-05,  -5.456349720E-09,   3.760599270E-13,
                -6.854568290E+04,  -4.704570180E+02] )
             ),
    note = "CIT/08" )
```

Figure 25: Example usage of thermodynamic coefficients with Cantera for 2-Butenal.

14 coefficients and three temperatures $(T_{min}, T_{mid}, T_{max})$. The format of the data in the cantera `.cti` file is

$$\text{thermo} = (\text{NASA}(\text{range} = (T_{min}, T_{mid}), \text{ coeffs} = (a_{0i}, a_{1i}, a_{2i}, a_{3i}, a_{4i}, a_{5i}, a_{6i}))$$
$$\text{NASA}(\text{range} = (T_{mid}, T_{max}), \text{ coeffs} = (b_{0i}, b_{1i}, b_{2i}, b_{3i}, b_{4i}, b_{5i}, b_{6i})))$$

As an example, a set of coefficients for $CH_3CHCHCHO$ (2-Butenal) is shown in Figure 25. The coefficients given in this example were obtained by performing a least-squares fit to tabulated data generated by evaluating at fixed temperature intervals the statistical mechanical functions with inputs from a semi-empirical model of the molecular structure.[8] The methodolgy behind the computation and fitting is described in the subsequent sections.

In our high-temperature reaction mechanisms distributed with the Toolbox, most species have typical values of $T_{min} = 200$ K, $T_{mid} = 1000$ K, and $T_{max} = $5000 to 6000 K. For the original mechanisms appearing in the version 1.7 Cantera distribution, most species are only defined to 3000 K. One of the motivations behind the present section is the need to create data sets that extend to the higher temperatures that occur in typical shock and detonation problems.

The thermodynamic parameters for each species are specified in the Cantera mechanism file and based on the original NASA format (McBride and Gordon, 1992, McBride et al., 1993). Compilations of this data have been made for many species through the JANAF-NIST project (Chase, 1998) and are available on-line. Coefficients of fits are available from NASA, NIST, BURCAT, and SNL. Note that for the Cantera 1.7 distribution, only the original NASA format is compatible, the newer releases which represent the thermodynamic properties with more than two temperature ranges are not supported. In addition, the newer versions of the NASA polynomials use a larger number of terms (there are 9 coefficients per temperature interval instead of 7) and Cantera is not compatible with these either.

E.2 Statistical Mechanical Computation of Thermodynamic Properties

The thermodynamic data provided with Cantera and used in the Shock and Detonation Toolbox come from many sources. As discussed above, the standard state enthalpy and entropy are determined from experimental data or semi-empirical data. However, the temperature dependence of the specific heat (and by implication, the enthalpy and entropy) are usually based on statistical mechanics. A basic sketch of this model is described below. Full details are given in textbooks, a simple one is Maczek (2004), and detailed presentations are given in McQuarrie (2000) and specifically for combustion in Chapter 8 of Kee et al. (2003).

The key concept in statistical mechanics is that there exists a *partition function* that contains all the information needed to determine the properties of a system consisting of a large number of molecules in thermodynamic equilibrium. The thermodynamic properties of the system, such as the internal energy, pressure, entropy, and enthalpy, can all be expressed in terms of functions of the partition function or its

---

[8]We thank Siddharth Dasgupta of Caltech for computing this data using the Lingraf program developed by the Goddard group.

derivatives. The partition function can be constructed by finding the quantum states and energy levels for the system of molecules.

The fundamental relation between thermodynamics and statistical mechanics connects the Helmholtz energy A and the *system partition function, $\mathcal{Z}$.*

$$A - A_0 = -k_B T \ln \mathcal{Z} \tag{351}$$

The constant A_0 and similar constants for the other thermodynamic potentials are introduced to make the statistical mechanics results consistent with the thermodynamic standard state. Statistical mechanics and the computational methods of quantum mechanics used to estimate energy levels in molecules consider the zero energy state to be nuclei and electrons separated by an infinite distance, see the discussion in the NIST Computational Chemistry Comparison and Benchmark Computational tutorial. However, the ground state (lowest energy) of the molecules where the electrons are bound most tightly to the nuclei corresponds to the thermodynamically stable state. The zero level of the heat of formation is chosen (arbitrarily) to be that of the reference elements at the standard state. In order to obtain the constants A_0 for each species that will agree with the thermochemical convention for heat of formation, a formation reaction has to be selected and the heat of reaction determined with ab initio comptuations of electronic structure of the other species and Hess' Law. Using the experimental standard state enthalpies of the other species in the reaction, Hess' Law and the ab initio heat of reaction can be used to define the standard state heat of formation of the species of interest and by subsequent computation, the constant A_0. Entropy is computed in a different fashion, using the Third Law of Thermodynamics to define the entropy at absolute zero and integrating all contributions from $T = 0$ to $T°$ as described in Irikura and Frurip (1998) and online at the NIST database.

For a system consisting of N independent and indistinguishable molecules (Maxwell-Boltzmann statistics), the partition function can defined in terms of the products of the partition function Z for each molecule

$$\mathcal{Z} = \frac{Z^N}{N!} \tag{352}$$

and is a function of the independent variables (N, V, T). The *molecular partition function Z* is determined from the geometry and fundamental properties of a molecule, such as the geometrical configuration (bond length and angles), mass of the atoms, moments of inertia, vibrational modes and frequencies, and electronic energy levels. Atoms are just a special case of molecules and the partition function for an atom is constructed in a similar fashion to that of a molecule but only translation and electronic energy states are considered.

The molecular partition function for a given molecule or atom is usually considered to be composed of a product of sub-partition functions corresponding to separable (independent) motions. These sub-partition functions are computed as the sum over all the possible quantum states for that type of motion. Each sub-partition function is represented as

$$Z = \sum_{states\ j} \exp\left(-\frac{\epsilon_j}{k_B T}\right) \tag{353}$$

where ϵ_j is the energy of state j relative to the energy of the ground state of the molecule. If the sum is done in terms of energy levels instead of quantum states (the case for electronic excitation) then the sum is written in terms of g_i is the degeneracy (multiplicity) of each moelcular energy level

$$Z = \sum_{energies\ j} g_j \exp\left(-\frac{\epsilon_j}{k_B T}\right). \tag{354}$$

The translational partition function is special case and the sum can be converted to an integral since there are such large number of states available in typical macroscopic volumes and the energy levels are closely spaced together. After carrying out the summation for the translational case, the result can be simply expressed as

$$Z_t = \left(\frac{2\pi m k_B T}{h_p^2}\right)^{\frac{3}{2}} V \tag{355}$$

where V is the system volume, m is the atom or molecule mass in kg, and h_p is Planck's constant. For polyatomic species, the rotational and vibrational motions are represented by additional sub-partition functions Z_r and Z_v, respectively. For the rotational modes, the basic model is that of the rigid rotator in each independent axis of rotation. For the vibrational modes, the basic model is that is each mode is represented as a simple harmonic oscillator with corrections associated with rotational stretching, low temperature rigid rotation, Fermi resonance, and anharmonicity and vibration-rotation interactions. The total number of vibration-rotational modes and the associated energy levels are determined by either by approximate solution of Schrodinger's equation or semi-empirical methods. The electronic contributions are represented by Z_e and for most combustion problems is usually possible to consider only the first excited state, at most. The vibration and rotational partition function used in most combustion thermochemistry computations are based on the ground electronic state configuration of the molecule. The net molecular partition function can be expressed as the product

$$Z = Z_t Z_r Z_v Z_e \tag{356}$$

or separating the motion into external (translation) and internal (rotation, vibration, and electronic) modes we can write

$$Z = Z_t Z_i \tag{357}$$

The internal energy, E relative to that of the ground state E_0, can be calculated for a system of N molecules by summing over all states and weighting the energy of each state by the expected number of molecules in that state.

$$E - E_0 = \sum_j N_j \epsilon_j \tag{358}$$

N_j is the number of molecules at in state j with an energy of ϵ_j relative to the ground state. This equation can be expressed in terms of the molecular partition function by using the *Boltzmann distribution* to define the expected fraction of the molecules in that state for a system that is in thermodynamic equilibrium

$$\frac{N_i}{N} = \frac{\exp\left(-\dfrac{\epsilon_i}{k_B T}\right)}{\sum_k \exp\left(-\dfrac{\epsilon_k}{k_B T}\right)} \tag{359}$$

Substituting this into (358), we can write the internal energy in terms of the molecular partition function as

$$E - E_0 = N k_B T^2 \left(\frac{\partial \ln Z}{\partial T}\right)_V \tag{360}$$

Since $Z(T, V)$, the number of molecules N does not enter in to the computation of the partial derivative.

The enthalpy, specific heats, and entropy can be computed using thermodynamic relationships and the relationship (351). To express the results in terms of the molecular partition function we will first observe that for a large number of molecules, Stirlings' approximation for the factorial can be used to simply the expressions.

$$\lim_{N \to \infty} \ln N! \approx N \ln N - N \tag{361}$$

The Helmholtz energy can be approximated as

$$A - A_0 = N k_B T \left(\ln Z - \ln N + 1\right) \tag{362}$$

The fundamental relation of thermodynamics for a fixed number of molecules can be written

$$dA = -S dT - P dV \tag{363}$$

which leads directly to the following expressions

$$S = -\left(\frac{\partial A}{\partial T}\right)_V \tag{364}$$

$$= N k_B \left[\left(\frac{\partial(T \ln Z)}{\partial T}\right)_V - \ln N + 1\right] \tag{365}$$

$$P = -\left(\frac{\partial A}{\partial V}\right)_T \tag{366}$$

$$= N k_B T \left(\frac{\partial \ln Z}{\partial V}\right)_T \tag{367}$$

Enthalpy is defined as

$$H = E + PV \tag{368}$$

$$= A - TS + PV \tag{369}$$

and for ideal gases

$$PV = N k_B T \tag{370}$$

so that

$$H - H_0 = N k_B T \left[T\left(\frac{\partial \ln Z}{\partial T}\right)_V + 1\right] \tag{371}$$

The definition for specific heat at constant pressure is

$$C_P = \left(\frac{\partial H}{\partial T}\right)_P \tag{372}$$

$$= N k_B \left[T\left(\frac{\partial^2}{\partial T^2}(T \ln Z)\right)_V + 1\right] \tag{373}$$

We can further simplify the result by using the splitting of the molecular partition function into translation and internal modes (357) and use (355) to compute the contribution of translation explicitly. The contribution of translation states to the thermodynamic function is equivalent to the thermodynamic properties of a monoatomic gas. The final results for the nondimensional temperature-dependent properties are found by considering one mole of substance ($N = N_A$):

$$\frac{c_P(T)}{R} = \frac{5}{2} + T\frac{d^2(T \ln Z_i)}{dT^2} \tag{374}$$

$$\frac{h(T) - h_0}{RT} = \frac{5}{2} + T\frac{d(\ln Z_i)}{dT} \tag{375}$$

$$\frac{s(T)}{R} = \frac{5}{2} + \frac{3}{2}\ln\left(\frac{2\pi m}{h_p^2}\right) + \frac{5}{2}\ln(k_b T) - \ln P + T\frac{d}{dT}(\ln Z_i) \tag{376}$$

The last term on the right-hand side of each of these expressions contains the contribution of all the internal degrees of freedom. To derive the pressure-independent portion of the entropy, use the definition

$$\frac{s_\circ(T)}{R} = \frac{s(T, P)}{R} + \ln\left(\frac{P}{P^\circ}\right) \tag{377}$$

to obtain

$$\frac{s_\circ(T)}{R} = \frac{5}{2} + \frac{3}{2}\ln\left(\frac{2\pi m}{h_p^2}\right) + \frac{5}{2}\ln(k_B T) - \ln P^\circ + T\frac{d}{dT}(\ln Z_i) \tag{378}$$

78

For a monoatomic gas with a mass of 1 amu (a hydrogen atom), the value of nondimensional entropy at a reference temperature of 1 K is known as the *Sackur-Tetrode* constant

$$\frac{s_\circ(T = 1 \text{ K})}{R} = -1.1517047 \qquad P^\circ = 100 \text{ kPa} \qquad Z_i = 1 \qquad m = 1 \text{ amu} \tag{379}$$

For a dicussion of the evaluation of the contributions of the internal partition function, see the JANAF table documentation (Chase, 1998) or the documentation for the NASA fitting program (McBride and Gordon, 1992). Note that the provided JANAF table documentation, Monograph 9, link points to a large 228MB pdf file. Therefore, one may also go to the NIST Monograph website, and use the "right click, save as" method to monitor the status of the download.

E.3 Estimating Heat Capacities

Some basic heuristics apply for estimating both the low and high temperature limits of the specific heats. These are useful for extending each species' properties to higher temperatures or for visually evaluating the success or failure of a least squares fit.

The heuristic models presented come from the classical result known as the equipartition of energy. The rule is that at sufficiently high temperatures that quantum effects can be ignored, each degree of freedom (DOF) of a molecule contributes $\frac{1}{2}k_B T$ to the internal energy. If the total number of degrees of freedom are f, then the internal energy per molecule can be written as

$$\epsilon = f\frac{1}{2}k_B T \tag{380}$$

and the internal energy per unit mass is

$$e = f\frac{1}{2}RT \tag{381}$$

The number of degrees of freedom f depends on the particular molecule. The effect of quantum mechanics is that the energy levels are discrete and for thermal energies ($k_B T$) that are comparable to or smaller than the energy level differences, the effective number of degrees of freedom will be a function of the temperature. Fewer degrees of freedom are excited at low temperatures and more are excited at higher temperatures. There are always three degrees of translational freedom for an atom, and similarly, there are three from the translation of the center of mass of a molecule. Equation 381 implies that the specific heat at constant volume is

$$c_v = \frac{f}{2}R \tag{382}$$

This is related to the specific heat at constant pressure through

$$c_P = c_v + R \tag{383}$$

$$\tag{384}$$

At low temperatures, the only contributions to a molecule's energy are the rotational and translational degrees of freedom. Therefore, with each atom fixed in the molecule (no vibrational energy), there are three degrees of translational freedom and two or three degrees of rotational freedom for the molecule as a whole. If the molecule is treated as a rotating rigid body, the total rotational degrees of freedom are two for linear molecules (e.g., O_2 or N_2) or 3 for non-linear molecules (e.g., H_2O or NH_3). The net result at low temperature is that

$$\lim_{T \to 0} c_P = \frac{7}{2}R \quad \text{linear} \tag{385}$$

$$\lim_{T \to 0} c_P = 4R \quad \text{nonlinear} \tag{386}$$

At high temperatures, all the vibrational modes of oscillation are excited in additional to rotation and vibration. Contributions from electronic excitation are usually small in the 3000 to 6000 K range and we will neglect these. The number of vibration modes can be computed by considering the atoms to move independently at high temperatures. There are a total of $3n_a$ independent motions per molecule with n_a atoms and if we substract center of mass translation and rotation, then we expect that at high temperatures there are $3n_a - 5$ vibrational modes for linear molecules and $3n_a - 6$ modes for nonlinear molecules. Each vibrational mode contributes two degrees of freedom, one for kinetic energy and one for potential energy. The total number of degrees of freedom for the high temperature limit is obtained by summing the translational, rotational, and vibrational degrees of freedom The final result can be used to express the high temperature specific heat limits as

$$\lim_{T \to \infty} c_P = \frac{6n_a - 3}{2} R \quad \text{linear} \tag{387}$$

$$\lim_{T \to \infty} c_P = \frac{6n_a - 4}{2} R \quad \text{nonlinear} \tag{388}$$

Note that if we neglect the electronic excitation of monatomic species, the specific heat is independent of temperature

$$(c_P)_{monatomic} = \frac{5}{2} R \ . \tag{389}$$

This is a good approximation for the temperatures of interest in ordinary combustion.

The utility of the limits for heat capacity are that these are a convenient way to check the validity of thermodynamic data and also provide a limiting values that can be used for extrapolating data valid for a limited range of temperature. Cantera uses the high-temperarture limiting value as a check on the polynomial fits when creating CTI files from NASA-style input data. As an alternative to recomputing the thermodynamic functions using statistical mechanics, it is possible in some cases to extrapolate data to higher temperatures. Programs for extrapolation are given on the Shock and Detonation ToolBox website. The idea behind the extrapolation[9] is that given a specific heat function $c_p(T)$ defined on $T_{min} \leq T \leq T_{max}$, the specific heat can be extrapolated using

$$\frac{1}{c_p} = \frac{1}{c_p(\infty)} - \frac{T_{max}}{T} \left(\frac{1}{c_p(\infty)} - \frac{1}{c_p(T_{max})} \right) \quad \text{for} \quad T \geq T_{max} \tag{390}$$

This method is simpler but less accurate than the more general extrapolation method developed by Wilhoit and implemented in the NASA code PAC91 (McBride and Gordon, 1992, see p. 7).

E.4 Least Squares Fit for Piecewise Thermodynamic Representation

Using the partition function definitions of thermodynamic properties, (374)-(376), we can calculate the specific heat, the enthalpy, and the pressure-independent portion of the entropy as functions of temperature. Since a large number of transcendental functions and sums have to be computed for each temperature, it is computationally expensive to evaluate the partition functions and derivatives each time a thermodynamic property is needed in a numerical computation. To circumvent this, the thermodynamic properties are evaluated ahead of time at fixed temperature increments over the range of interest and fit to an approximating polynomial that is computationally inexpensive to evaluate. For example, the tables in the JANAF compilation are generated directly from evaluating the partition function expressions and the NASA polynomial coefficients are obtained by fitting these data. In order to obtain reasonable fits of polynomials to specific heats over a wide temperature, the temperature range is divided into segments and data on each segment fit separately. The method developed by NASA in the 1960s, which is still widely used today, is to divide the temperature range into two segments that share a common mid-point temperature T_{mid}.

Of the many ways of computing the polynomial fit coefficients, the most suitable method is to simultaneously optimize the fit to all three properties in the least-squares sense with the additional constraints

---

[9]This is due to Hai Wang of USC, who generously provided information about this procedure and Fortran programs for carrying out the fitting process.

of continuity at the matching temperature, T_{mid}. Other constraints, such as continuity of derivatives and high and low temperature limit boundary conditions, can also be considered. A common past practice has been to evaluate the properties from the partition function expressions at at 100 K intervals from 200 K to 3000-6000 K and match the two temperature ranges at 1000 K.

An example of the statistical thermodynamic data and the fit for c_P/R with $T_{min} = 200$ K, $T_{mid} = 2500$ K, and $T_{max} = 5000$ K is shown in Figure 26. This figure was constructed using the coefficients from the 2-Butenal ($CH_3CHCHCHO$) example shown in Figure 25. The piecewise function was fitted using a

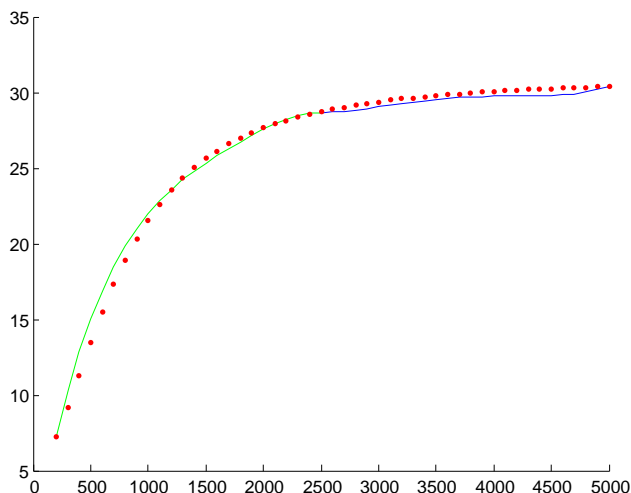Figure 26: Comparison of c_P/R for 2-Butenal ($CH_3CHCHCHO$) calculated from the statistical mechanics representation (points) to the piecewise polynomial fit (solid lines).

constrained least-squares method in Matlab. All three piecewise functions for the non-dimensional properties, $c_{Pi}(T)/R$, $h_i(T)/RT$, and $s_{\circ i}(T)/R$, were simultaneously optimized and constrained for the best overall fit. The constraints include continuity for $h_i(T)/RT$ and $s_{\circ i}(T)/R$ and continuity for both $c_{Pi}(T)/R$ and its derivatives. Also, the boundary point constraints for $c_{Pi}(T)/R$ and $h_i(T)/RT$ are included. There are a number different possible combinations of constraints; however, care must be taken not to over-constrain the system of equations to be optimized.

The constrained optimization problem for a piecewise fit is formulated in Matrix form with two non-square systems of equations, one for the least squares minimization

$$Ax = b \tag{391}$$

and one for the constraint equations

$$A_{eq}x = b_{eq} \tag{392}$$

where x is the 14×1 vector of coefficients

$$x = [a_{0i}, a_{1i}, ..., a_{6i}, b_{0i}, b_{1i}, ..., b_{6i}]^T \tag{393}$$

with $[.]^T$ representing the transpose. After constructing the matrices A, A_{eq} b, and b_{eq}, Matlab's *lsqlin()*, iterative constrained least-squares optimization function is used to find the best fit for the coefficient vector x. The constraints are handled by the method of Lagrange multipliers and the solution is iterated until user-specified convergence criterion are met.

The general form of the linear least-squares problem without constraints can be written as the matrix equation

$$Ax = b \tag{394}$$

81

where A is dimension $m \times n$, x is dimension $n \times 1$, and b is dimension $m \times 1$. The dimension m depends on the number of temperature intervals that are used to evaluate the partition function expressions. The standard solution method is to construct a square $(n \times m)$ linear system by augmenting the matrix A and using a standard numerical linear algebra routine to find the unknown vector x.

$$(A^T A)x = (A^T b) \tag{395}$$

However, for the constrained problem, additional steps are required, which Matlab conveniently handles through the function *lsqlin()*.

The user-defined input for the fitting program includes the temperature ranges, the standard state enthalpy of formation and standard state entropy, the species name, and the species molecular composition. For example, the input Matlab script used contains

```
Tmin = 200; % in Kelvin
Tmax = 5000;
Tmid = 2500;
% Standard state entropy and enthapy of formation at approximately 298.15 K
so_over_R_298 =  40.06;  % so/R at 298.15 K and 1 bar
ho_over_RT_298 = -109.7/8.314472*1000/298.15; % ho/RT at 298.15 K and 1 bar (enthalpy of formation)
substance = 'CH3CHCHCHO'; %species name to apear in chemkin II output
                          %the output file appears as substance_output
```

The molecular composition is specified by typing at the Matlab prompt at run time. For this example, there are 3 types of atoms, four carbon, six hydrogen, and one oxygen atom so the interactive input to the demonstration script will be:

```
input number of element types 3
first element (in CAPS) C
multiplicity 4
second element (in CAPS) H
multiplicity 6
third element (in CAPS) O
multiplicity 1
```

The Matlab program is run from the script demo_interp_thermo.m, which then calls the function interp_thermo, located in interp_thermo.m. Input for the program is the LINGRAF thermodynamic data for the example molecule 2-Butenal and user-defined values input at the Matlab prompt. The thermodynamic input data is given a Matlab matrix in the script twobutenal.m. The output from the program fitting program includes the coefficients a_{ni} and b_{ni}, optimization diagnostics, goodness of fit measures, plots showing the fits, and output files, CH3CHCHCHO_output, in the CHEMKIN format that can be used in Cantera with the ck2cti utlility to create the .cti format. Also, included is Cantera output in the .cti file format.

All of these files can be found at the following website. By independently obtaining thermodynamic data from molecular modeling and statistical mechanics software such as LINGRAF, one may easily adapt this Matlab program for constructing fits for any desired species.

F Functions

This section is intended to be a quick reference for learning and usage. Please refer to the website for installation details.

Below we have provided a brief description of the functions in the Shock and Detonation Toolbox that numerically calculate shock jump conditions. The basic syntax, input, and output are provided for Matlab. The syntax for Python is very similar. Finally, for each function, we give links to the Matlab and Python implementations of these functions. All functions except the equilibrium sound speed-based *CJSpeed* functions are supported in Matlab. Not all of the Python functions have been implemented in Windows.

Note: For constant volume explosions and one-dimensional detonation structure (ZND model) see the companion document from the Shock and Detonation Toolbox website (see Browne et al., 2005).

F.1 Core Functions

- **CJSpeed**
  Calculates CJ detonation velocity.
  Matlab Function - CJSpeed.m
  Python Function - CJSpeed (in PostShock.py)

  ```
  SYNTAX:
  [cj_speed,curve,goodness,dnew] = CJSpeed(P1,T1,q,mech,plt_num)
  INPUT:
  P1 = initial pressure (Pa)
  T1 = initial temperature (K)
  q = string of reactant species mole fractions
  mech = cti file containing mechanism data (i.e. 'gri30.cti')
  plt_num = 0 if no plot, else number for plot of w1 vs density ratio
  OUTPUT:
  cj_speed = CJ detonation speed (m/s)
  curve = least squares fit curve
  goodness = goodness of curve fit
  dnew = CJ density ratio
  ```

- **CJspeed2**
  Calculates CJ detonation velocity and CJ state
  Matlab Function - N/A
  Python Function - CJSpeed2 (in CJ2.py)

  ```
  SYNTAX:
  [cj_speed, gas] = CJspeed(P1, T1, q, mech)
  INPUT:
  P1 = initial pressure (Pa)
  T1 = initial temperature (K)
  q = string of reactant species mole fractions
  mech = cti file containing mechanism data (i.e. 'gri30.cti')
  OUTPUT:
  cj_speed = CJ detonation speed (m/s)
  gas = gas object at CJ state
  ```

- **PostShock_eq**
  Calculates equilibrium post-shock state for a specified shock velocity.
  Matlab Function - PostShock_eq.m
  Python Function - PostShock_eq (in PostShock.py)

```
SYNTAX:
[gas] = PostShock_eq(U1, P1, T1, q, mech)
INPUT:
U1 = shock speed (m/s)
P1 = initial pressure (Pa)
T1 = initial temperature (K)
q = string of reactant species mole fractions
mech = cti file containing mechanism data (i.e. 'gri30.cti')
OUTPUT:
gas = gas object at equilibrium post-shock state
```

- **PostShock_fr**
  Calculates frozen post-shock state for a specified shock velocity.
  Matlab Function - PostShock_fr.m
  Python Function - PostShock_fr (in PostShock.py)

```
SYNTAX:
[gas] = PostShock_fr(U1, P1, T1, q, mech)
INPUT:
U1 = shock speed (m/s)
P1 = initial pressure (Pa)
T1 = initial temperautre (K)
q = string of reactant species mole fractions
mech = cti file containing mechanism data (i.e. 'gri30.cti')
OUTPUT:
gas = gas object at frozen post-shock state
```

- **reflected_eq**
  Calculates equilibrium post-reflected-shock state assumming u1 = 0.
  Matlab Function - reflected_eq.m
  Python Function - reflected_eq (in reflections.py)

```
SYNTAX:
[p3,UR,gas3] = reflected_eq(gas1,gas2,gas3,UI)
INPUT:
gas1 = gas object at initial state
gas2 = gas object at post-incident-shock state (already computed)
gas3 = working gas object
UI = incident shock speed (m/s)
OUTPUT:
p3 = post-reflected-shock pressure (Pa)
UR = reflected shock speed (m/s)
gas3 = gas object at equilibrium post-reflected-shock state
```

- **reflected_fr**
  Calculates frozen post-reflected-shock state assuming u1 = 0.
  Matlab Function - reflected_fr.m
  Python Function - reflected_fr (in reflections.py)

```
SYNTAX:
[p3,UR,gas3] = reflected_fr(gas1,gas2,gas3,UI)
INPUT:
gas1 = gas object at initial state
gas2 = gas object at post-incident-shock state (already computed)
```

```
gas3 = working gas object
UI = incident shock speed (m/s)
OUTPUT:
p3 = post-reflected-shock pressure (Pa)
UR = reflected shock speed (m/s)
gas3 = gas object at frozen post-reflected-shock state
```

F.2   Subfunctions

- **CJ_calc**
  Calculates the wave speed for the Chapman-Jouguet case using Reynolds' iterative method (see Section 7.2).
  Matlab Function - CJ_calc.m
  Python Function - CJ_calc (in PostShock.py)

```
SYNTAX:
[gas,w1] = CJ_calc(gas,gas1,ERRFT,ERRFV,x)
INPUT:
gas = working gas object
gas1 = gas object at initial state
ERRFT,ERRFV = error tolerances for iteration
x = density ratio
OUTPUT:
gas = gas object at equilibrium state
w1 = initial velocity to yield prescribed density ratio
```

- **equilSoundSpeeds**
  Calculates equilibrium and frozen sound speeds. For the equilibrium sound speed, the gas is equilibrated holding temperature and pressure constant.
  Matlab Function - N/A
  Python Function - equilSoundSpeeds (in CJ2.py)

```
SYNTAX:
[aequil,afrozen] = equilSoundSpeeds(gas)
INPUT:
gas = working gas object (modified inside function)
OUTPUT:
aequil = equilibrium sound speed (m/s)
afrozen = frozen sound speed (m/s)
```

- **eq_state**
  Calculates equilibrium state given T and ρ.
  Matlab Function - eq_state.m
  Python Function - eq_state (in Thermo.py)

```
SYNTAX:
[P,H] = eq_state(gas,r1,T1)
INPUT:
gas = working gas object
r1,T1 = desired density and temperature
OUTPUT:
P,H = equilibrium pressure and enthalpy at constant temperature and specific volume
```

- **FHFP_CJ**
  Uses the momentum and energy conservation equations to calculate error in current pressure and the

enthalpy guesses (see (112) & (111)). In this case, state 2 is in equilibrium.
Matlab Function - FHFP_CJ.m
Python Function - FHFP_CJ (in PostShock.py)

```
SYNTAX:
[FH,FP] = FHFP_noshk(gas,gas1,w1)
INPUT:
gas = working gas object
gas1 = gas object at initial state
w1 = current guess for initial velocity (m/s)
OUTPUT:
FH,FP = error in enthalpy and pressure
```

- **FHFP_CJ2**
  Uses the momentum and energy conservation equations and equilibrium sound speed to calculate error in current pressure and the enthalpy guesses (see (112) & (111)). In this case, state 2 is in equilibrium.
  Matlab Function - N/A
  Python Function - FHFP_CJ2 (in CJ2.py)

```
SYNTAX:
[FH,FP,cj_speed] = FHFP_CJ2(gas,gas1,gas2)
INPUT:
gas = working gas object
gas1 = gas object at initial state
gas2 = dummy gas object (for calculating numerical derivatives)
OUTPUT:
FH,FP = error in enthalpy and pressure
cj_speed = CJ detonation speed (m/s)
```

- **FHFP_fr**
  Uses the momentum and energy conservation equations to calculate error in current pressure and the enthalpy guesses (see (112) & (111)). In this case, state 2 is frozen.
  Matlab Function - FHFP_fr.m
  Python Function - FHFP_fr (in PostShock.py)

```
SYNTAX:
[FH,FP] = FHFP_fr(U1,gas,gas1)
INPUT:
U1 = shock speed (m/s)
gas = working gas object
gas1 = gas object at initial state
OUTPUT:
FH,FP = error in enthalpy and pressure
```

- **FHFP_reflected_fr**
  Uses the momentum and energy conservation equations to calculate error in current pressure and the enthalpy guesses (see (112) & (111)). In this case, state 3 is frozen.
  Matlab Function - FHFP_reflected_fr.m
  Python Function - FHFP_reflected_fr (in reflections.py)

```
SYNTAX:
[FH,FP] = FHFP_reflected_fr(u2,gas3,gas2)
INPUT:
u2 = current post-incident-shock lab frame particle speed
```

```
gas3 = working gas object
gas2 = gas object at post-incident-shock state (already computed)
OUTPUT:
FH,FP = error in enthalpy and pressure
```

- **gruneisen_eq**
  Computes the equilibrium Grüneisen coefficient by equilibrating the gas object at constant temperature and pressure.
  Matlab Function - gruneisen_eq.m
  Python Function - N/A

  ```
  SYNTAX:
  G_eq =  gruneisen_eq(gas)
  INPUT:
  gas = working gas object (not modified in function)
  OUTPUT:
  G_eq = equilibrium Gruneisen coefficient [-de/dp)_v = -(v/T)dT/dv)_s]
  ```

- **gruneisen_fr**
  Computes the frozen Grüneisen coefficient.
  Matlab Function - gruneisen_fr.m
  Python Function - N/A

  ```
  SYNTAX:
  G_fr =  gruneisen_fr(gas)
  INPUT:
  gas = working gas object (not modified in function)
  OUTPUT:
  G_fr = frozen Gruneisen coefficient [-de/dp)_v = -(v/T)dT/dv)_s]
  ```

- **hug_eq**
  Algebraic expressions of equilibrium (product) Hugoniot pressure and enthalpy. Passed to root solver 'fsolve'.
  Matlab Function - hug_eq.m
  Python Function - hug_eq (in Thermo.py)

  ```
  SYNTAX:
  [x,fval] = fsolve(@hug_eq,Ta,options,gas,array)
  INPUT:
  Ta = initial guess for equilibrium Hugoniot temperature (K)
  options = options string for fsolve
  gas = working gas object
  array = array with the following values
     vb = desired equilibrium Hugoniot specific volume (m^3/kg)
     h1 = enthalpy at state 1 (J/kg)
     P1 = pressure at state 1 (Pa)
     v1 = specific volume at state 1 (m^3/kg)
  OUTPUT:
  x = equilibrium Hugoniot temperature corresponding to vb (K)
  fval = value of function at x
  ```

- **hug_fr**
  Algebraic expressions of frozen (reactant) Hugoniot pressure and enthalpy. Passed to root solver 'fsolve'.
  Matlab Function - hug_fr.m
  Python Function - hug_fr (in Thermo.py)

```
SYNTAX:
[x,fval] = fsolve(@hug_fr,Ta,options,gas,array)
INPUT:
Ta = initial guess for frozen Hugoniot temperature (K)
options = options string for fsolve
gas = working gas object
array = array with the following values
   vb = desired frozen Hugoniot specific volume (m^3/kg)
   h1 = enthalpy at state 1 (J/kg)
   P1 = pressure at state 1 (Pa)
   v1 = specific volume at state 1 (m^3/kg)
OUTPUT:
x = frozen Hugoniot temperature corresponding to vb (K)
fval = value of function at x
```

- **LSQ_CJspeed**
  Determines least squares fit of parabolic data.
  Matlab Function - N/A
  Python Function - LSQ_CJspeed (in Thermo.py)

```
SYNTAX:
[a,b,c,R2,SSE,SST] = LSQ_CJspeed(x,y)
INPUT:
x = independent data points
y = dependent data points
OUTPUT:
a,b,c = coefficients of quadratic function (ax^2 + bx + c = 0)
R2 = R-squared value
SSE = sum of squares due to error
SST = total sum of squares
```

- **PostReflectedShock_eq**
  Calculates equilibrium post-reflected-shock state for a specified shock velocity.
  Matlab Function - PostReflectedShock_eq.m
  Python Function - PostReflectedShock_eq (in reflections.py)

```
SYNTAX:
[gas3] = PostReflectedShock_fr(u2,gas2,gas3)
INPUT:
u2 = current post-incident-shock lab frame particle speed
gas2 = gas object at post-incident-shock state (already computed)
gas3 = working gas object
OUTPUT:
gas3 = gas object at equilibrium post-reflected-shock state
```

- **PostReflectedShock_fr**
  Calculates frozen post-reflected-shock state for a specified shock velocity.
  Matlab Function - PostReflectedShock_fr.m
  Python Function - PostReflectedShock_fr (in reflections.py)

```
SYNTAX:
[gas3] = PostReflectedShock_fr(u2,gas2,gas3)
INPUT:
u2 = current post-incident-shock lab frame particle speed
```

```
gas2 = gas object at post-incident-shock state (already computed)
gas3 = working gas object
OUTPUT:
gas3 = gas object at frozen post-reflected-shock state
```

- **shk_eq_calc**
  Calculates equilibrium post-shock state using Reynolds iterative method (see Section 7.2).
  Matlab Function - shk_eq_calc.m
  Python Function - shk_calc (in PostShock.py)

```
SYNTAX: [gas] = shk_eq_calc(U1,gas,gas1,ERRFT,ERRFV)
INPUT:
U1 = shock speed (m/s)
gas = working gas object
gas1 = gas object at initial state
ERRFT,ERRFV = error tolerances for iteration
OUTPUT:
gas = gas object at equilibrium post-shock state
```

- **shk_calc**
  Calculates frozen post-shock state using Reynolds iterative method (see Section 7.2).
  Matlab Function - shk_calc.m
  Python Function - shk_calc (in PostShock.py)

```
SYNTAX:
[gas] = shk_calc(U1,gas,gas1,ERRFT,ERRFV)
INPUT:
U1 = shock speed (m/s)
gas = working gas object
gas1 = gas object at initial state
ERRFT,ERRFV = error tolerances for iteration
OUTPUT:
gas = gas object at frozen post-shock state
```

- **soundspeed_eq**
  Computes the equilibrium sound speed by equilibrating the gas object at constant temperature and pressure.
  Matlab Function - soundspeed_eq.m
  Python Function - N/A

```
SYNTAX:
aequil =  soundspeed_eq(gas)
INPUT:
gas = working gas object (not modified in function)
OUTPUT:
aequil = equilibrium sound speed (m/s)
```

- **soundspeed_fr**
  Computes the frozen sound speed.
  Matlab Function - soundspeed_fr.m
  Python Function - N/A

```
SYNTAX:
afrozen =  soundspeed_fr(gas)
```

```
INPUT:
gas = working gas object (not modified in function)
OUTPUT:
afrozen = frozen sound speed (m/s)
```

- **state**
  Calculates frozen state given T and ρ.
  Matlab Function - state.m
  Python Function - state (in Thermo.py)

  ```
  SYNTAX:
  [P,H] = state(gas,r1,T1)
  INPUT:
  gas = working gas object
  r1,T1 = desired density and temperature
  OUTPUT:
  P,H = pressure and enthalpy
  ```